SOLID STATE PARTICLE COUNTER

(An investigation into the use of aluminium oxide as an alpha particle detecting medium)

by

E. Dennis, B.Sc., (Adel)

January, 1967

A thesis prepared from research performed in the laboratories of the Physics Department, Royal Military College of Australia, Duntroon, A.C.T. under supervision of the Physics Department of University of Adelaide, for the degree of Master of Science at the University of Adelaide.

This thesis contains no material which has been accepted for the award of any other degree or diploma in any University, and to the best of my knowledge and belief, this thesis contains no material previously published or written by another person, except when due reference is made in the text of the thesis.

C O N T E N T S

Page

SUMMARY

An investigation was conducted into the use of aluminium oxide films and a single crystal as detecting media for alpha particles.

Existing detection methods and their limitations are discussed and reasons for investigating aluminium oxide stated.

Methods of preparing the oxide by anodisation, evaporation and cathodic oxidation are reviewed, and the known electrical properties of each type summarised.

Spark cutting and electropolishing equipment was developed and is described together with the other measuring equipment used.

Electrical conduction in the oxide is considered from a theoretical viewpoint and in the process values of the electron mobility are calculated.

Experimentally, the conduction mechanism in the films is shown to involve field enhanced thermionic emission of trapped electrons into the conduction band, although some evaporated films exhibited negative resistance characteristics.

Anodic and evaporated films did not respond to alpha particles, whilst cathodic oxide films thicker than 3500 Å produced measurable pulses when irradiated.

The oxide single crystal behaved as a detector when two adjacent electrodes were deposited on one face. From the pulse height and rise time a carrier mobility of 5 ± 2 $cm^2 V^{-1} sec^{-1}$ and a carrier trapping time of $4{\cdot}5 \times 10^{-7}$ sec were calculated.

Possible future work is indicated.

CHAPTER 1

INTRODUCTION

This investigation arose from the need for a physically small detector for protons of energy in the vicinity of some few kilo-electron volts. For reasons discussed later, aluminium oxide films were chosen as the detecting medium. The range of 100 keV protons in this material is of the order of 1 micron. Alpha particles of energy 5 MeV give approximately this amount of energy to this thickness of oxide.

Consequently, because of the ease of acquiring and mounting suitable sources, initial experimental investigations were restricted to the detection of alpha irradiation with the intention of extending the investigation at a later stage, to particles of more local interest.

This thesis then, is a report on the work performed in the development of an aluminium oxide based solid state alpha particle detector.

The characteristics of currently available detection methods are briefly discussed, in Chapter 2, with particular emphasis on the low energy region. It is concluded that whilst windowless gas-based counters have sufficient sensitivity, the non-confinement of the gas renders them unsatisfactory for the eventual purpose. Scintillation counters are considered, but excluded because of a sensitivity limit of about 75 keV.

The characteristics of solid ion chambers, which encompass crystal counters, and semiconductor detectors, including homogeneous, junction and surface barrier types, are dealt with in the remainder of the chapter. In particular the effects of the leakage currents inherent in the use of low energy band gap material are stated, and a case made for the use of a solid with a large energy band gap.

This is based upon the recognition that the small charge release associated with the interaction of a low energy particle with the solid can be masked by the random fluctuations of the leakage current.

Finally, in this chapter, the expected advantages of using aluminium oxide as the medium are detailed, with the added suggestion that the investigation will shed some light on the basic conduction mechanism of this material, and lead to a value of the charge carrier mobility.

Chapter 3 is a survey of the previous work on aluminium oxide. The various forms of the oxide and their physical structures are reviewed.

Methods of preparation of anodic films, both porous and non porous, and the techniques used in measuring their physical parameters are analysed in some detail in view of the variations reported by the earlier workers.

Oxide film production by evaporation and cathodic oxidation is described, and an indication given of other methods which would be worth investigating at a later stage.

Some attention is given to the known electrical properties of single crystal and amorphous forms of the oxide in section 3·3. This includes the observations made on photoconductivity and electron tunnelling, as well as an account of some of the irradiation experiments which have been conducted.

A description of the materials, apparatus and methods used in the present experiment forms chapter 4. The processes of spark machining and electropolishing of aluminium specimens up to one inch in diameter, and the apparatus developed to perform these functions are included in the initial sections of the chapter. Then follows an account of the techniques and apparatus used to produce the oxide films which form the basis of the investigation.

Details are given of the procedures and equipment to produce oxide films with consistent characteristics, by anodisation, evaporation and cathodic oxidation. This last type having not previously been investigated in detail.

The means used to measure the thickness of the films is discussed in section 4·27.

The chapter concludes with brief outlines, supplemented by diagrams, of the specimen and source mounts and the electrical measuring equipment.

For the pulse type measurements, a low noise charge-sensitive preamplifier using E810F pentodes was designed and constructed. To increase the sensitivity of the Tektronix 585 oscilloscope, which was used for all the pulse shape measurements, a wide-band, (150 MHz) low noise amplifier was developed. Circuit diagrams and performance data of these are included as an appendix.

The mechanisms of electric conduction in insulators, and particularly aluminium oxide are considered from a theoretical viewpoint in Chapter 5. Experimental values of charge carrier mobility in aluminium oxide have not been published, and because of the importance of this quantity in the charge collection process, several calculated values of the mobility are included in this chapter. Models due to Frohlick and Mott and the semi-empirical approach of Suchet were used, resulting in the widely varying values of 9·05 and 800 $cm^2\ V^{-1}\ sec^{-1}$ respectively.

Electronic conduction in amorphous materials is also considered, with the emphasis on field enhanced thermal excitation of trapped electrons into the conduction band. The suggestion is made that a plot of the log of current density against the square root of the electric field is a more convenient relationship to consider, rather than one involving the square root of the applied potential.

The final part of Chapter 5 is concerned with the charge carrier generation associated with alpha particle irradiation, and the effects of carrier mobility, charge trapping and recombination, and film thickness on the collection of the released charge.

The results of the experiments and the conclusions drawn from them comprise Chapter 6. Here it is shown that for the films investigated, field enhanced thermionic emission of trapped electrons into the conduction band is the most probable process by which steady currents flow through the oxide.

The resistivity of anodic films is less than that of the best resistivity evaporated films of the same thickness. This is ascribed to the increased disorder associated with the latter type of film.

Some evaporated films, which showed evidence of contamination, exhibited marked discontinuities in the current-voltage relationships. Negative dynamic resistance effects were observed, in which the current under some conditions increased as the applied potential was decreased.

Cathodic oxidation film current-voltage curves also support the theory of field enhanced emission, with several films displaying a lateral displacement of the line. A tentative explanation in terms of the density of trapped electrons is suggested.

The latter part of Chapter 6 is concerned with the alpha particle counting experiments. These results may be briefly summarised. Anodic and evaporated films did not show any detectable effects on irradiation. This was put down to their structural disorder.

Most films produced by cathodic oxidation produced measurable pulses; in some instances there was evidence of some kind of charge multiplication effect. The high capacity of the detectors rendered resolution studies difficult, because the associated pulses were just above the input noise level of the amplifier used.

Chapter 6 also includes a report on the conduction and alpha particle counting characteristics of an aluminium oxide single crystal. For this specimen the log of the current density is proportional to the half power of the applied field, with the same slope as for thin films, suggesting a similar conduction mechanism, at least at low fields.

Alpha particle counting did not occur over the 1 cm of depth of this crystal. However, quite satisfactory counting took place when a high electric field existed between two electrodes spaced along one side of the crystal.

The resultant pulses were sufficiently well defined to permit a determination of the surface carrier mobility and mean life time. The mobility value was subject to uncertainties in the point of incidence of the alpha particles, and the capacity of the detector; a value of 5 ± 2 cm^2 V^{-1} sec^{-1} is reported. Mean lifetime from the experiments was $4{\cdot}5 \times 10^{-7}$ seconds.

The experiments did not permit the type of charge carrier to be identified.

Finally, it is concluded that thin aluminium oxide films can be manufactured with sufficiently low static leakage currents to allow them to be used as particle detectors, and good quality single crystals of the oxide can also act as detectors.

Some directions in which future work may proceed are also indicated.

CHAPTER 2

REVIEW OF PARTICLE DETECTORS

2.1 Review of non-solid alpha particle detectors.

Initially a review of existing detection methods and apparatus was made to determine which system merited further detailed study, having in mind the ultimate aim.

Of the non-solid types of detector, the gas based ones have been most used for alpha particles; cloud chambers of the expansion or diffusion type (Wilson 1951, Das Gupta and Ghosh 1946, Snowden 1953), Geiger and proportional counters (Curtis, Heyd, Olt, and Eichelberger 1955) and ion chambers (Wilkinson 1950), being the most commonly used. Some early work (Greinacher 1936, Chang and Rosenblum, 1945) with spark chambers has been performed, although these devices seem to have more application in the very high energy field.

All gas counters, except the atmospheric spark chamber, are such that the gas or gas plus quenching vapour, must be confined in some manner. This necessitates that either the alpha source is located within the detector, as in the gas flow counters, or that an extremely thin and therefore fragile window be incorporated in the device.

The window has an appreciable effect on the efficiency of the detector as a result of the absorption of some of the incident particles. If the window thickness is expressed as an air equivalent, as is usually the case with alpha particles, the collection efficiency for a given configuration can be calculated from the equivalent geometry. A window of 0·5 mg. cm^{-2} aluminium (air equivalent 0·3 cm) results in a collection efficiency of 85% when a source of 5 MeV alpha particles is placed 0·2 cm. from the window. (Sharpe, 1964, p. 27, p. 86).

Flow counters have been extensively used for alpha particle counting, principally because they avoid the need for windows. (Simpson 1947, Sharpe and Taylor 1951, Sharpe 1953). They have the advantage that when operated in the proportional mode it is possible to discriminate between alpha, and beta and gamma particles, because of the low specific ionisation of the latter types of radiations. They have been used for the measurement of absolute particle flux, because their overall efficiency depends on a small number of factors, e.g. geometry, back-scatter, self-absorption and small dead time correction, which can all be evaluated with acceptable accuracy.

Another advantage of the flow-counter is their inherently low background count, which makes them suitable for measuring low level alpha fluxes.

The sensitivity of the gas counters can be greatly increased by the multiplication of charge carriers that results when the counters are operated with high electric fields. The avalanche collision induced ionisation can give rise to a measurable discharge even when only one electron-ion pair is produced within the gas by the initial interacting particle.

Even with high values of charge carrier multiplication ($> 10^3$) the proportional counter can be designed to respond to X-rays and gamma rays in the region of 0·5 to 100 keV, with acceptable energy resolution.

The operation of gas ion chambers has been described on a number of occasions (Price, 1964, Chap. 4, Sharpe 1964, Chap. 6). The range of usefulness, and the limitations of both mean level and pulse ion chambers are well known. Typical limiting parameters as far as low

energy particle detection is concerned are considered by Sharpe (Sharpe 1964, p. 181) where a minimum particle energy of 38 keV is derived for parallel geometry. The gridded ion chamber (Frisch 1944, Bunemann, Cranshaw and Harvey 1949) is capable of higher sensitivity, and values of the order of 18 keV are possible.

The requirements that the detector was to be physically small and should have good energy resolution for particles with energy below 100 keV were so restrictive that no kind of gas based counter appeared capable of being adopted to the task.

2.2 Solid detectors

2.21 Scintillation counters.

In this type of detector the energy of the incident particles is converted into electromagnetic quanta, which are in turn detected by a photo-sensitive device. The scintillation counter has been most useful for the detection of gamma radiation. The alkali halides, suitably doped to suppress the long wavelength exciton radiation [e.g. the 0·3μ radiation in pure NaI, quenched by small concentrations of thallium (Van Sciver and Hofstadter 1955)] can be grown sufficiently large and strain free for this purpose.

The detection process requires two energy conversions, viz., incident particle energy into photons, and photons to photoelectrons, with attendant energy loss at each conversion.

At low energies (< 400 keV) the photoelectron yield is not linearly related to the energy of the incident particle (Taylor, Jentschke, Remley, Eby and Kruger 1951; Engel Kemeir 1956; Iredale 1961).

The scintillation counter is suited to the detection of single particles because the process takes place in a time of the order of microseconds. Further, since the electrical output pulse in most instances can be made a function of the incident particle energy, then the counter can supply information about this energy.

Detectors of this type have been used for registering alpha as well as other particles. The scintillators used differ from that for x-rays and gamma rays principally because the energy transfer processes are different, resulting in the penetration depth of the alpha particles in the solid being much less.

A typical alpha sensitive scintillation counter is described by Sharpe (Sharpe 1964, p. 127). The scintillator commonly used is activated zinc sulphide, which is deposited directly on a photo-multiplier surface, or on a light guide which is optically coupled to the surface.

Sharpe (Sharpe 1964, p. 130) considers the characteristics of a representative alpha particle detector and suggests a threshold energy of 75 keV. This figure could be reduced by the selection of phosphor and photocathode materials, as well as by reducing the temperature of the environment. It was felt that the investigation of an alpha particle detector based upon the scintillation counter with materials then available, would not lead to a system which would satisfy the ultimate need.

2.22 Solid ion chambers.

In detectors of this kind, the ionisation produced in a solid by the incident radiation is measured, either directly or indirectly.

As in the gaseous ion chamber the radiation interacts with the material to produce charge carriers. These carriers can be caused to drift through the medium under the influence of an electric field. Information about the ionising radiation would result from measurements of:

(a) the change in electric current through the medium,
(b) the electrical capacity change,
(c) the change in electric potential across the medium,
(d) some or all of the electric charge separation.

Usually (a) or (d) is measured, although the capacity has been used as the variable parameter of a parametric amplifier (Chase 1961).

A further possibility would be to use the detecting element as part of the input circuit of a self-quench super-regenerative detector, in which case the arrival of ionising particles would initiate oscillation. The effect of the residual noise of the input circuit of a super-regenerative circuit such as this would be difficult to eliminate, thus rendering it not very useful as a pulse counter. However the combination could be of value as a mean level detecting system.

The advantage of recording the shape of the current pulse lies in being able to determine the mobilities and trapping times of the generated charge carriers. The effect of trapping and recombination of carriers has been considered for a range of situations. (Gibson and Miller, BNL 5391, Northrop andSimpson 1962).

The integrated charge released by the interaction is a measure of energy lost by the particle in the medium. If the particle is completely stopped within the detector, this becomes a measure of the particle energy.

A charge sensitive preamplifier, the output voltage of which is proportional to the charge released inside the detector, treated as a capacitor, is coupled to the detector, and apart from recombination and trapping processes, the output signal is a measure of the interaction energy.

Alternatively, a thin counter permits a measurement of $^{dE}/_{dx}$ for the interaction thus permitting particle identification.

The detector consists of a piece of suitable material with electrodes attached, and between which an electric field is maintained. The required characteristics of the material, particularly for use in low energy interactions are discussed in detail in the remainder of this chapter.

A variety of materials has been used for such detectors. The state of the art up to 1949 has been reviewed by Hofstadter (Hofstadter, 1949), where the earlier work (Van Heerden, 1945; McKay 1948, Yamakawa 1949, Ahearn 1947, and others) using silver chloride, silver bromide, diamond and cadmium sulphide crystals is discussed.

In the later work zinc sulphide and mixtures of lithium and silver bromide were used to detect alpha particles and slow neutrons respectively (Ahearn 1948, Yamakawa 1951). Some considerable additional work has been performed on diamond (Ess and Rossel 1951).

The requirements that the detecting medium should have low conductivity and be free from physical defects, and usually, impurities, resulted in experiments being conducted with silicon and germanium single crystals. A crystal of n-type silicon would have a maximum resistivity of about 3600 ohm cm and if the dimensions were 0·6 cm thick and area 1 cm^2, at room temperature (electron mobility 1,360 $cm^2\ V^{-1}\ sec^{-1}$) the rise time of the pulse would be about 400 nanoseconds for a 1000 V cm^{-1} field. The fluctuations of the leakage conduction electrons would be of the order of 10^6. This would be equivalent to a minimum detectable particle energy of 2 MeV. Reducing the temperature to 77°K would increase the electron mobility by a factor of 10; decreasing the pulse rise time to 40 n sec, the fluctuations to 500, and the equivalent energy to about 1 keV. Consequently, whilst homogeneous detectors based upon silicon would be satisfactory at low temperatures, their performance at room temperature would be unacceptable.

The realisation that the depletion layer which exists across a back biased PN junction possessed most of the requirements for a

detection medium resulted in work using first germanium (McKay, 1949; Orman, Fan, Goldsmith and Lark-Horovitz, 1950) and later silicon junctions (McKenzie and Waugh, 1960) as detecting materials.

It has been pointed out (Northrop and Simpson 1962) that as the purity of the basic material increases, the PN junction detector approaches more nearly that of a homogeneous conduction detector.

An alternative form of semiconductor detector consists of a piece of silicon or germanium on one side of which an insulating oxide layer has been grown by exposing the cleaned and etched surface to the atmosphere for several days. A thin conducting gold electrode is deposited on this oxide. The characteristics of these surface barrier detectors have been considered in detail (Sharpe 1964, p. 166, Dearnaley and Northrop, 1964).

The sensitivity and energy resolution of these semiconductor detectors, particularly at low temperatures, have resulted in their wide application.

The diffusion of lithium ions into the silicon results in impurity produced charge carrier compensation being possible over quite extensive volumes. Detectors with active depths up to one centimetre have been reported.

Consequently it was decided to investigate a conduction counter with greatly reduced standing current. A search of the literature revealed that whilst many experiments had been performed on particle energy-range relationships for aluminium oxide over a wide variety of particles, and investigation of the change in electrical properties of single crystal alumina under large radiation doses, no attempt had been made to study it as a particle detecting medium.

Further, oxide films of the required thickness could be produced by many methods which would result in different but reproducible characteristics.

In addition, investigation showed that the basic electrical conduction mechanism in thin aluminium oxide films was not understood. Some of the current theories and experimental values of conductivity are discussed in Chapter 3.

No generally accepted value of the energy band gap for pure single crystal aluminium oxide has been published. (A figure of 10 eV is usually assumed.) The conduction process appears to be electronic, with p-type characteristics predominating. The mobility of the charge carriers has not been determined; nor have the mean lifetimes and mean free paths.

The dependence of these properties on the manner in which the oxide was produced and the relationship between structure and properties has not been carefully investigated.

In those instances where alpha particle irradiation produced measurable electrical pulses some estimate of these properties would be possible.

2.221 Pulse height-energy relationship.

The interaction of charged particles with solid matter has been widely studied. (Whaling, 1958).

The relationship between particle type and the atomic number of the stopping medium for energetic particles is well known. This relationship (Livingston and Bethe 1937) is found to hold well for proton and alpha particles with energy greater than 100 keV.

The stopping power is given by:

$$-\frac{dE}{dx} = \frac{4\pi e^4 NZ}{mv^2}\left[\ln\frac{2mv^2}{I} - \ln(1-\beta^2) - \beta^2\right]Z^2$$

where z = charge number of incident particle

N = number of atoms cm^{-3} of stopping material

Z = atomic number of stopping material

V = velocity of incident particle

$\beta = V/c$, where c = speed of light

I is the average excitation potential of the atom

($I \approx 10ZeV$).

In cases where the energy is less than 100 keV, empirical values of the stopping power are used. When the stopping medium contains more than one kind of atom, the energy loss can be taken at the sum of the individual losses.

For 5 MeV alpha particles incident upon aluminium oxide the initial rate of energy loss is 140 keV per micron. Hence an oxide thickness of one micron ($= 10^4$ Å, equivalent to anodising at 800V.) will have deposited in it 140 keV of energy. When 100 keV protons are incident upon the same thickness of oxide, they will be completely absorbed, and thus the effect of these lower energy protons can be simulated by the 5·1 MeV alpha particles.

The stopping process involves the exchange of energy between the incident particle and the electrons in the solid. A useful concept is the average energy (ϵ) required to generate an electron-hole pair. The number of charge carrier pairs generated within an absorber is directly proportional to the energy absorbed, over a wide range of energies.

$$Q_g/e = n_g = \frac{E}{\epsilon}$$

where Q_g is the charge generated when n_g electron-hole pairs (charge e) are produced as a result of kinetic energy E being lost by the particle to the medium.

A simple model for this type of interaction process has been

proposed (Shockley, 1961) in which the predicted value of ϵ is:

$$\epsilon = 2{\cdot}2\ E_g + r\ E_r,$$

where E_g is the forbidden energy gap, E_r is the highest optical mode phonon energy, and $r = L_i/L_r$ is the ratio of the mean free path between ionising collisions (L_i) and the mean free path for phonon collisions (L_r).

Empirical values of ϵ have been determined for some solids and those used for particle detection are listed in table 6 of Sharpe (1964).

The variation in the measured values of ϵ can be partly ascribed to the incomplete collection of the charge carriers generated, due to recombination and trapping effects.

The temperature dependence of ϵ for silicon and germanium has been investigated (Emery and Rabson, 1965).

A value for ϵ for aluminium oxide for alpha particle irradiation has not been published. The energy loss for electrons in aluminium oxide has been observed to occur in multiples of 22·3eV. (Young, 1959). If the Shockley model is applicable to this material a value between 20eV and 30eV would be expected.

Once ϵ for the material of a detector and the charge collection efficiency have been determined, particle energies can be measured by measuring the total collected charge. A convenient method is to use a charge sensitive amplifier following the detector. The linear relationship between charge generated and hence voltage pulse out and particle energy makes the solid ionisation chamber satisfactory for energy spectrometry. The departure from this linear relationship for proton energies below 100 keV means that a detector would have to be calibrated for these energies.

Whilst the 5·1 MeV alpha particles lose the same amount of energy in a one micron thick aluminium oxide detector as 100 keV protons, they do not unambiguously permit a measurement of energy resolution. The spread in the total charge collection will however be an indication of the resolution that could be expected, for these lower energy protons.

2.222 Noise characteristics.

The unwanted electric currents that flow through the detector as a result of the applied charge collecting field tend to mask the charge pair generation process of the incident particles.

These currents arise from several sources.

(a) Direct leakage through the active volume of the detector due to charge carriers that exist because of impurities and lattice defects.
(b) Leakage produced by charge carriers thermally excited into the conduction band or an impurity level.
(c) Leakage currents which migrate across the surface of the specimen, and which frequently bear little relationship to the bulk properties of the material of the detector.
(d) Currents which arise from the injection of charge carriers at the electrode-medium interface.

Some, or all of these currents will be environment dependent.

Since these currents fluctuate with time, the fluctuations put a limit on the minimum detectable particle energy.

A complete treatment of such noise has not been made. The major sources and their effects on energy resolution have been summarised. (Dearnaley and Northrop, Chapter 4, 1964).

The prime requirement is that the spurious redistribution of charge should be minimal.

2.223 Charge multiplication

If a sufficiently high electric field is maintained across the sensitive region of a detector, the charges produced by the incident particle could be accelerated sufficiently to produce additional charge carriers by ionisation by collision. This form of multiplication process is used with considerable success in gaseous detectors.

To date this approach has not been applicable to solid detectors. This has been primarily due to the inability to eliminate leakage currents, which would also be subject to the multiplication process. The overall increase in signal to noise has been marginal. A marked reduction in the leakage current could result in a significant charge multiplication being worthwhile.

A possible alternative approach would be to make use of the charge multiplication process that has been observed when semiconductors are doped with suitable amounts of transition element impurities. Multiplication ratios of 10^4 have been measured in germanium containing manganese impurity (Tyler, Newman and Woodbury, 1955).

2.3 Detection of low energy particles.

The requirements for satisfactory detection of low energy particles are quite restrictive. Since the total particle energy is small the total charge separation produced is small. This necessitates a very efficient charge collection process, which in turn implies a very low concentration of recombination and charge trapping centres. Further, the collection potential across the detector needs to be sufficiently high to ensure the collection efficiency. An inevitable consequence of a high collecting potential is the corresponding increase in leakage current through the detector.

An important parameter is the depth of penetration of the particles. Low energy particles permit the use of thin detectors. The effect of traps and recombination centres can be reduced by reducing the length over which the charges are collected, because even if the density of these defects remains constant (and assuming the reduced thickness does not produce a marked change in mobility), the time for the collection will be less for a given collecting field.

The desirable characteristics of a low energy detector can be summarised.

(a) Small leakage currents.
  (i) High purity; minimum structural defects.
  (ii) Small number of thermally excited carriers; i.e. energy band gap large; temperature low.
  (iii) Area of detector as small as consistent with environment - the leakage current through the detector will be a simple function of the area of the detector.
  (iv) Minimum potential across detector consistent with efficient charge collection.
  (v) Surface currents excluded from measuring circuit by guard ring techniques.
  (vi) All other insulating material of high quality.

(b) Efficient charge collection.
  (i) Product of carrier lifetime and mobility high; i.e. high mobility; high purity; minimum structural defects.
  (ii) Thin detector.

(c) High charge generation by interaction.
  (i) Low value of ϵ - implies a low energy band gap.
  (ii) Little energy lost exciting phonons - i.e. long mean free path for phonon collisions.

Some of these requirements are not compatible with some of the others and in particular, the condition of a wide forbidden energy gap for low leakage currents, and a narrow gap for maximum generation of charge carriers.

It was considered that the dominant problem was the leakage current and that this could be reduced substantially by decreasing the number of thermally excited carriers $\left[\alpha \exp\left(-\frac{E_g}{2kT}\right)\right]$, by using a material of wide energy band gap, but at the same time the number of charge carriers produced would only fall approximately linearly with energy gap.

Further, because structural characteristics were so important, it was felt that some gain would accrue from observing the one material in four physical states; amorphous, polycrystalline, and single crystal films, and thick single crystal.

Aluminium oxide was chosen as the material because;

(a) it is relatively easily prepared in these four forms,
(b) photoconductivity is well developed in the amorphous form,
(c) no publications were sighted using this material as a detector,
(d) the measured conductivity of all forms is low.

In addition the basic electrical conduction mechanism is not understood, even in relatively pure single crystals and no value of charge carrier mobility has been published. It was anticipated that the experiments conducted would supplement the work already done.

CHAPTER 3

SURVEY OF PREVIOUS WORK ON ALUMINIUM OXIDE

3.1 Introduction.

Aluminium oxide occurs extensively in nature. Only one basic oxide Al_2O_3 is known to exist, although this occurs with varying amounts of impurity (giving rise to the gems; sapphire, blue, due to Co, Cr, or Ti dioxides; ruby, red, due to Cr_2O_3), and varying degrees of hydration. A variety of minerals include the oxide as one of their principal constituents.

Two non-hydrated forms of the oxide exist, the α-oxide which is hexagonal (rhombohedral division) and the η-oxide which has cubic (spinel) structure. A particular form of the η structure, the white microcrystalline, is frequently called γ-oxide or γ- alumina. At elevated temperatures (650°C, Hass, 1949) the γ forms transform to the α structure.

The crystal structure of α-Al_2O_3 has been reviewed recently by Gamble et al (Gamble, Bartram, Young, Gilliam and Levy, 1964). The basic crystal structure is rhombohedral with space group $D_3D^6(R\bar{3}c)$. The bonding appears to be predominately ionic (Bersohn 1958) with approximately a 20% covalent contribution. (Laurance, McIrvine, and Lambe, 1962).

The crystal can be considered as a hexagonal close packing of oxygen ions (O^{2-}) with pairs of trivalent aluminium ions (Al^{3+}) at intersticial sites along the c axis, sharing equilateral triangles of oxygen between them.

The shared triangles are slightly reduced in size by the electrostatic forces between the two different kinds of ions, resulting in a small distortion of the hexagonal close packing. This results in a slight enlargement and rotation about the c axis of the

adjoining triangle, which consist of oxygen ions from three adjacent coplanar molecules. Rotations in both senses occur in equal numbers throughout the lattice. The rotation is 3·9° (Newnham and de Haan, 1962).

The thin film of oxide produced by anodisation usually gives rise to electron and X-ray diffraction patterns corresponding to γ-Al_2O_3 (with or without hydration.)

In γ-Al_2O_3 the cations in the spinel structure are ordered, and in γ^1-Al_2O_3 the cations are randomly arranged. (Burghers, Claassen and Zernike 1932). In both these materials 70% of the metal ions are in the octahedral sites and 30% in the tetrahedral sites. The unit cell of γ-Al_2O_3 contains 32 oxygen ions and is built up in a regular array from smaller cells each containing four oxygen atoms. Some of the small cells contain aluminium ions in 6 coordination only, some with 4 coordination only.

Aluminium metal on exposure to air acquires an oxide layer which has been estimated to be between 20 Å and 60 Å thick (Charlesby 1953, van Geel and Schelen, 1957). Holland (Holland 1956, p. 344) quotes Hass (Hass 1947) as reporting initial rapid growth to 15-20 Å, followed by further slow growth to 45 Å after one month. A thickness of 10 Å in less than one minute was claimed for evaporated aluminium film (Stern and Uhlig 1952). The layer is classed as highly transparent and amorphous.

The literature abounds with references to the work done on aluminium oxide; its preparation and properties; chemical, electrical, crystallographic. Many of the results are at variance in one or more important aspects and in some cases, even self contradictory. The measurement of electrical properties of oxide layers produced in the laboratory has been mainly limited to films formed electrolytically; the so called anodic method.

A good selection of the work on anodic aluminium oxide is reviewed in the book of Young (Young 1961).

For this project it was decided to investigate oxide films which could be made with acceptably reproducible characteristics, by three different methods. Materials so produced would be investigated with the view to determining what characteristic they had in common and where they diverged; and which showed most promise as the basis of a particle detector.

The previous work on these three oxide types is summarised in this chapter.

3.2 Oxide types and formation.

3.21 Anodic oxide films.

Earlier it was generally recognised that when aluminium was oxidised by making it the anode of a suitable electrolytic cell, two types of oxide structure could be produced. The principal variation required to make these types was in the selection of the electrolyte. The temperature of the solution also contributed to which type was formed in a particular circumstance. These two types have been given a variety of names e.g. amorphous and insulating (Charlesby 1953), porous and non-porous (Young 1961), high and low resistance, crystalline and amorphous. The two terms used commonly are porous and non-porous, and whilst this is a relatively unsatisfactory distinction, these terms will be used.

Porous films are produced when the electrolyte contains sulphuric, phosphoric, oxalic or chromic acid. The thickness of the oxide layer is not determined by the potential applied across the cell, but will grow at constant potential to a thickness of many microns.

The structure of these films has been examined by a variety of methods. Optical microscopy showed that the films were fibrous in structure with pores associated with the fibres. (Rummel 1936, Baumann 1939, Edwards and Keller 1941, 1944). Pore concentration was estimated at about 10^8 cm^{-2}. From water uptake and electrical resistance measurements Rummel considered the pore diameter to be of the order of 10^3 Å. Pores became wider with increasing anodising voltage in oxalic and sulphuric acid electrolytes.

When stripped films were placed in suitable media and the birefringence measured (Huber 1945; Huber and Gaugler 1947, 1948), a plot of birefringence against refractive index gave a minimum $\mu = 1{\cdot}65$ - the refractive index of the film. The variation in birefringence was due to the uptake of the medium in which the film was immersed (it was not due to any crystalline structure of the oxide). Using a theoretical model due to Weiner, it was concluded that in the film measured the pore volume was 4.3% near the metal and 16% near the electrolyte. Crystals up to 0.8 mm in thickness were examined. Direct electron micrographs of stripped oxide layers as well as replicas of the outer (electrolyte) layers and the inner (metal oxide interface) and cross-sections through the oxide have been examined. (Edwards and Keller 1944, Keller and Geisler 1944; Keller, Hunter and Robinson 1953, Heidenreich and Peck 1953).

The oxide was found to consist of hexagonal cells whose outer and inner surfaces bulged into the solution and metal respectively. One pore was counted in transmission microscopy for each cell counted in replica photographs. It was concluded that each cell has a centrally situated pore.

The linear size of the cells increased with the formation voltage ($S = aV + b$, b = diameter of pore, aV = twice the wall thickness). Cells first appeared along sub-grain boundaries, and then filled out into the whole area.

The number of cells per unit area was very large. For example, for a layer formed at 20V in 15% H_2SO_4 at 10°C a value of $5{\cdot}2 \times 10^{10}$ cm^{-2} was calculated.

The pores did not completely penetrate the film. The name barrier-layer thickness has been used to describe this region of unpenetrated film.

These porous films did not appear to be pure Al_2O_3. Films formed at 20°C in 10% sulphuric acid have been reported (Liechti and Tredwell 1947) to contain 13% of "SO_3" as well as a few per-cent of bound water. The stripped films were very hygroscopic.

The rate of oxidation depended upon the crystal face of the aluminium if the oxidation rate were greater than that produced by 15 ma cm^{-2} (Herenguel and Le Long, 1951). The thickness was greatest in [111] direction and least in the [100].

The relative permittivity (at low frequencies) of dry films was 7·58 (Treadwell and Obrist 1941). This would correspond (on the basis of the estimated size of pores) to an oxide relative permittivity of approximately 10.

The A.C. impedance of the film immersed in conducting solutions was dominated by the leakage conductance due to the pores. The series equivalent capacity of films with graphite and other conductors replacing the electrolyte varied by large factors (as high as 10^2) depending on the relative humidity of the air.

There is no generally accepted theory of growth of these oxide layers. Factors which must be accounted for are the persistence of the pores, (that is, they show no tendency to become blocked as the process is continued) and the independence of the thickness of the layer of such variables as applied potential, type and temperature of electrolyte. Experiments have indicated that the mobile ion in this type of film is oxygen (i.e. O^{2-}) rather than the metal (Lewis and Plumb 1958) though the OH^- ion moving through the oxide to

the metal and releasing H^+ ions which move back through the oxide (Hoar and Mott 1959), as well OH^- and H^+ ion (Treadwell and Orbist 1943), have variously been suggested as the principal growth mechanism.

Non-Porous Films. The second type of anodised film has a structure and therefore properties differing from the porous type. There exists some appreciable difference of opinion as to the precise structure and composition of these layers.

The method of production is the factor that essentially separates them from the porous layers. Typical detailed descriptions of the formation of these layers are given by Barrett and Winterbottom (1961) and by van Geel and Schelen (1957).

In the first case high purity aluminium (99.99) were subjected to a homogenising anneal for 24 hours at 500°C. The resultant hardness was 15 Brinell.

The specimen was machined to dimensions and ground on waterproof carborundum paper immersed in white spirits.

Two alternative procedures were then adopted.

(a) The specimen was electropolished in a perchloric acid - alcohol electrolyte.

(b) The specimen was fine ground with 3μ diamond dust, polished with alumina on selvyt before electropolishing.

It is claimed that generally acceptable surfaces were produced by both these methods, as long as the homogenisation of the material was performed, and provided that the rectified output of the polishing current supply unit was suitably smoothed.

The specimens were then anodised in an electrolyte (after Hass 1949) containing 3% ammonium tartrate, pH 5·5, at 20°C.

This solution was prepared by taking a 3% tartaric acid solution and adjusting it to pH 5·5 with ammonium hydroxide. The anodising was performed using a power supply, with variable voltage but electronically stabilised to the preset value. Specimens were anodised at 500V at 250 ma.

No mention was made in this work to the naturally occurring oxide layer, since it presumably was removed in the process of mechanical polishing.

The process of van Geel and Schelen comprised:

(a) Aluminium of purity 99·9% was cleaned in one of three different ways.

(i) The aluminium was immersed in a cleaning solution consisting of 6 gm. per litre of potassium bichromate added to equal parts by volume of water and concentrated sulphuric acid, for at least 1½ min at 90°C.

(ii) The aluminium was cleaned in alcohol only. This did not remove the 60 Å layer of oxide formed in air.

(iii) The aluminium was immersed for at least 1 min in a bath at 60°C containing 200 gm of potassium hydroxide per litre of water. After being rinsed the aluminium was dipped alternately in baths of dilute acids and bases. Finally the aluminium was put in boiling water. This method was found to produce a layer of Boehmite (the monohydrate form of the oxide $Al_2O_3\ H_2O$).

The report stated that process (i) was preferred.

(b) An aluminium plate was oxidised at room temperature up to 340 volts in an electrolyte solution of 40 gm of boric acid and 10 gm of borax per litre of water.

In the latter process, the oxide films were stripped by dissolving the aluminium in a solution of bromine and anhydrous methanol (1 : 12) and the density determined to be $3{\cdot}1 \pm 0{\cdot}2 g\ cm^{-3}$.

The thickness of the oxide layer was directly related to the anodising potential. If the anodising were carried on until the current dropped to a very low value (of the order of microamps), the film thickness (d) was given consistently by

$$d = 12{\cdot}7V \text{ Å}.$$

If the leakage current remained significant this relationship was no longer valid. This dependence of film thickness upon the anodising potential was one of the most important differences between the porous and non-porous oxides.

van Geel and Schelen investigated the crystal structure of the oxide with an X-ray spectrometer and found the layer to be mainly amorphous. They state: "In general it can be said that the amorphous Al_2O_3 is made up of oxygen atoms arranged in a close-packed lattice which is often, but need not necessarily be, cubic. Moreover the close packed lattice need not be strictly periodic. The aluminium atoms are irregularly distributed over the octohedral and tetrahedral spaces.

After cleaning by method (i) ($K_2Cr_2O_7 + H_2SO_4$) amorphous Al_2O_3 was only formed in oxidation at room temperature. If the oxidation were performed at 100°C, γ-Al_2O_3 was also formed. Owing to the higher temperature crystalline aggregates were produced. The same result was obtained in the oxidation of the aluminium which had only been superficially cleaned and had retained its film of oxide.

Aluminium cleaned by method (iii), in which aluminium was immersed in boiling water, was always covered during cleaning by a layer of boehmite ($Al_2O_3\ H_2O$). This layer does not act as an insulator in the electrolyte. If such a boehmite coated plate is oxidised and the thickness of the film produced is calculated from the oxygen taken up, and compared with the thickness determined experimentally, then the experimental thickness will be found to be greater than that which follows from the oxygen yield. On weighing the plate before and after oxidation only a small increase in weight is found. The most plausible explanation is that during oxidation part of the boehmite is converted into γ^1-Al_2O_3. That γ^1-Al_2O_3 is formed during oxidation even at room temperature is evident from the X-ray patterns.

Summing up it can be said that oxidation at 100°C always gives rise, not only to amorphous but also to γ^1-Al_2O_3. Oxidation at room temperature gives amorphous oxide only, except when there is a layer of boehmite in the aluminium prior to oxidation; in this case γ-Al_2O_3 is also formed."

A good survey of the work performed by others is included in Young (1961). A variety of results has been reported (Burghers et al 1932, Verwey 1935, David and Welch 1956, Blewe 1936, Harrington and Nelson 1940, Hass and Kehler 1941, Taylor et al 1943, Hass 1949) which in turn show evidence of crystalline, amorphous structure, with and without pores, both hydrated and anhydrous, when formed at low voltages and high.

Surface preparation seems to be of considerable importance (Hulik and Nowatny 1957), and the presence of adsorbed chlorine is believed to stimulate the production of a hydrated oxide on the surface.

Plumb (1958) using radioactive phosphorous P^{32} found that films formed in phosphate electrolytes contain some 8% of the phosphate radical.

Franklin (Young 1961 p. 214) states that at least three types of oxides are formed in boric acid and borax electrolytes.

(i) A hydrated layer is formed near the oxide-solution interface. (It was detected using tritiated water).

(ii) Crystalline γ^1-Al_2O_3 (cubic, cell size 3·91) occurred as irregular patches within the anodic layer.

(iii) Amorphous oxide normally constitutes the bulk of the film.

Both metal and oxygen were believed to be mobile since changes in topography occurred at both metal/oxide and oxide/solution interfaces. This has been investigated by Lewis and Plumb (1958) who produced a radioactive marker layer using sulphuric acid containing radioactive sulphur, S^{35}. Non-porous films were produced in 3% ammonium tartrate electrolyte. Duplex and sandwich films were formed, and these were sectioned by chemical dissolution; plots of radioactivity against amount dissolved indicated that the last layer formed was on the outside, i.e. that the metal was mobile.

This mobility of the metal, rather than the oxygen was further supported by the work of Vermilyea (1954) on tantalum oxide formation. Whilst there is some agreement that in all probability the oxide grows at the oxide/electrolyte interface, the mechanism by which the metal ions move through the oxide layer is far from understood. There does not appear to be much clear evidence that the oxide is particularly metal ion rich near the metal/oxide interface, or metal ion deficient at the other interface.

The mechanism of metal ion transport in tantalum oxide has been considered (Verkerk, Winkel and de Groot 1958) without any finality being reached. The question of a gradient of metallic ions across the oxide has been investigated for both aluminium and tantalum (Winkel and de Groot 1958), but the data reveals no indication that these layers have any strongly asymmetric structure. Some work with niobium oxide lends support to the ion gradient idea. (Young 1951)

Whether the oxides formed in tartrate and borate electrolytes have pores has also been the subject of some debate. Franklin (1957) reported cell concentrations of 1.4×10^{8} cm^{-2} in oxide layers formed on aluminium at 500 V in an electrolyte of 3% boric acid and 0.05% borax at 20°C. The radius of the cells was about the same as the thickness of the film. This number of cells per unit area is considerably less than the 10^{10} cm^{-2} for the porous material measured by Keller, Hunter and Robinson.

More recent work (Grosskreutz and Shaw 1964) on the structure of coherent anodic layers grown on the (100) faces of aluminium in tartaric acid - ammonia electrolytes has been performed using replicas and transmission electron microscopy.

At pH 5·5 the layers were pore free to 10 Å to 15 Å and faithfully replicate the original surface formed during electropolishing. Anodic layers grown at pH 2.0 or 10.5 were highly porous and an electropolishing action took place. An ultrastructure with characteristic spacing of 50 Å was observed on surfaces polished in perchloric acid mixtures. The structure was also seen on the electrolyte interface of the anode layer. It was proposed that this structure was not an artefact of the shadowing process but that it may correspond to particles of aluminium hydroxide formed during growth of the anodic layer.

It is very apparent that over the years a large number of conflicting results has been produced. There are a variety of factors which not all workers have considered. Such things as, amount and type of impurity in the aluminium, the crystal structure, and size, surface preparation, elastic strain, type of polishing used, the cleaning process after polishing, the purity of the materials forming the electrolyte, the specific conditions of electrolysis, temperature, amount of agitation, current density, to name some are obviously going to be significant when irregularities of the order of 20 Å are being considered.

In this investigation, work on anodic oxide films will be restricted such that as few untoward variables as possible will be involved. Non porous films prepared by the method of van Geel and Schelen (van Geel and Schelen 1957), on polycrystalline aluminium rod of known composition, and on high purity single crystals, and the method of Grosshreutz and Shaw on aluminium single crystals will only be considered.

The material and methods are treated in Chapter 4.

3.22 Vacuum evaporation of oxide films.

Aluminium oxide melts at 2050°C and boils at 2250°C when the ambient pressure is one atmosphere. It can be vaporised in a vacuum evaporator (vapour pressure = 10 microns at 1781°C) using a tungsten spiral heater, and the vapour deposited upon a suitable substrate. The layer so formed is considered to be deficient in oxygen as a result of some decomposition (the dissociation pressure 10^{-8} Torr). (Weinrich 1947,).

The presence of water vapour and diffusion pump oil has a marked effect on the structure of the deposited oxide.

The metal oxide may be further modified as a result of chemical reaction with the evaporator heater. Al_2O_3 is reduced by tungsten above 2000°C (Wartenberg and Moehl, 1947). It was stated (Johnson 1950) "at high temperatures the limiting factor for refractories is not the melting point, but the stability when in contact with other substances and the rate of volatilisation."

The lower metal oxides are more volatile than the higher oxides e.g. Al_2O_3 is less volatile than AlO, and hence the decomposition product evaporates more readily than the pure oxide (Holland 1950 p. 449).

The tendency to decompose increases with temperature and consequently, purer oxide layers can be produced by slow rather than

rapid evaporation.

Hass (1949), describes the layer evaporated on to a cold polycrystalline aluminium substrate as amorphous, while those formed at higher temperatures are crystalline γ-Al_2O_3. Temperatures in the range 450°C to 500°C are required to get any significant crystalline structure. If the amorphous oxide films are annealed in vacuo at 680°C the structure becomes crystalline, corresponding to cubic γ-Al_2O_3. (Hiesinger and Koenig, quoted by Holland L. 1956).

The difficulties associated with the evaporation of aluminium oxide are discussed by Holland. The matter is considered again in Section 4.25.

3.23 Oxide films by cathodic oxidation.

Reactive Sputtering.

Sputtering is the process whereby material is moved from the cathode when a low pressure discharge occurs. The disintegrated material may leave as free atoms or in chemical combination with the ambient gas.

The processes involved have been extensively investigated but as yet no generally accepted explanation has been proposed.

If a pure deposit of the cathode material is required, it is preferable to produce the discharge in an inert atmosphere. The sputtering rate appears to increase with increasing atomic number of the gas used; consequently argon is the most commonly used medium.

The sputtering process is a means of producing a clean cathode surface, by permitting the removal of contaminants and unwanted oxide layers.

If the cathode surface has been polished prior to the sputtering process, etch figures can be produced on it by the ion bombardment (McCutcheon, 1949; McCutcheon and Pahl, 1949).

Oxide layers may be deposited by performing the sputtering operation in an oxygen or an oxygen/argon atmosphere. This process has been called reactive sputtering (Veszi, 1953, Preston 1950). The investigations have generally been concerned with the type of deposit produced on the walls of the container rather than on any product that occurs at the cathode.

However, it is possible to produce well oriented oxide layers on the cathode by a mechanism similar to that used in reactive sputtering.

This technique has recently been developed (Hilbert (1962), Czarnecki and Hilbert (1962) (1), Czarnecki and Hilbert (1962) (2) for the production of coloured epitaxial oxide films on a variety of surfaces.

The process was reviewed and extended to additional materials in an article in Jena Review (Hilbert and Lorenz 1963).

The material was first cut to size and the surfaces to be examined were rendered smooth by mechanical and/or electropolishing. The surface finish was similar to that required for standard metallographic examination. The specimen was then placed in a container which could be evacuated, and to which suitable gases could be admitted. A positive electrode, a source of longitudinal magnetic field and a water cooled cathode were inside the container. The apparatus was similar in kind to that depicted in figure 4.5.

The container was evacuated to 10^{-4} Torr, then thoroughly flushed with argon gas. A discharge in the gas between the specimen and the anode at a pressure of 8×10^{-3} Torr with an anode supply of 5 kV and

current density of 0·2 to 0·5 mA cm^{-2} was maintained for a suitable period.

The magnetic field was used to confine the discharge to the region near the specimen. The water cooling at the cathode was aimed at keeping the specimen temperature as low as possible.

Depending upon the specimen, this argon ion bombardment-cleaning process was continued for periods of from 2 min (for uranium, U_3S_{12} and steel, 0·08%C) to 2 hr. 30 min.(for zirconium sheet). In this latter case the specimen was classed as being deeply etched.

At the termination of this sputter clean process, the argon was pumped out and replaced with air or oxygen at a pressure of 5×10^{-2} Torr. A 5 kV discharge in this atmosphere at a current density of 1 to 2 mA cm^{-2} was maintained for periods of from 1 to 10 min.

The surface of the cathode became covered in a layer of oxide, the thickness being dependent upon the time of discharge.

The only variation in the procedure from one material to another, was in the length of the etching and oxidising times. Some difficulties were encountered in the process. Metals such as nickel and aluminium which have a naturally occurring oxide layer on the surface needed to be deeply etched by the argon ion cleaning process before they would exhibit any oxidation. This indicated that the oxidation mechanism was appreciably different from the electrolytic case (where the aluminium is the anode, and the residual oxide layer does not restrict any additional oxidation.) That the aluminium needs to be etched for an appreciable time is in general agreement with the experience of others (Holland 1956 p. 439).

Surface preparation prior to etching was most important, and best results were obtained with electropolished specimens which had been electrolytically etched to remove the viscous polishing layer.

If the oxidation process were continued for some time, the layers produced became dark, probably due to the inclusion of some of the cracked products of the diffusion pump oil being incorporated in the film. No detailed analysis of the composition of these layers has been published.

The rate of growth of the oxide was dependent upon the crystal structure of the specimen. The oxide was stated to have grown epitaxially on the specimen, although no direct evidence of this was given. Assuming that this were the case, the refractive index of the oxide layer would also be dependent upon the crystal orientation. The colours exhibited by the films were interpreted in terms of the depth of the layer and the refractive index of the material. An important feature of the method was that thicknesses of a given material were readily reproducible.

No information has been published on the electrical properties of aluminium oxide layers formed in this manner and consequently it was considered that an investigation of these single crystals would supplement the work on anodised and evaporated films.

3.24 Other methods of producing oxides.

There are many other methods of producing aluminium oxide layers of known thickness. Two that would be of interest, but which have been excluded from the present investigation, but will be studied later, are (chemical) vapour plating, and plasma anodising.

Vapour Plating. This is the process whereby the required compound is produced by a suitable chemical reaction in the region where the compound is to be deposited. It has the advantage over many processes in that refractory materials (e.g. carbides, nitrides, oxides) can be produced at quite low temperatures. High purity materials have been produced by the process.

In one case (Powell, Campbell and Gonser 1955) reaction of a volatile metal halide (e.g. $AlCl_3$) with a hydrogen-carbon dioxide mixture at a heated surface results in a coating of the oxide on that surface. The reaction is of the form:

$$2AlCl_3 + 3H_2 + 3CO_2 \longrightarrow Al_2O_3 + 6HCl + 3CO$$

Typical conditions were:

Vapour temperature	130 to 160°C
Specimen temperature	800 to 1000°C
H_2 flow rate	300 $cm^3\ min^{-1}$
CO_2 flow rate	100 to 300 $cm^3\ min^{-1}$
Coating time	0·2 to 2 hrs.

Plasma anodising. In this process aluminium is anodised in a gaseous discharge instead of in the more conventional electrolyte. (Miles and Smith 1963, Tibol and Hull 1964, Tibol and Kaufman 1965).

A plasma of charged particles is formed as a result of a continuous electrical discharge in a bell jar at about 5×10^{-2} Torr. A d.c. potential applied between the aluminium anode and a cathode causes a current to flow and the aluminium becomes oxidised by oxygen ions. The oxide growth is a function of the anodising voltage; about 22 Å per volt, with a relative permittivity of 8·5. The time required is approximately 1 hr. for 15V with plasma current of 20 mA. The material produced is an excellent dielectric for condensers. The structure of the oxide has not been determined.

3.3 Electrical characteristics of Aluminium Oxide.

3.31 Single Crystal Data.

At low temperatures (i.e. 300°) purified crystalline aluminium oxide is an insulator. At elevated temperatures it behaves like an

electronic semiconductor. (Cohen 1959, Ryshkurich 1960). It has been shown recently that much of the bulk conductivity that exists at room temperature is probably due to iron impurity (Harrop and Creamer 1963). Ionic conduction, at least up to 1300°C is negligible. The addition of chromium has the effect of reducing the conductivity. Thermo-electric e.m.f.'s of about 1.4 mV $°C^{-1}$ were determined at high temperatures, the hot junction being negative indicating p type conduction.

The energy band gap is of the order of 10 eV.

The values of conductivity measured by Harrof and Creamer, when extrapolated to room temperature indicate that the conductivity of their single cyrstals was of the order of 10^{-60} mho cm^{-1}. The impurity content was less than 20 ppm.

Typical room temperature values quoted for alumina are 10^{-11} to 10^{-14} mho cm^{-1} (Gregg 1961), whilst alumina based ceramics have approximately the same range. The apparent discrepancy between these data is due to the different sources of charge carriers in the two cases. The impurity levels which are mainly responsible for the measured conductivity at room temperatures are all essentially ionised at higher temperatures. The temperature variation of conductivity will then depend upon the energy band gap, i.e. will be characteristic of the pure bulk material. The ℓn (carrier density) plotted against $1/T°K$ will be a straight line with slope of $-Eg/2k$.

At lower temperatures the slope is dependent upon $E/2k$, where E is the activation energy of the mechanism which gives rise to the conduction.

3.32 Anodic Oxide films.

In much of the work performed on oxide films, the resistance of specific devices is given, but without unambiguously stating the dimensions. A reliable determination of resistivity is not possible

in these cases. Frequently authors have been more concerned with variation in resistance or resistivity with illumination and temperature change rather than in absolute values.

The amorphous insulating films produced by anodising, in general exhibit a current flow which increases roughly exponentially with applied field over many decades. Hence to consider absolute resistance or absolute resistivity, without stating clearly under what conditions measurements were made is of little value.

Winkel and de Groot (1958) detailed the equivalent series capacity and resistance for aluminium oxide condensers of area 6 cm^2 for the range of anodising voltages 10 to 150V. Taking values at frequency 100 Hz and a condenser formed at 60V, with oxide layers produced at 13 Å V^{-1} as being representative, the parameters are:

area (A) = 6 cm^2; thickness of dielectric (d) 800 Å series capacity 0.8 uF; series resistance, 22 Ohm; equivalent parallel resistance (R_p), 2 x 10^5; resistivity 1.5 x 10" Ohm cm.

The material of the dielectric had a low frequency conductivity near that of the higher conductivity aluminas. As would be expected the value was many orders of magnitude less than that of the pure single crystal material.

From a curve due to Masing and Young (Young 1961, p. 144), the resistance of a Ta/Ta_2O_5/metal, cell of area 2 cm^2 and oxide thickness 3000 Å was of the order of 10^9 Ohm with 10V applied to the cell. This corresponds to an oxide conductivity of about 10^{-14} mho cm^{-1}.

It is generally agreed that, at low temperatures, and low (i.e. less than formation potential) voltages the conduction through these anodised films is essentially electronic. Various mechanisms have been proposed to account for the observed currents. Charlesby (1953) assumed that the flow of electrons was inhibited by a potential barrier of height U, and half width 'a'. The barrier was considered

to occur at or near the metal-oxide surface. He proceeded to develop the relationship:

$$i = A \sinh {}^{V}/_{V_1}$$

where i was called the "flow of electrons".

$$A = 2Ne\sqrt{}\exp(-U/kT)$$

$$V_1 = (dkT/ae)$$

where N electrons were available to carry the current.

$\sqrt{}$ = the probability (per second) of a transition in the absence of a barrier,

e = electron charge,

d = film thickness,

k = Boltzmann constant,

T = temperature, °K,

V = applied potential.

Values of U and 'a' were obtained from measurements of i and V, and the variation of i with temperature. For aluminium oxide layers formed at 50V at 20°C values of a $\approx$ 1.4 Å (and for data given by Guntherschulze and Betz, a, lies between 1.2 Å and 2 Å.) and U $\approx$ 0.5 to 0.6eV.

The origin of the electron current from the electrolyte surface was considered to be one of, quantum tunnelling, strong field emission, or thermionic emission. The temperature dependence of the current was considered to favour the last hypothesis. The electrons were presumed to arise from the presence of impurities, "since there is evidence that these determine the magnitude of the electron current. With very pure specimens the electron flow, at a given field intensity, is much lower than for less pure specimens.

Intrinsic conduction by the film cannot account for the observed electron currents. For such conduction the conductivity σ is of the form;

$$\sigma = \sigma_o \exp(-U/kT)$$

with $\sigma = 100$ mho cm^{-1}. In our case $\sigma_o = 10^{-4}$ mho cm^{-1}".

This mechanism was criticised by Vermilyea (1954) on the grounds that barriers of the magnitude proposed by Charlesby would be penetrated by wave mechanical tunnelling. (Tunnelling probabilities would be of the order of 10^{-1}, while thermal jumping rates would be 4×10^{-4}).

Vermilyea proposed a trapping mechanisn, whereby a trap was represented by a positive charge such that the potential energy near the trap was

$$V = \frac{-e^2}{4\pi\epsilon r}$$

where e = electron charge,
r = radial distance.

With an applied field E,

$$V = \frac{-e^2}{4\pi\epsilon r} - eEr$$

The maximum is at $X_o = \left(\frac{e}{4\pi\epsilon E}\right)^{\frac{1}{2}} \approx 4$ Å

The activation energy to leave the trap was calculated from V(r)., from which the conductivity σ was obtained.

$$\sigma = A \exp(W/2kT)$$

where $A = 3 \times 10^{10} \mu N^{\frac{1}{2}}$

where μ = mobility,

N = concentration of traps.

The resutling expression was:

$$\log i \propto V^{\frac{1}{2}}$$

This was considered a better fit to Charlesby's data than the sinh law. The ordinary formula for high field emission when applied to the solution/oxide interface gives an expression of similar form.

Vermilyea (1956) obtained evidence that weak spots were responsible for much of the cathode current. Young (1959) proposed that fissures in the film were the sources of these weak spots. Young made use of this weak spot theory to explain the rectification properties of metal/oxide/electrolyte systems. The work of Winkel and Verkerk (1958) does not completely support the idea of rectification at weak spots, although they concede that "spots will contribute to secondary effects, especially to the leakage current."

The rectification properties of these systems (which would need to be accounted for in a complete theory of electron transport through thin films) was not part of the present investigation and consequently will not be discussed, except in so far as it throws any light on the conduction mechanism. In attempting to explain rectification effects observed, van Geel (1951, 1955) proposed that a p-n junction within the oxide was responsible. This theory has been independently proposed by Taylor and Haring (1956). However according to Young (1961 p. 142) it has not been shown in detail how a p-n junction could account for the observed behaviour.

Smith (1957) reported $^{i}/V$ plots for aluminium oxide and gave reasons for rejection of the p-n junction and space charge theories to explain rectification. The models would give too much current for the present thin films. He considered the oxide must be regarded as an insulator with the entry of carriers (i.e. electrode processes) controlling the current. In a later paper (Smith 1959) he concludes that defects in the film are responsible for the currents observed.

Young (1961 p. 147) considers that with flawless films the current flow will be governed by similar conditions to that applying to electrodes attached to semi-conductors. The thinness of the oxide is an important point of departure however.

Tantalum can be anodised similarly to aluminium, and such oxides have been well investigated. The system $Ta/Ta_2O_5/Au$ has been considered in some detail (Mead 1962). For this system (and the cases where the gold electrode was replaced in turn with platinum and aluminium), the mechanisms considered were:

(i) ionic flow
(ii) space charge limited flow with distributed traps
(iii) Schottky effect
(iv) tunnelling.

(A detailed analysis of this work will be treated in Section 5.23)

Tunnelling and ionic currents were eliminated as the means of charge transport by the lack of agreement between the measured and predicted temperature dependence in the first case, and the complete lack of ion transfer in the second.

Schottky emission predictions also fail to satisfy the observed temperature dependence. The variation of potential across a cell to keep a constant current of 1 mA through the cell as the thickness of the insulating layer is varied, leads to a result incompatible with the idea of space charge limited currents with distributed traps.

The mechanisms proposed by Mead as the rate-limiting step in the current flow through tantalum oxide and similar films are:

(i) At low applied voltages and high temperatures current is carried by thermally excited electrons hopping from one isolated state to the next. This yields an Ohmic characteristic, exponentially dependent upon temperature.

(ii) At high fields and low temperatures, the rate limiting step is field ionisation of trapped electrons into the conduction band.

(iii) At high fields and high temperatures the rate limiting step in the current flow is field-enhanced thermal excitation of trapped electrons into the conduction band.

3.33 Photoconductivity.

Anodically formed oxide layers of aluminium and tantalum have been observed to show variations in conductivity when suitably illuminated. Photovoltaic and electroluminescent effects have also been investigated. Most of this work has been concerned with the system, metal/oxide/electrolyte (Young, 1961, Chap. 10), although the investigation of van Geel et al (Van Geel, Pistorius and Winkel, 1958) included the cases of thin transparent metal (cu) and transparent semi-conducting (Cu I) electrodes as well as the electrolyte.

The wavelength cut-off for aluminium oxide was determined as 2600 $\pm$ 100 Å, although most of the measured effects were produced by the 2527 Å line from a mercury lamp.

The mechanism assumed in the explanation of the effects involves modified band theory (Frohlich, 1947) and lends support to the use of this theory in considering amorphous structures.

No measurements have been made on the detection of individual photons by this effect.

3.4 Irradiation experiments.

No published information was sighted on the use of aluminium oxide films or single crystals as alpha particle or proton detectors.

Some investigations have been performed on the determination of the range of particles in the oxide (Young 1961).

As well a significant amount of work has been done on the irradiation of single crystals of α-aluminium oxide by ultra-violet, gamma-ray, neutron and high energy electron radiation, to produce ionised lattice defects.

The modified properties of the irradiated crystals have been studied by measurement of optical absorption spectra (Hunt and Schuler 1953, Levy and Dienes 1955, Levy 1961, Mitchell, Rigden and Townson 1960), long wavelength neutron scattering cross-sections (Antal and Goland 1958) thermal conductivity (Berman, Foster, Schneidmesser, Tirmizi 1960) lattice expansion (Martin 1955) and thermoluminescence. (Gabrysh, Eyring, Le Febre and Evans 1962). Some electron spin resonance studies have been made to determine the nature of the centres produced by the radiation damage (Gamble, Bartram, Young, Gilliam and Levy, 1964).

The alpha particle flux used in the present investigation was insufficient to produce any significant change in the properties of the oxide layers used.

3.5 Electron tunnelling.

If it is assumed that a rectangular potential barrier of height 0.85 eV and width, the width of the oxide layer exists for a system $Al/Al_2O_3/Al$, then quantum mechanical tunnelling through the barrier can occur for films of 35 Å or less. (Hartman and Chivian, 1964). For films thicker than this, the probability of tunnelling is so small, that any observed currents are due to thermionic or Schottky emission.

The barrier height has been observed to be as high as 1.8 eV (Collins and Davies 1964), reducing still further the effective tunnelling length.

If the barrier is shaped other than rectangular, the tunnelling thickness may be increased, but not sufficiently to have any influence on the films considered in this investigation.

CHAPTER 4

EXPERIMENTAL APPARATUS AND METHODS

4.1 Aluminium specimens.

4.11 Types of aluminium

The aluminium used in the experiments was from two different sources.

Rods, with dimensions, length 15 cm and diameter 6.35 cm supplied by Johnson, Matthey & Co. Ltd., were used for some of the experiments for the production of the oxide films, and for all the evaporated aluminium electrodes. The impurities in these rods, as determined by spectroscopic analysis were:

Impurity	p.p.m.
magnesium	20
zinc	8
iron	3
cadmium	2
silicon	2
copper	1
silver	1

The rods were polycrystalline in structure, although a selected number of them contained some crystals of about 3 m m in length.

Single crystals of zone refined aluminium, 2.5 ± 0.1 cm diameter and spark planed flat (< 200 μm pits) to a thickness corresponding to 20 S.W.G. were supplied by Metals Research Ltd. The amount and type of impurity was not quoted, although total impurities were of the order of less than several parts per million.

The crystals were orientated with their (100) planes parallel to the spark planed surfaces.

4.12 Methods of preparation

It was reported by Barrett and Winterbottom (Barrett and Winterbottom 1961) that more uniform anodised films were produced if the aluminium were "homogenised" at 500°C for 24 hours prior to anodising. Consequently all specimens produced from the rods were annealed under these conditions either before or after being cut to length. This annealing in some cases produced a marked increase in crystal size. In one instance (specimen No. 32) the etch pattern produced when the naturally occurring oxide was removed indicated that the same crystal covered the whole of one flat face. This was not the case before annealing. Whether this growth was influenced by the spark machining process or not has not been determined.

An advantage of the annealing process after cutting the rods to length is that some of the structural damage associated with the parting off process would be reduced.

4.121 Spark machining.

To ensure that the annealed rods were as free from strain as possible, it was necessary to cut them into the wanted lengths by a method which subjected them to a minimum stress. A spark machining device based upon that due to Cole et al (Cole, Bucklow and Gregson 1961) was designed and constructed. The essentials of the machine are illustrated in Figures 4.1 and 4.2.

The published information on spark machining contains relatively little information on the construction and operating conditions of the machines. Consequently, a significant amount of development effort was required to produce a useful, reliable machine.

Because the rate of cut consistent with small pit size is slow, it was essential that the cutter should run virtually unattended. In the commercial version of the Cole machine (Metals Research Ltd. "Servomet")

FIGURE 4.1

Spark Cutter

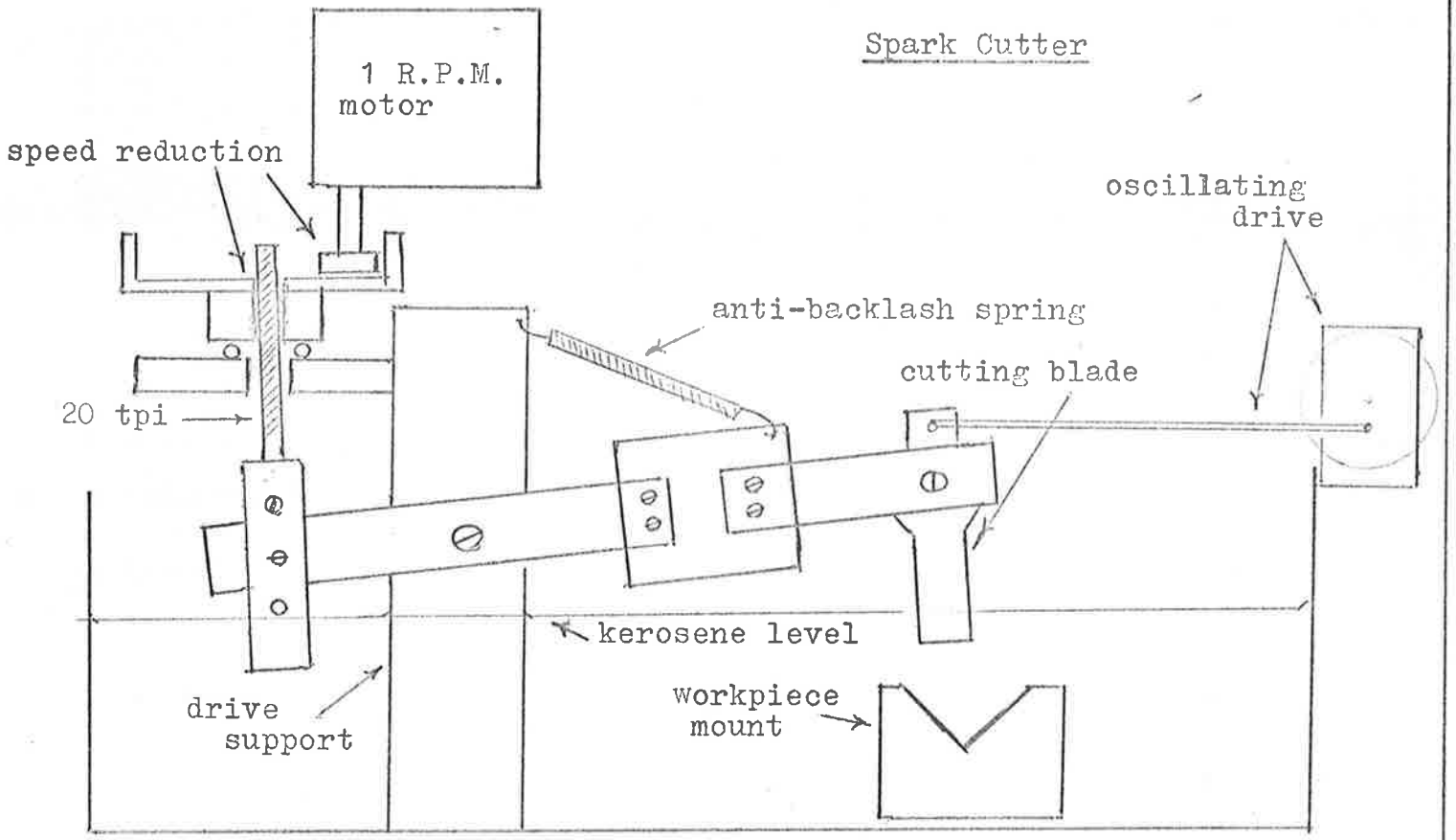

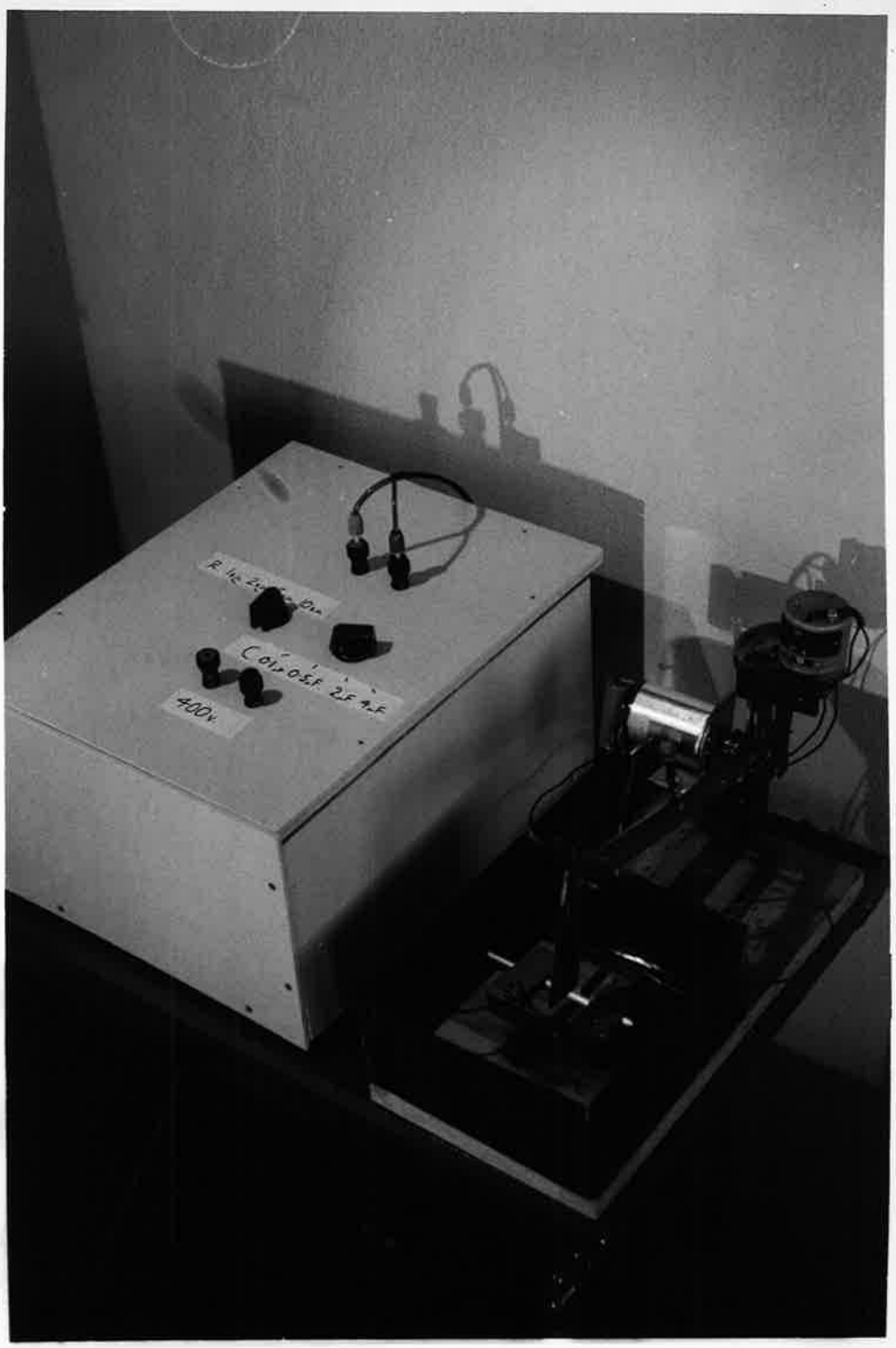

FIGURE 4.2

a servo-control varies the rate of travel of the cutter so that the cutting rate is maintained and yet at no time does the cutter physically contact, and probably weld to, the specimen.

Detailed experiments showed that by being prepared to accept a slow rate of cut, and restricting the machine to a particular size of specimen, a servo-control was not necessary. However, when the cutter was used for larger diameter specimens ($\frac{1}{2}$ and 1 inch) some control of the drive speed was essential. A simple control which disconnected the mains supply from the motor whenever the sparking rate became too great was designed. The circuit is included in the appendix.

A significant problem (mentioned by Cole et al) was the effective removal of the eroded metal and the carbon particles that resulted from the spark discharge in the insulating liquid, in this instance kerosene. The presence of these metallic and carbon particles between the cutter and the work piece seemed to result in a substantial number of welds occurring between these parts; almost independent of the rate of advance of the cutter. That the particles should remain in this region is surprising, in view of the considerable agitation produced in the liquid by the sparking.

This problem was solved most effectively by causing the cutter blade to oscillate in its own plane, i.e., along the direction of the cut at about 4Hz with an amplitude of approximately $\frac{1}{2}$ inch.

A variety of cutting tool materials was tried to determine the one best suited to parting off the aluminium rods. A stainless steel (302) cutter was eroded at about three times the rate of the aluminium rod being cut. Aluminium cutters were eroded at approximately the same rate as the specimen, as were the copper tools, although with the latter material, microscopic examination revealed a noticeable number of flecks of copper metal transferred to the cut edges of the specimen.

Brass proved the most useful of the materials tried. The erosion rate was less than one-quarter that of the aluminium cutters, and no detectable metal transfer occurred. The cutter loss was independent of the thickness for the range from 16 gauge to 26 gauge. There appeared to be some tendency for an increased carbon deposit on the cut surfaces when using brass.

The rate of advance of the cutter was set at one-quarter inch per forty minutes - this being a good compromise between cutting time and insurance that no welding should take place. Under these conditions pit diameters of 70 to 180 μm, (measured with a Cooke image shearing eyepiece), with an estimated depth of 20 μm were produced, when the supply potential was 400V, charging resistor 5000 Ohm, and capacitor 4 μF. Pit diameters increased to between 200 and 400 μm when the capacity was increased to 8 μF.

The width of the cut was 1·1 mm when a brass blade of thickness 1 mm was used.

To produce plane faces the high voltage was connected to both sides of the specimen. Figures 4.3 (a) and (b) are photographs of a severed rod,

(a) immediately after the cut was completed,
(b) after the aluminium was etched in chromic acid.

The carbon particles present in (a) were removed by the etching process.

There is some evidence (Wilms and Wade 1956) that spark cutting is not strain free when the cutter is permitted to contact the work-piece. A more detailed investigation (D.S.L. Annual Report 1961-62) of the non-contacting cutter process indicates that for low energy sparks (that is small spark pits) and for ductile materials like aluminium, the amount of strain should be small. In the present investigation a significant thickness of material was removed by electropolishing after the spark machining and that this would result in at least the melted and recrystallised material being removed.

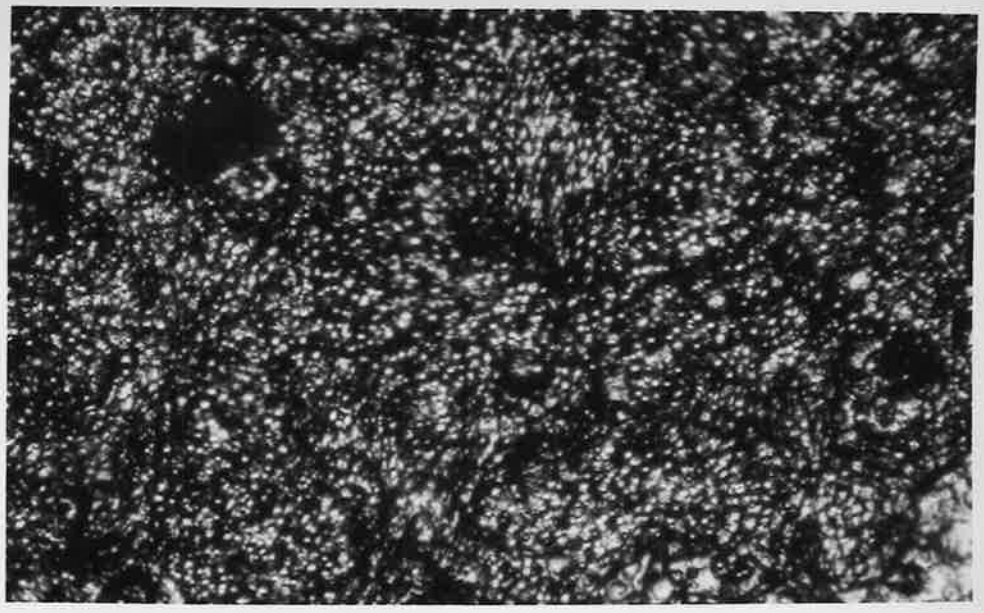

FIGURE 4.3 (a)

FIGURE 4.3 (b)

4.122 Electropolishing

Electropolishing permits the production of smooth surfaces, without the attendant difficulties of mechanical polishing. The problems of plastic flow and imbedding of impurities makes mechanical polishing unsatisfactory as a preparation method for aluminium for an investigation of this type which relies especially upon structure of the outer layers of material.

The spark machined rods were etched for 90 seconds in a solution of H_2SO_4, 500 ml; H_2O, 500 ml; $K_2Cr_2O_7$, 5 gm. kept at 90°C, to remove the products of the machining process, and to reduce the size of the pits. In most cases the metal was then further annealed at 500°C for an additional 24 hours, after which the etch process was repeated to remove the naturally occurring surface oxide layer, and to generally clean the specimen.

A variety of electropolishing solutions were tried, based upon:

(i) aluminium and zinc chlorides in ethyl alcohol (Evans 1960 p. 225),

(ii) phosphoric and sulphuric acids (Evans p. 257),

(iii) the original Jacquet solution of perchloric acid and acetic anhydride (Evans p. 258),

(iv) a solution similar to (iii), modified by the addition of aluminium powder to the solution immediately prior to polishing (Tegart 1956),

(v) a solution of methanol and methyl glycol (Jena Review 1960, 1963).

Best results, that is, the least amount of free material produced in the vicinity of the rod, most uniform removal of metal and the minimum polishing times, were obtained with method (iv) and (v). The latter method had the further advantages of little risk of an explosion and that the viscous layer, required for the polishing process, could

be moved from the rod by reducing the polishing potential for a short time. The other recommended method of removing the polishing layer (Tegart 1956) by washing with a strong jet of cold water, was not always effective.

For all processes it was found essential to keep the temperature of the solution at or near room temperature. For the larger (one inch diameter) specimens this necessitated the electrolyte being cooled.

Whilst it was not difficult to polish the surface of the aluminium, it was not easy to keep the surface flat. This problem has been considered before. Barrett and Winterbottom (Barrett and Winterbottom 1961) were able to get "generally acceptable surfaces . . . (by) . . . smoothing the rectified output of the polishing current supply unit." Tegart suggested a potentiometric supply should be used; that agitation of the solution only, produced grooving of the anode, and that it was necessary to rotate the anode at about 100 revolutions per minute.

The best method was found, independently, to be similar to that of Snouse (Snouse 1961). In this case the specimen and the disc cathode were both rotated in the solution.

The processes involved in electropolishing are not well understood, and more detailed investigation of the polishing mechanism would be worth while.

The apparatus used for most of the specimens is illustrated in Figure 4.4

The polishing procedures adopted as the most consistent were:

(i) Electropolishing solution

Methanol (methyl alcohol)	175 ml
methyl glycol (ethylene gycol monomethyl ether)	100 ml
Glycerine	25 ml
Perchloric acid (S.G. 1·6)	8 ml

FIGURE 4.4

Polishing machine

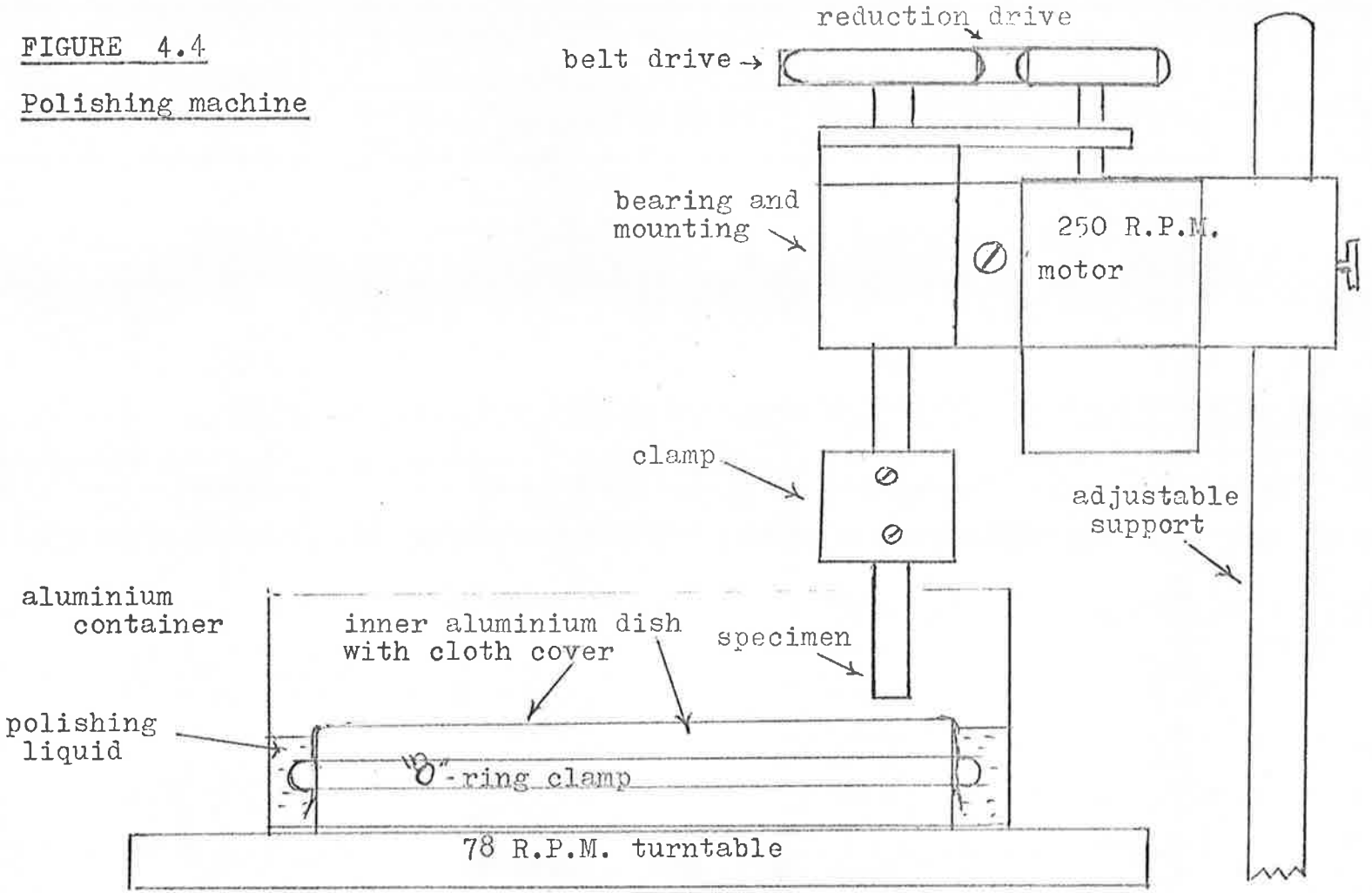

(ii) The specimen was made the anode of the polishing cell, and both the specimen and the cathode rotated in the same direction at approximately 150 and 78 revolutions per minute respectively.

(iii) The polishing potential across the cell was maintained at 40V, and the current density kept at 80 to 100 Ma cm^{-2} by manually adjusting the separation between the two electrodes.

(iv) Polishing was continued until the surface appeared flat when viewed under a low powered (x 25) microscope. Investigation showed that these surfaces were also substantially flat when viewed at 1500 x.

(v) The polishing potential was reduced to 18V for 3 to 10 seconds to remove the viscous polishing layer.

4.123 Vacuum Evaporation

To eliminate the use of mechanical and chemical means to produce good aluminium surfaces on which to deposit the evaporated layers of aluminium oxide, some thick (2,000 to 3,000 Å) layers of aluminium were evaporated on to glass substrates. Aluminium wire (99.99) was evaporated in a commercial vacuum evaporator, Hitachi, HUS-3, which was not equipped with a liquid nitrogen cold trap. The residual gas pressure was in the vicinity of 10^{-6} Torr.

Optical microscopy 3" x 1" glass slides were used as substrates. They were cleaned in a sulphuric acid - potassium bichromate solution maintained at 90°C for 3 min, placed in a Dawe "Soniclean" ultrasonic cleaner for 5 min with cold distilled water and 2% surface active agent RBS25, rinsed in distilled water, agitated in distilled water in the ultrasonic cleaner for a further 5 min, blown dry, dried with filtered warm air, washed in clean alcohol, shaken, and placed directly into the evaporator.

The aluminium was deposited normally on the glass surface from a spiral tungsten basket mounted 10 cm below the substrate.

This procedure resulted in aluminium layers which adhered well to the glass substrate, and which were in the main, free of pin holes and similar blemishes.

4.2 Oxide films

4.21 Introduction.

Aluminium oxide films were produced by three different processes:

(i) anodic oxidation in an electrolytic cell,
(ii) oxidation by an electrical discharge in an oxygen atmosphere,
(iii) the vacuum evaporation of aluminium oxide.

The purpose in using these three distinct methods was to have available a range of reproducible oxide materials, which probably differed greatly in structure. The D.C. leakage and alpha particle induced currents could then be compared to determine the variations inherently produced by the different oxide types. Very little intercomparison work of this kind has been performed.

Further a piece of high purity (99.999%) aluminium oxide single crystal was purchased from Semi-Elements Inc., Saxonburg, U.S.A. The pulse characteristics of this material was compared with that of the three other structures.

4.22 Surface film produced by electropolishing

In order to get satisfactory smoothing of the aluminium by electropolishing, it is necessary, at least in certain types of electrolytes to produce a partially insulating viscous layer around the region being polished. Although some investigations of the composition and action of this layer have been made, the situation is still far from clear (Tegart 1956).

It was found essential to remove these films from the polished aluminium, to ensure that the resultant surface would behave in a predictable manner. Incomplete removal resulted in excessive bubble formation during anodising, and very patchy, non-adherent oxide films.

The procedure outlined in Jena Review No. 1., 1963 in which the polishing potential was reduced at the completion of the polishing process was found to be successful on most specimens. Some specimens, cut from the same bar as others did not seem to respond to this treatment. In these cases it was found necessary to agitate the polished specimens in the ultrasonic cleaner, using the process previously described (section 4.123) for the cleaning of glass slides.

In every case a light etch in hot sulphuric acid - potassium bichromate solution proved an effective way of removing the layer.

4.23 Anodising procedure.

Two types of anodising electrolyte were used. These were the boric acid-borate solution of van Geel and Schelen which is detailed in section 3.21, and later the method due to Hass (Hass 1949) in which 3% ammonium tartrate solution was produced from 3% tartaric acid, adjusted to pH 5.5 with ammonium hydroxide.

In every case the anodisation was performed at room temperature. The temperature of the solutions was never permitted to rise above 25°C, and in most cases would have been in the range of 20° to 22°C.

Oxide layers were produced at potentials ranging from 50 volt to 800 volt. Most of the measurements were performed using layers produced at 100 and 500 volt. In every case the current density was kept below 10^{-3} A. cm^{-2} at the anode. For some of the higher formation potentials, it was necessary to begin the process at a lower potential, ans as the thickness of the oxide increased, to raise the potential. It proved difficult to get consistent oxide formation above 500 volt. This is in agreement with the work of Charlesby (Charlesby 1953).

The cathode of the electrolytic cell was a loop of gold wire.

Slight agitation or rotation of the anode made no significant difference to the current through the electrolyte. This was probably because the bubble formation at the anode was very slight.

Some specimens did not oxidise uniformly; irregular bubble patterns developed, some dendritic crystals were produced, and the current did not decrease as the layer thickness built up. This behavious was attributed to the partial removal of the electropolishing products. In several specimens it proved impossible to perform the oxidation satisfactorily. These specimens have been preserved with the intention of studying their surface structure in more detail at a later date.

The materials for the electrolytes were analytical grade reagents in every case. The impurity level in these was seldom less than 20 p.p.m. Some improvement in the reproducibility of results would doubtless follow from the use of extremely pure materials.

4.24 Epitaxial films by cathodic oxidation.

4.241 Introduction.

The method used was based upon the work performed by Hilbert and Lorenz (Hilbert and Lorenz 1963), although in their case aluminium proved very difficult to oxidise. This method has been outlined in section 3.23.

The polycrystalline aluminium rods and the single crystal discs were spark machined, and electropolished as described in section 4.122. The electropolishing layer was removed by electrolytic etching and ultrasonic cleaning. This procedure did not leave the surface in a satisfactory state to be oxidised by this method.

Consequently it was necessary (as reported by Hilbert and Lorenz) to subject the aluminium to a prolonged etch by argon ion bombardment. Initially a relatively high pressure (10^{-1} Torr) discharge was used with an effective potential difference of 2·5kV across the chamber. Inspection of the surface of the specimen, even after a discharge lasting 10 hours showed no evidence of etching in the metallographic sense.

The pressure was reduced to 10^{-2} Torr, and to get a satisfactory electrical discharge it was necessary to introduce a longitudinal magnetic field. The surface was suitably etched by a discharge of 3 mA cm^{-2} for a period of 60 min.

It was considered that the surface was clean enough to permit reproducible oxide films without the surface having undergone any major structural changes.

All specimens prepared by this cathodic oxidation were treated in this manner.

The oxidation process was performed under similar conditions, i.e. with a longitudinal magnetic field and oxygen pressures of the same order.

4.232 Apparatus.

The bell jar and vacuum assembly used is illustrated in Figures 4.5 and 4.6.

Gases used were commercial grade welding argon and oxygen. Liquid nitrogen traps were interposed between the cylinders and the chamber to remove any residual hydrocarbon, water vapour and carbon dioxide from the gases. The chamber itself was separated from the air cooled oil diffusion pump by a liquid nitrogen trap. Care was taken to reduce the number of sources of contamination. The bell jar, with the high purity aluminium anode attached, was baked initially for 48 hours at 300°C before the unit was assembled. Prior to the baking it was cleaned in distilled water containing a commercial surface active agent (Decon

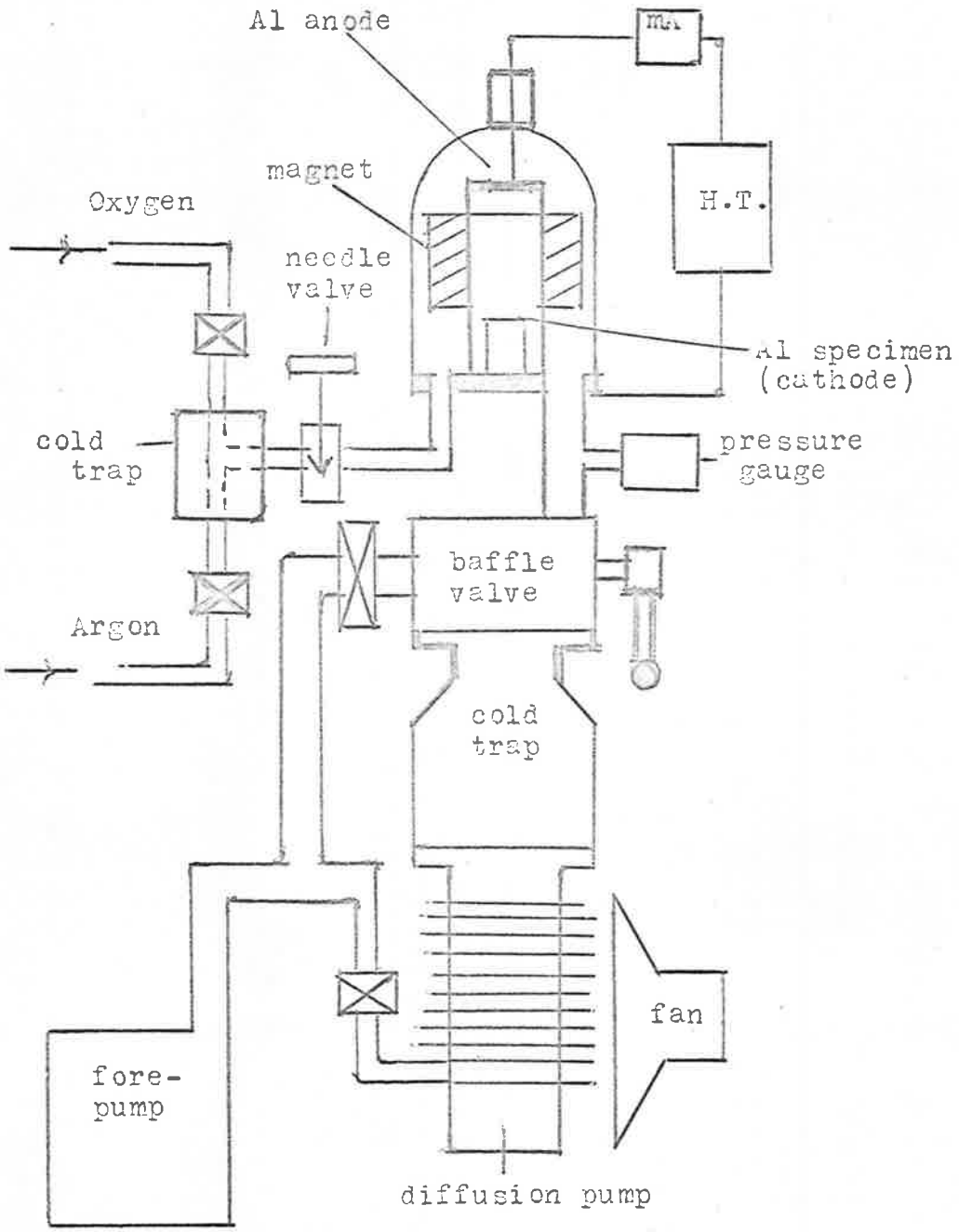

FIGURE 4.5 Cathodic Oxidation Apparatus

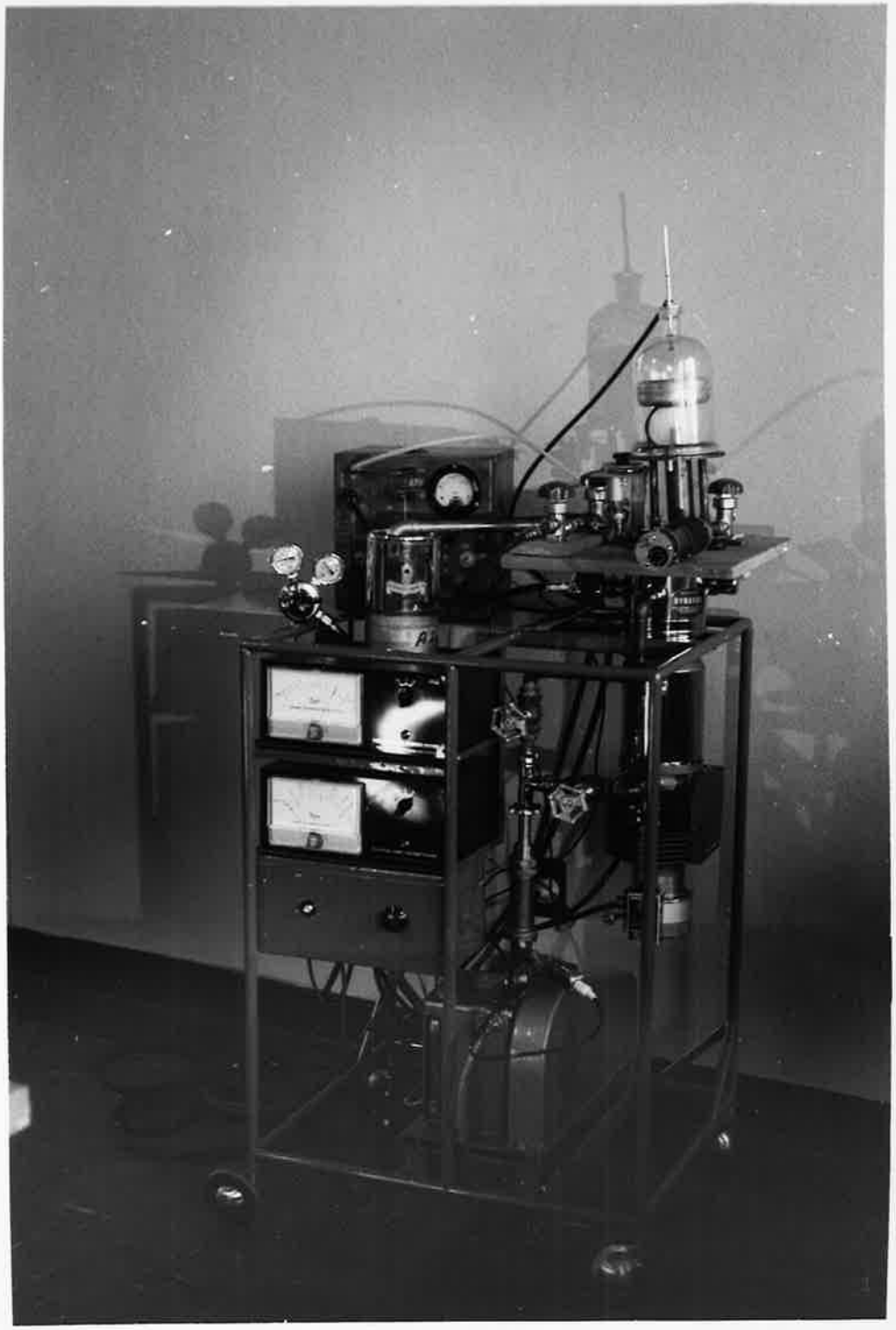

FIGURE 4.6

75) rinsed thoroughly in distilled water, and finally washed in ethyl alcohol.

Trays of artificial zeolite pellets (Linde 5A) which had also been extensively baked were included in the chamber.

The magnet assembly consisted of a coil of fine copper wire enclosed in a soft iron sheath which had a $\frac{3}{8}$" gap in the inner section. This section was sealed by an aluminium tube, held in place by an epoxy glue. The whole unit was mechanically and chemically cleaned, and finally given a substantial coating of evaporated high purity aluminium. The evaporation was performed after the coil assembly had been kept at a pressure of less than 10^{-6} Torr for 48 hours.

At all times the pieces of apparatus for use within the chamber were stored in air tight containers with dessicating material.

The major sources of any hydrocarbon contamination in the system would probably be the single neoprene "O" ring of the main seal, and the bombardment induced material from the epoxy glue and potting compound.

4.243 Procedure.

Electropolished and cleaned aluminium rods and discs were argon ion etched under the following conditions:

gas pressure	10^{-2} Torr
current density	3mA cm^{-2}
electric potential difference across chamber	2·5 to 3·5kV
time	up to 60 min.

The chamber was pumped out until the residual gas pressure was less than 10^{-6} Torr for one hour. Argon gas at atmospheric pressure was admitted, and the chamber pumped again to 10^{-6} Torr. This procedure of flushing and pumping was repeated 3 times for each sample to be cleaned.

The pressure was finally maintained at 10^{-2} Torr by allowing the diffusion pump to continue operating and bleeding a small flow of argon through the inlet needle valve. This continuous gas flow was aimed at pumping out any contaminants as they were produced.

After etching the specimens were oxidised using the following steps:

(i) the system was flushed with fresh argon,

(ii) this argon was pumped out till the pressure was less than 10^{-6} Torr,

(iii) this argon flushing was repeated twice,

(iv) oxygen was admitted at atmospheric pressure and pumped out to pressure less than 10^{-6} Torr,

(v) this oxygen flushing was repeated twice,

(vi) finally the oxygen pressure was kept at 5×10^{-2} Torr during the oxidation process, which was performed when a discharge of current density 2mA cm^{-2} was maintained across the cell by a potential of 2·5 to 4 kV. The oxidation proceeded until the desired oxide thickness was obtained.

The measurement of the thickness of these oxide films is treated in section 4.27.

4.25 Evaporated oxide films.

4.251 Apparatus.

A commercial vacuum evaporator, Hitachi HUS-3 was used for the manufacture of these films. The evaporator was capable of a minimum pressure of 10^{-6} Torr. It was not equipped with a cold trap. Considerable difficulties were experienced in the production of films with reproducible characteristics. If the evaporation procedure extended over an appreciable period of time (say 15 min.) the layers produced were invariably darkened. This indicated a source of contamination; most probably the diffusion pump oil. A non-refrigerated isolation trap after Biondi (Biondi 1959) was inserted in the system for the

later experiments. This improved the colour of the deposits, although the electrical properties were still variable.

4.252 Powder characteristics.

Two sources of aluminium oxide were used, both being in the powdered form. High purity chromatographic grade, produced by May and Baker Ltd., England, and aluminium oxide of analytical reagent grade produced by British Drug Houses Pty. Ltd. were selected as representative of the materials readily available. The latter material was stated to contain less than 0·005% chloride, 0·01% sulphate, 0·01% Fe, with a loss on ignition of less than 1%.

The mean size of the powder particles was measured using an optical microscope and a Cooke A.E.I.image splitting eyepiece, which combination was calibrated against an optical diffraction grating. The particles were remarkably uniform in size.

4.253 Substrate

A glass microscope slide 3" x 1" was used as the supporting member for these films. The slide was cleaned and dried and a relatively thick layer (> 2,000 Å) of high purity aluminium vacuum evaporated on to it. Rapid evaporation of the aluminium resulted in few optically detectable flaws in the film. This layer of aluminium was then masked to leave several exposed areas approximately $\frac{1}{4}$ inch square, and on to these exposed regions the oxide was deposited.

4.254 Procedure.

A variety of ways were tried to produce layers of oxide with reproducible characteristics. Several alumina crucibles supported on multistrand conical tungsten baskets (After Olsen, Smith and Crittenden, 1945) were used; in some cases they resulted in rather large clumps of oxide particles being deposited on the substrate.

The most readily reproducible layers were deposited from a depression in a strip of tungsten foil. (Holland, p. 119, type (b). A small quantity of oxide powder was placed in the depression, and the temperature of the tungsten raised to approximately 1300°C to permit any volatiles present to be ejected. The substrate was covered during this process.

The vapour pressure of Al_2O_3 is 10 millitorr at 1780°C. Consequently, maintaining the source in the vicinity of 1900 to 2000°C ensured steady evaporation of the oxide. The heating current required to produce this temperature was determined for a test strip of tungsten using a Pyrolux optical pyrometer. The size of the strip (length 10 cm, width 1 cm, thickness 0·1 mm), magnitude of indentation (2 mm), the amount of oxide and the heating current were kept constant for all films. The only parameter varied was the deposition time.

All powdered material used, whether previously suspended in water, baked at 800°C in air for some hours or used straight from the bottle, showed a marked tendency to eject lumps of material. It proved somewhat difficult to get deposits which were free of these lumps. A subsidiary tungsten strip, heated to about 2500°C mounted above the vapour source and angled towards the substrate which was shielded from direct deposition by an aluminium plate served to re-direct some of the vapour, but not the lumps. Films prepared by this process were essentially lump free. However, the deposition time was substantially prolonged.

4.26 Single crystal of aluminium oxide

A single crystal of approximately 1 cm^3 of high purity (< 10 p.p.m. impurity) aluminium oxide was purchased from Semi-Elements, U.S.A.

This material was supplied sawn to size, and was polished mechanically, using diamond paste and aluminium oxide powder. The surface was finally etched and polished using hot orthophosphoric acid.

4.27 Determination of film thickness

The work of van Geel and Schelen (van Geel and Schelen 1957) on the structure of anodised aluminium oxide films in a borax-boric acid electrolyte was checked for one thickness of oxide (formed at 500V) using an optical interference method.

A piece of aluminium was partially masked and the unmasked section anodised at 500V. Portion of the anodised section was then additionally masked and the unprotected oxide region etched away in hot sulphuric acid and potassium bichromate solution. After removal of the masking material a uniform layer of aluminium was vacuum evaporated over the three sections of the specimen.

The difference in height between the three layers was measured using an optical microscope and a Watson interference objective.

The agreement with the values given by van Geel and Young (Young 1961) was sufficiently close to accept their more detailed work as being applicable to the films being studied, viz. 12·8 Å per volt across the anodising cell.

The advantage of the evaporated upper layer of aluminium was that the refractive index of the oxide was not simultaneously being measured. The reflected beam from all three regions was also of the same intensity.

A similar procedure was used to measure the thickness of the evaporated and cathodic oxidised layers.

An accurate thickness value was required for some of the thin evaporated and cathodic oxidised films. In these instances many measurements were made visually, and as well photographs were taken for three different values of fringe separation. The positions of

the maxima were located by a photometer using an enlarged transparency. It is considered that the estimate of error at ± 200 Å for a 2000 Å film is reasonable. Once the thickness of a particular layer had been determined accurately, the depth of similar ones was gauged by ascertaining the thickness of the measured oxide which exhibited the same interference colours.

The presence of the gold front electrode enhanced the colours and made the comparison easier.

Films prepared by evaporation and cathodic oxidation exhibited appreciable variations in thickness, even when utmost care was taken during their preparation.

In particular, for the evaporated films, the film colour was variable. This coupled with the marked variation in electrical conductivity reported in section 6.13, suggests that the oxide only was not being deposited. Some suboxides have been reported (Holland, p. 449, 1956), but this does not appear to be sufficiently great to account for the scatter of the readings.

A possible conclusion is that the absence of satisfactory trapping in the vacuum system permitted a significant amount of oil vapour and its products to be incorporated in the films.

It is proposed to repeat the experiments with evaporated films, using a clean vacuum system which will incorporate a refrigerated zeolite roughing pump and a titanium sputter ion pump. The system will be all glass, capable of being baked and containing no rubber demountable seals.

A multiple interference optical system will be used to measure more precisely the variation in film thickness.

4.3 Mechanical structure of cells.

4.31 Introduction.

The oxide films were sandwiched between two conducting electrodes. In the cases of those specimens formed by oxidation of aluminium the material itself was made sufficiently robust to permit easy mounting and to form one of the electrodes.

4.32 Electrodes.

For all specimens measured, one electrode (referred elsewhere as the back electrode) consisted of aluminium, either part of the region which was not oxidised, or in the case of evaporated layers, as a previously evaporated back electrode.

The other, a front electrode, was evaporated gold.

Preliminary measurements were made to ensure that readily reproducible electrodes could be manufactured. Typical values used were gold ≈ 100 Å and aluminium ≈ 200 Å. These electrodes were deposited from a tungsten basket containing 1·0 cm of 20 S.W.G. gold wire or 1·0 cm of 18 S.W.G. aluminium wire, spaced normally 15 cm from the substrate, and the tungsten heater operated at 15 amp for 5 seconds.

Thickness was estimated by performing the evaporation (using a different tungsten basket each time) and advancing a 3" x 1" glass slide past a mask, 1/10" at a time. In this way a series of steps consisting of from one up to twenty layers was produced on the slide. The last step was arranged to be between the first and the twentieth layer - this giving directly the total depth of the layers. This last distance could be measured with some accuracy using the interference objective. Inspection using the optical microscope showed a fairly uniform trend in thickness with each layer.

Examination of the electrode structure under the electron microscope indicated a generally continuous cover of the surface, with a minimum of globules being formed.

Electrical connections were made to these front electrodes by a very fine copper wire attached by a droplet of dag suspension of silver in M.I.B.K., produced by Acheson Colloids Ltd.

4.33 Cell dimensions.

The cell produced from the oxidised aluminium rod for both the guarded and unguarded versions were defined mainly by the size of the front electrode. This was kept a disc of diameter 2 mm (or a No. 30 drill size). This allowed a guard ring separated from the front electrode by 1 mm. to be deposited, and the two types compared directly.

Two cells were produced using the one inch diameter aluminium discs, anodised at 100V, with front electrodes 1·5 cm diameter, and one of these was guarded.

Two further discs were anodised at 100V and 500V respectively and the front electrodes deposited through a mesh of 2 mm apertures, separated by 1 mm strips, thus producing more than 30 usable cells on each disc.

Similarly, four discs were oxidised by gaseous bombardment to produce films as near in thickness to the anodically produced ones, and guarded, single front electrodes were deposited on two of them and multiple electrodes on the other two.

4.34 Heat Treatment

No heat treatment was carried out on any of the cells. Although marked changes in oxide structure occur at 650°C (Hass 1949), the use of aluminium back electrodes precluded the possibility of investigations at near this temperature.

Because the structural changes produced by this type of treatment would have a marked effect on the electrical properties, it is proposed to investigate this in more detail. Some anodised films will be formed from aluminium which has been vacuum deposited on to a previously vacuum deposited platinum film on a mica substrate; the aluminium thickness being chosen so that at the anodising potential, all the aluminium will be converted into oxide.

A front electrode of platinum will permit the variation of leakage current with temperature cycle to be measured.

4.4 Measuring equipment and methods.

4.41 Introduction.

Two main types of experiments were performed, viz. the static current-voltage relationship for the cells, and the measurement of the height and shape of the electric current pulses produced when the cells were irradiated with alpha particles.

4.42 Evacuated measuring chamber.

The experiments in which alpha particles were incident upon the cell were all conducted in an evacuated chamber. The pressure was always less than 10^{-6} Torr. The physical configuration of the chamber, with the position of the measuring leads is shown in figure 4.7.

It will be observed that the source was able to be rotated through 180°, effectively eliminating any alpha particles falling on the cells. Further, suitable shields were inserted between the source and the cells, to ensure that no other region in the vicinity of the cells was subjected to bombardment. This was aimed at reducing to a minimum any spurious alpha induced current in parts of the system which were not under test.

FIGURE 4.7.

Evacuated Measuring Chamber

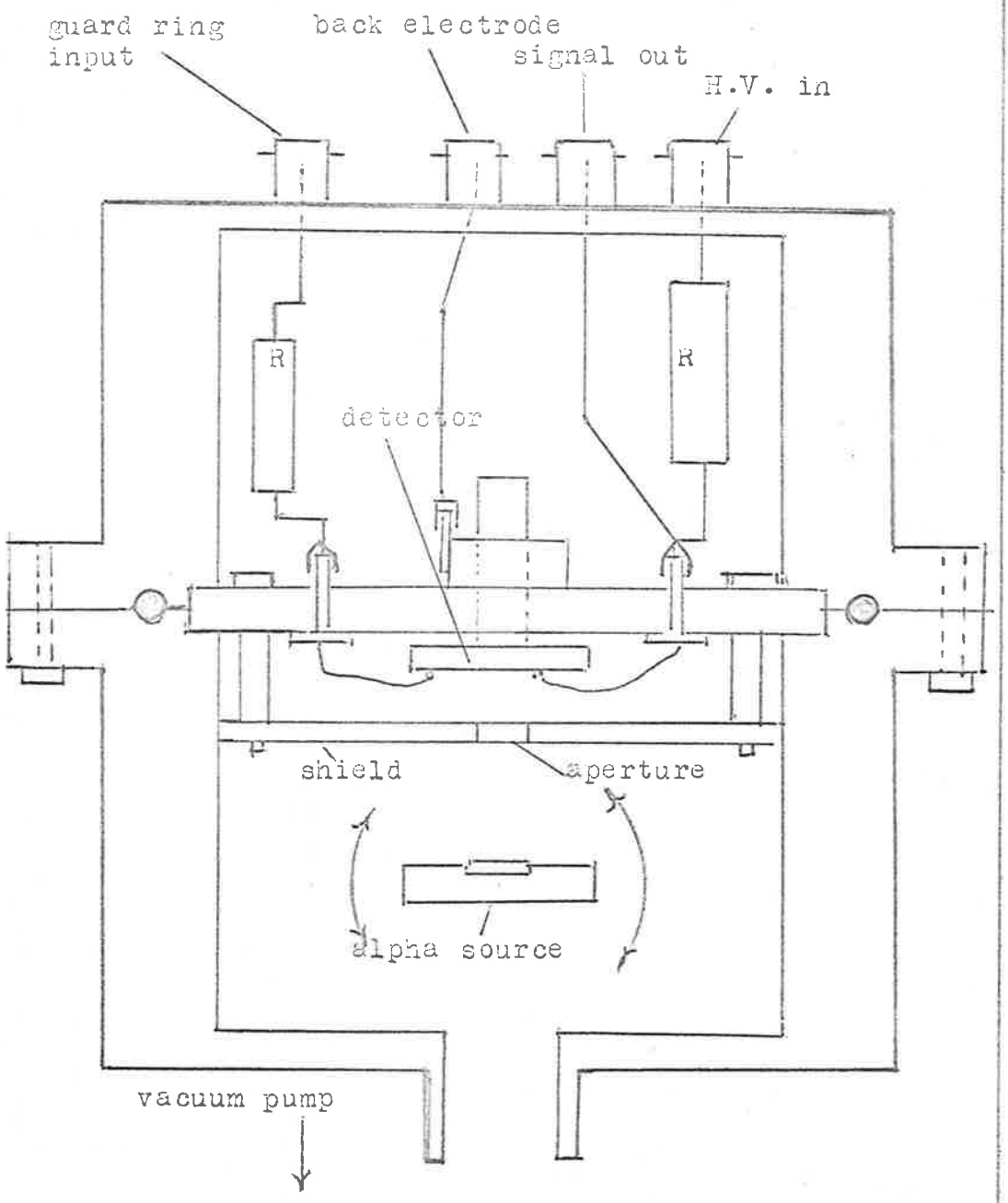

The alpha particle source was a calibrated plutonium-239 reference source supplied by the United Kingdom Atomic Energy Authority, under the identification: RCC PU-239 R636 Code No. PIRC.3, with a certified total radioactive content of $2.29 \times 10^5 \pm 3\%$ disintegrations per minute. The alpha emission from the front face was one half this disintegration rate. Up to 2% Americium-241 could have been present. The average alpha particle energy was 5·14 MeV. The angle subtended by the 8·6 mm^2 cells (that is with front electrode of No. 30 drill size) at the source was approximately 10^{-2} ster-radians, resulting in a particle flux of 3 per second.

Alternatively the source could be mounted between the shield and the detector. The 8·6 mm^2 detector then intercepted 100 particles per second.

Current leakage tests on the chamber, with and without the alpha source present, and with the active side of the source remote from the measuring cables were performed.

4.43 Static measurements equipment.

For the first set of measurements a variable, low noise well filtered D.C. power supply adjustable from 0 to 1,450 volts was used as a source of potential. The current flowing through the cell was measured using a Keithly 610A electrometer.

A typical circuit is shown in figure 4.8. For the unguarded cells the guard lead was not connected.

With this configuration any leakage to ground from the specimen, was not registered by the electrometer. The applied potential 'V' was measured with a Beckmann digital multimeter model 4014VH.

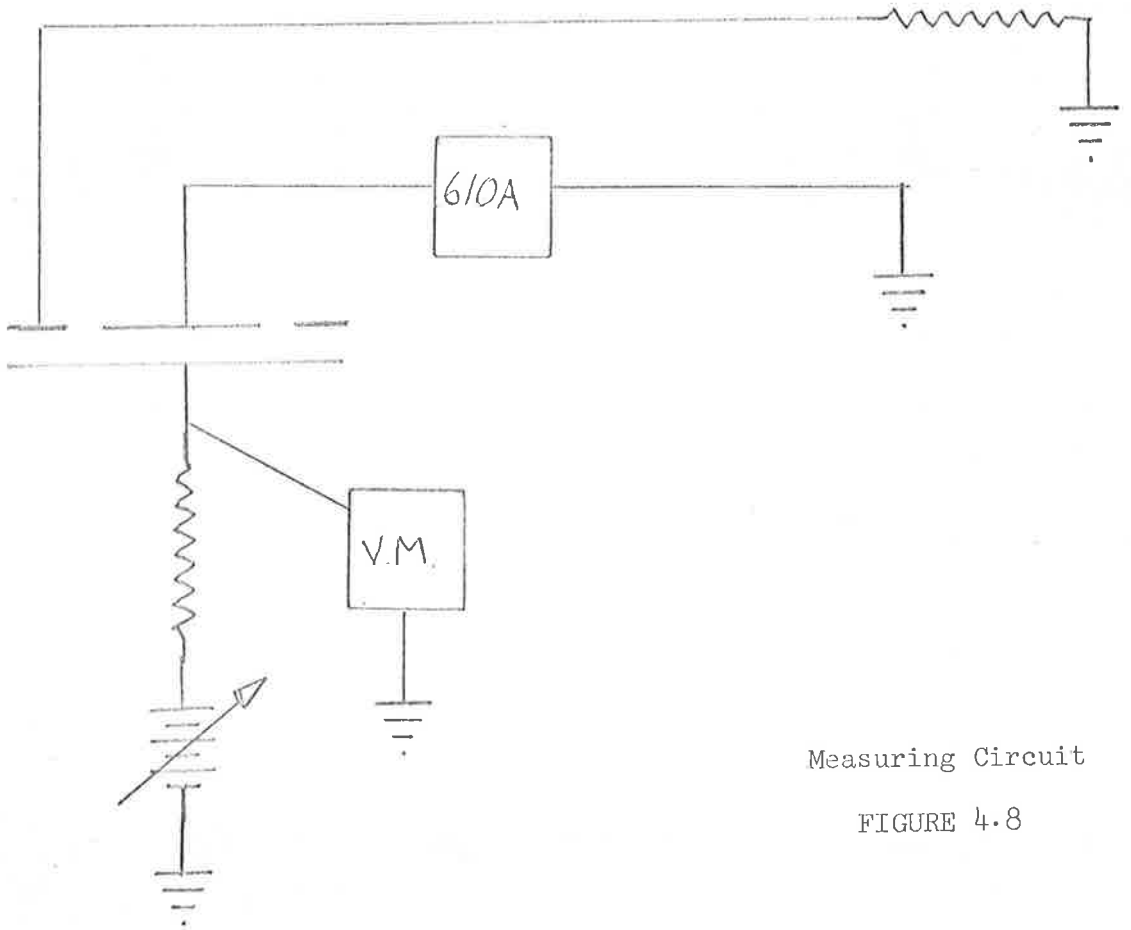

Measuring Circuit

FIGURE 4.8

4.44 Pulse measuring equipment.

4.441 General

Three types of measurements on the cells as a result of alpha particle irradiation were required. Firstly, it was necessary to determine if the arrival of particles could be detected at all, either as individual current pulses through the cell, or as a change in the D.C. leakage current. Secondly, for the individual alpha particles that could be detected, the rise and decay times of the ensuing current pulse was needed to permit some determination of carrier mobility, carrier life time, the density and possibly the distribution of trapping and recombination centres. Thirdly, the total charge separation produced by the interactions was needed to measure the energy loss of the alpha particles to the aluminium oxide.

The change in leakage current due to the alpha flux was measured somewhat similarly to the D.C. leakage current, as described in section 4.43. In this case however, the electrometer was used as an amplifier, and its output was rectified by a low leakage silicon diode, and this value integrated by means of a capacitor, and the result recorded by a potentiometric chart recorder. The record on the trace with alpha source was compared to the case without alpha source.

4.442 Charge sensitive pre-amplifier

To measure the total energy loss to the specimen by the alpha particles, it was necessary to integrate the total charge produced. For the case where trapping and recombination effects were negligible, this could be performed by using the charge-sensitive amplifier technique of Cottini et al (Cottini, E, E. Gatti, G. Giannelli and F. Rossi, 1956).

Two such amplifiers were constructed. The circuit of ORNL Q-2069B-3 preamplifier was copied with minor modifications. In an attempt to reduce even further the equivalent noise input of the preamplifier, a design centred around the high gain, low noise pentode E810F was devised. Further improvements were made by using type EL80F for successive stages in lieu of the original 6DJ8 triodes. The complete circuit, together with that of the post amplifier is included in the appendix.

4.443 Wide-band amplifier.

A tektronix 585 oscilloscope, with dual trace type 82 amplifier, with a maximum sensitivity of 10 mv cm^{-1} of trace, and a rise time of < 3n sec, together with a high speed (F = 1·5, 1 : 1 Tektronix C19) Polaroid back camera was available for the pulse rise and decay time measurement.

To increase the sensitivity a wide band (> 150 mHz) low noise amplifier was developed. Use was made of the then newly introduced E810F pentode, which had an equivalent noise inputof 100 ohm, a gain bandwidth product of 250 mHz and a mutual conductance of 50 millimhos. The circuit is included in the appendix.

The amplifier, together with the separate closely regulated power supplies was constructed in three units, two of voltage gain 25, and one of gain 5, and capable of being connected in cascade. Whilst this resulted in a physically large unit, the ability to get a change in gain by patching out one or more sections rendered the device highly useful.

4.444 Scaling

A Hewlett Packard model 521C scaler was used for pulse counting, whilst a Philips type PW4082 single channel discriminator, together

with a PW4072/01 linear amplifier were available for pulse height measurement and counting.

4.5 Equipment evaluation.

4.51 Test procedures.

The electrometer was checked periodically by the standard methods of:

(a) for voltage ranges, against a standard cell;

(b) for the magnitude of the resistors, by the time of discharge of a low leakage condenser.

The charge sensitive preamplifiers were calibrated and the noise measured by the method due to Fairstein (Fairstein 1961). The full width half maximum equivalent noise input for the ORNL preamplifier corresponded to 10keV for 100 pF input capacity. This was about 20% worse than the value quoted by the designers.

The E810F preamplifiers on the other hand had a measured noise at the input of 2·5 keV. Such a value could be expected for this valve in this type of circuit.

The wide-band amplifier was tested for gain frequency response, noise, and pulse response, including the recovery from overload characteristics.

4.52 Commercial detector.

A commercial silicon detector, a Solid State Radiations Inc., NPS series, type NPS 10 x 10 - 5000 - 25, was used as an alpha particle detector as a comparison device. Once the apparatus had been calibrated, and the response of this particular detector to alpha radiation determined, any other experimental arrangement could be easily checked by inserting this detector. This proved to be an extremely simple means of verifying that the equipment was operating satisfactorily.

CHAPTER 5

THEORY

5.1 Introduction.

Aluminium oxide is a good insulator with essentially ionic bonding of its constituents. However, under the usual conditions of preparation both of single crystals and amorphous films, a measurable conductivity is observed at room temperature, at electric field strengths well below that of dielectric breakdown.

Further, charge carriers released by the interaction of ionising radiation with the oxide, can give rise to electrical conduction.

Both of these sources of electric current are relevant in that they determine the noise characteristics and the suitability of the material as a detecting medium.

5.2 Electric currents in ionic solids.

In pure single crystals of ionic solids at 0°K, the valence energy band is filled and the conduction band is empty. This type of solid is characterised by a relatively large energy gap between these bands.

Consequently at room temperature the electronic conductivity of these materials is low because so few charge carriers are excited into the conduction band.

In real materials there are isolated energy levels between the bands, due to impurity atoms, vacancies and intersticials, which can give rise to electronic conductivity. In addition, electron-hole traps will be associated with these defects, and the density of these traps will depend upon the density of the deformations of the lattice field.

Ionic conductivity, due to the migration of positive and negative ions, is facilitated by certain types of lattice defects and the presence of suitable impurity atoms.

At low temperatures the conductivity of these real materials is still small; the electronic contribution is small because of the small number of charge carriers, and the ionic contribution is small due to the low mobility of the ions.

At low field strengths the ionic conductivity for most ionic materials is usually greater than the electronic conductivity. This predominance of ionic conductivity occurs at all temperatures. The ionic conductivity is almost independent of the electric field, whilst the electronic conductivity is frequently very strongly field dependent.

At low temperatures the ionic conductivity is so low that the material can support larger electric fields, and hence under these conditions electronic conductivity can predominate.

For single crystal materials, in the region where carrier mobility is field independent, the electronic conductivity can be expressed:

$\sigma_e = (n_n e \mu_n + n_p e \mu_p)$, where n_n and n_p are the electron and hole charge carrier concentrations respectively, e is the electronic charge, and μ_n and μ_p the electron and hole mobilities.

For a forbidden energy gap E_g, the number of electrons n_n (or holes n_p) in the conduction (or valence) band, due to thermal excitation, is,

$$n_n = n_p = 2(2\pi kT/h^2)^{\frac{3}{2}} (m_n^* m_p^*)^{\frac{3}{4}} \exp(- E_g/2kT)$$

where m_n^* and m_p^* are the effective electron and hole masses respectively, the remaining symbols having their usual significance. If $m_n^* \approx m_p^* \approx m_o$, then at room temperature,

$$n_n = n_p \approx 10^{19} \exp(- E_g/2kT).$$

A typical value for E_g for an ionic solid (KCl) is 9.44 eV and the measured electron mobility is 300 $cm^2\ V^{-1}\ sec^{-1}$, and hence at room temperature:

$$n_n \approx 10^{-59}\ cm^{-3}, \text{ and } \sigma_e = 5 \times 10^{-76}\ mho\ cm^{-1}.$$

The ionic conductivity is determined by the diffusion coefficient of the ions and the type and number of defects. For alkali halides, where Schottky defects predominate, and one kind of ion is much more mobile than the others,

$$\sigma_i = (e^2\ a^2\ \nu_o\ n_o/kT)\ (n\ -/n_o)\ \exp(-\ E\ _-/kT)$$

in the intrinsic region.

Where, ν_o is the jump frequency, a is the lattice constant, $n\ -/n_o$ is the concentration of intersticials, and E - is the activation energy.

For KCl at room temperature, $\sigma_i \approx 10^{-10}$ mho cm^{-1}. This ionic conductivity is further increased by the presence of impurity atoms.

The electronic contribution to the measured conductivity of an assumed pure, perfect crystal at room temperature is thus negligible.

The situation is not quite so straight forward for amorphous (or polycrystalline) materials. The basic band theory model arises from the assumed periodicity of the structure of the material. This structural regularity is to a large extent absent from amorphous materials, with the result that conventional band theory does not apply.

However, because many amorphous materials are aggregates of crystallites, some of the properties of bulk crystals can be incorporated in a suitable model. In particular, effects such as photoconductivity and electroluminescence imply some kind of energy level structure.

A convenient model (Frohlich, 1947) is based on the assumption that the energy band structure of the single crystal applies with additional energy levels appearing in the forbidden region. For simplicity these levels are considered to be of two types: shallow traps which extend over a small range of energy below the conduction band; and deep traps which lie appreciably below the conduction band.

This model has been partially successful in accounting for photoconductivity and dielectric breakdown.

The increased number of trapping centres present in amorphous materials compared to single crystal materials results in significant changes in electrical characteristics. The conduction mechanism assumed is that the charge carriers spend a significant time in these traps; that they are thermally excited from one trap into another.

This hopping process results in very low effective mobilities; ($< 10^{-3}$ cm^2 V^{-1} sec^{-1}) values which are frequently not simply related to the single crystal value. The hopping conduction is essentially Ohmic and exponentially dependent upon temperature (Mott and Twose p. 107, 1961).

It is now doubted that mobilities measured in amorphous materials are at all indicative of the mobilities to be expected for single crystals of the same materials (Bosman, 1966).

The most direct way of differentiating between band and hopping conduction is to measure the temperature dependence of the mobility. In the latter case the mobility increases exponentially with temperature while in the former, for pure materials it exhibits a power law decrease.

It was pointed out in section 4.34 that temperature dependencies were not measured in the present investigation. It is intended to measure the charge carrier mobilities of the various aluminium oxide types by some of the recently proposed methods (Davies, 1966, Gibbons 1966).

5.21 Electronic conduction in aluminium oxide.

Measurements of diffusion coefficients for single crystal aluminium oxide, (Paladino and Kingery 1962, Cable 1958) suggest that cation diffusion predominates and causes a conductivity of 10^{-9} mho cm^{-1} at 1500°C. When extrapolated to room temperature, the ionic contribution to the measured conductivity is negligible.

The number of charge carriers in the conduction band for pure aluminium oxide at room temperature would be about the same as that of KCl. The energy band gap of aluminium oxide at room temperature has been reported as being 8·56eV, (Chubb and Friedman 1955), although it could well be as high as 10eV.

The expected electronic conductivity of intrinsic aluminium oxide at room temperature would therefore be quite small. The extrapolated conductivity curve of Harrop and Creamer (1963) suggests a value of 10^{-60} mho cm^{-1}. Obviously the measured values of 10^{-14} mho cm^{-1} are defect and/or impurity produced.

Consequently it is not possible to get a reliable value of charge carrier mobility from conductivity measurements.

Further, values of the electron and hole mobilities for aluminium oxide have not been measured.

In view of the considerable importance of the charge carrier mobility to the investigation, attempts were made to calculate the electron mobility for the oxide.

Two models were considered. The relationship of Frohlick and Mott as modified by Bardeen (Yamakawa 1951) for the mobility of electrons in the conduction band of an ionic solid can be expressed:

$$\mu_e = 2\,(3/\pi m^* k\theta)^{\frac{1}{2}}\, e\, r_o\, [\exp(\theta/T) - 1]\,(\epsilon_r\, \epsilon_{ro}/\epsilon_r - \epsilon_{ro})$$

where $\theta = (hc/k\lambda)\,(\epsilon_r/\epsilon_{ro})^{\frac{1}{2}}$ and

where λ = reststrahlen wavelength (≈ 20 μm for Al_2O_3),

r_o = first Bohr radius,

m^* = effective electron mass,

ϵ_r = relative permittivity at optical frequencies and is $(1{\cdot}78)^2$

ϵ_{ro} = relative permittivity at low frequencies and ≈ 10 for thin pore-free oxide films.

The other symbols have their usual significance.

If the electrons excited into the conduction band are considered to have an effective mass approximately equal to the rest mass, then substituting we get:

$$\mu_e = 9{\cdot}05 \text{ cm}^2 \text{ sec}^{-1} \text{ V}^{-1} .$$

This is about an order of magnitude less than the measured values of the ionic materials which have been used for detecting particles. For example, silver bromide at 77°K has a measured mobility of 200 $cm^2\ sec^{-1}\ V^{-1}$, and the corresponding calculated value of 308 $cm^2\ sec^{-1}\ V^{-1}$. (For the same temperature (77°K) the calculated value for aluminium oxide would be 60 $cm^2\ sec^{-1}\ V^{-1}$). This mobility is not as low as has been expected from photoconductivity measurements on amorphous oxide films.

Another method of calculating the electron mobility is based upon the crystallochemical model of Suchet (Suchet 1965). This model is concerned mainly with semiconductors, although a satisfactory agreement is reached between the calculated and measured values of ZnO which has a relatively wide energy band gap of 3·2eV.

The approach is semi-empirical, and some of the constants developed may not be rigorously applicable to aluminium oxide. The expression can be written:

$$\mu = 3 \times 10^6 \exp - 9(\lambda_o + q/n)$$

where $^{q}/_{n}$ is the ratio of the effective charge carried by the atoms of the compound to the maximum number that would be carried if the bonding were completely ionic. This ratio can be calculated from a knowledge of the ionic radii, the total electronic charge carried by the ions, and an empirical constant.

$$^{q}/_{n} = [1 - 0{\cdot}01185\ (Z/r' + Z'/r)]$$

where Z, Z' are the number of electron charges carried by the cation and anion respectively and r and r' are the ionic radii, in Angstrom units of the ions.

For aluminium oxide, $Z = Z' = 10$, $1/r' = 0{\cdot}715$, $1/r = 2$.

λ_o is the atomic ionicity, and is determined by the position of the elements in the periodic table and the bond type.

$\lambda_o = (1 - {}^{n}/_{c})$, where the 'c' shared bonding pairs formed by an atom with its near neighbours make up the 2c valence electrons (basic coordination concentration).

$\lambda_o = 0{\cdot}25$ for Group III, Group VI, compounds.

The calculated electron mobility for aluminium oxide using this approach is:

$\mu_e = 800\ cm^2\ sec^{-1}\ V^{-1}$.

This is significantly higher than the value determined from the Frohlich-Mott model.

As a check on the adaptability of this approach to a strongly ionic crystal, the value of electron mobility for silver bromide was calculated, and found to be 150 $cm^2\ sec^{-1}\ V^{-1}$. This is in acceptable agreement, both with the measured value and the value predicted by Frohlich and Mott.

It has been suggested (Zhuze 1955) that, for semiconducting elements and compounds a relationship exists between the heat of formation (Q) and the electron mobility.

$\log \mu = - C \log Q$, where C is a constant, dependent to some extent upon the crystal structure. A plot was made of the logarithm of the heat of formation against the logarithm of the measured mobility for a number of materials. Whilst it was not possible to find a rigorous relationship between Q and μ, a definite trend was observed.

Extrapolating this to include aluminium oxide, indicated an electron mobility for this material of the order 10 $cm^2\ V^{-1}\ sec^{-1}$. This could be in error by an order of magnitude.

Consequently, while no real agreement existed between the values of mobility calculated by the several methods, the values were sufficiently high as to justify attempting to use the alpha particle induced charge separation as a means of measuring the mobility. The material in single crystal form could also have sufficiently high mobility to be satisfactory as a solid ion chamber.

In all probability the effective mobility of the amorphous and polycrystalline forms would be appreciably less than the single crystal values. The probability of these being successful as particle detectors is much lower.

A survey of the attempts to account for the experimental conduction properties of amorphous aluminium oxide has been included in section 3.3. The most successful work for materials of this kind was that of Mead (Mead 1962) where a detailed systematic study of anodised tantalum oxide was reported. The current-voltage relationships for a range of oxide thickness over a wide temperature range were measured.

The conclusions can be summarised:

(a) The poor structure of the films resulted in a large density of isolated states distributed throughout the forbidden energy band.

(b) The characteristics were those of the material of the oxide and not electrode effects.

(c) The influence of the difference in work function between the tantalum and the second electrode was principally on the effective electric field across the oxide, and as such was noticeable at low fields.

(d) Three different regimes could be identified, and are considered as (i), (ii), and (iii) below.

(i) Low applied fields and high temperatures. The conduction mechanism here is by thermally excited electrons hopping from one isolated state to the next. This yields an Ohmic characteristic, exponentially dependent on temperature.

(ii) High fields and low temperatures. This system is characterised by field ionisation of trapped electrons into the conduction band. The current-voltage characteristic is independent of temperature and has the form (Chynoweth p. 95, 1960):

$$J = J_o(\underset{\sim}{E}/\underset{\sim}{E}_o)\ \exp(-\underset{\sim}{E}_o/\underset{\sim}{E}),$$

where $E_o = [4(2m^*)/3\ \hbar.e]^{\frac{1}{2}}\ W^{3}/2$

J is current density, $\underset{\sim}{E}$ is the electric field, and W is the depth of the trap potential well.

[Alternatively (Piper and Williams 1955),

$E_o = 10^7\ E_g^{\frac{1}{2}}\ W^{3}/2$ where the field is in volt cm^{-1}, and the energy gap E_g as well as W are in electron volts.]

(iii) High fields and high temperatures. The rate limiting step in the current flow in this case is field-enhanced thermal excitation of trapped electrons into the conduction band (Frenkel, 1938).

$J = J_{o\sim}E \exp(\beta V^{\frac{1}{2}} - W)/kT$

where V is the applied voltage, and

$\beta = (e^3/\pi\epsilon d)^{\frac{1}{2}}$, with d, the thickness of the dielectric of permittivity ϵ.

Because anodised aluminium oxide so closely resembles tantalum oxide, the room temperature current voltage relationship would be expected to be of a similar form to (iii), above, for high fields, and like (i) for lower fields. The influence of the work functions of the electrodes would also be noticeable.

Vacuum evaporated oxide layers have a similar disordered structure, and similar relationships would be expected.

The single crystal films, whilst not free of defects would have appreciably less than the amorphous and polycrystalline material. Measurements of the current-voltage characteristics for these structures would permit the conduction process to be compared with that of the amorphous films.

5.3 Alpha particle induced charge separation

5.31 Introduction.

The mean energy (ϵ) per hole-electron pair production when radiation interacts with a solid can be expressed as:

$\epsilon = 2{\cdot}2E_g + rE_r$, $r = L_i/L_r$ where these terms are all defined in section 2.221.

If the phonon mean free path L_r is assumed to be defined by, $L_r = 3K/vC_v$ where v is the phonon velocity (taken here to be the velocity of sound), C_v the specific heat per unit volume and K the thermal conductivity, then for aluminium oxide, $L_r \approx 5 \times 10^{-7}$ cm.

If a 5·1 MeV alpha particle loses 130 keV in the first micron of aluminium oxide, and if ϵ were tentatively assumed to be 30 eV, $L_i \approx 2{\cdot}5 \times 10^{-8}$ cm.

This results in an overestimate of L_i, and hence of r. Thus, $r \approx 1/20$, and hence $\epsilon \approx 2{\cdot}2\ E_g \approx 22$ eV.

Consequently in the first micron of its passage through aluminium oxide the alpha particle will produce,

$N_g \approx$ 6000 charge carrier pairs.

5.32 Charge Collection

The effect of trapping and recombination on the collection of the charge generated has not been rigorously solved. The most complete treatments due to Northrop and Simpson (Northrop and Simpson 1962) and Gibson and Miller (Gibson and Miller BNL 5391). Northrop and Simpson consider four situations.

(a) Complete collection: all charge carriers of one sign completely and promptly collected without trapping or recombination.

(b) Short term trapping: some carriers spend some time in traps, but are eventually collected in less than the dielectric relaxation time.

(c) Partial recombination: some pairs of carriers combine without being collected.

(d) Long term trapping: the time spent in traps by some carriers exceeds the dielectric relaxation time.

Representative detector current rise and fall curves for detectors exhibiting these properties form figures 3.6 to 3.7 of Dearnaley and Northrop's book, (Dearnaley and Northrop 1964).

When the crystal dimensions are large compared to the particle penetration depth, and when the particle enters at one electrode (resulting in one type of charge carrier being collected rapidly) a simple analysis is possible.

In the case of a single crystal 1.0 cm thick, the whole of the alpha particle energy will be deposited in the vicinity of one electrode; and carriers of one sign will have to drift, under the influence of the applied electric field, to the other side of the crystal.

If n_g free electrons are produced by one alpha particle penetrating the negative electrode, then when one of these moves distance x across crystal, a charge q, $q = ex/d$, is induced on the electrodes, with $x = \mu \tilde{E} t$. If the mean trapping time for electrons is T, the number drifting towards anode at time t is $n = n_g \exp(- t/T)$. Hence the total charge appearing on the capacitance is:

$$q = (n_g e/d\ \mu\ \tilde{E} t) \int_0^d x \exp(- x/\mu \tilde{E} t)\ dx + n_g e \exp(- d/\mu \tilde{E} T).$$

The pulse height will be

$$q = (n_g e\ \mu \tilde{E} T/c)\ [1 - \exp(- d/\mu \tilde{E} T)]$$

If the range is taken as $I = \mu \tilde{E} T.$, the charge dq induced in time dt, is $dq = (n_g e\ \mu \tilde{E}/d) \exp(- t/T)\ dt.$, so that total charge after time t is $q(t) = (n_g I/d)\ [1 - \exp(- t/T)]$ if electrons have not reached anode. Whence a measurement of pulse rise time gives a value of the trapping time T, and a measurement of pulse height gives the range, I, and hence the mobility.

The maximum pluse height produced in a 1 cm^3 crystal (capacity $\approx$ 1 pF) would be approximately 40 mV, if there were no recombination. The corresponding lifetime for an assumed mobility of 10 $cm^2\ V^{-1}\ sec^{-1}$ and a collecting potential of 1000V, would need to be 100 microseconds. If, on the other hand, a mobility of $10^3\ cm^2\ V^{-1}\ sec^{-1}$ were realised, then with 5 kV applied to the crystal, a carrier lifetime of $\approx 10^{-7}$ seconds only is required.

The case of a thin detector poses a different set of problems. Carrier lifetime ceases to be a limitation because charge collection times across a 1μm detector with 100 volt applied potential are of the order of 10^{-12} seconds.

However, with only 6000 charge carrier pairs generated, and with the increased capacity of the detector, caused by the reduced thickness, the maximum signal voltage becomes of the order of microvolts. Consequently, the ability to detect signals will largely depend upon the preamplifier.

Typical expected values for a 1μm thick aluminium oxide detector of area $5mm^2$ would be: capacity, 500pF; number of charge carriers generated, 6000; signal voltage across capacitor 2μV.

The output pulse from the charge sensitive preamplifier with feed back capacitor of 5pF would be 190 microvolt, rendering a low noise post amplifier essential.

The input noise level of the E810F charge sensitive amplifier with a detector of this capacity (500pF) would be equivalent to an input charge of 3000 electrons.

Consequently the expected signal would only just be detectable above the amplifier noise.

The leakage current through the detector under these conditions ($\sigma \approx 10^{-14}$ mho cm^{-1}) would be 10^{-13} amp, the fluctuations of which would be well below the signal produced by an alpha particle.

CHAPTER 6

RESULTS AND CONCLUSIONS

6.1 Static characteristics

6.11 Introduction.

Polished polycrystalline aluminium rods and single crystal discs were anodised in borate and tartrate electrolytes as described in section 4.23. In each case the current density was less than 1 mA cm^{-2}, and the anodising procedure continued until the ion current fell to a low value.

No essential differences were produced by the different anodising methods. The time rate of change of current at fixed applied potential was virtually the same for both types of aluminium and for both electrolytes. In some cases the specimen could not be anodised (section 4.23), and these were excluded from further investigation.

In addition, evaporated aluminium oxide films were produced (section 4.25), and as well aluminium polycrystalline rods and single crystals were oxidised by bombardment with oxygen ions at reduced pressure.

One electrode in each case was always of aluminium, and the other a thin layer of gold.

The current-voltage characteristics of the various cells were measured and analysed.

From the variation in characteristics it was apparent that some surface effects were being observed in addition to the conduction through the films. Much of the variation between specimens prepared in similar ways was rendered very small by the use of a guard ring electrode.

Cell area varied between 1 cm^2, 8.6 mm^2 and 4 mm^2. The difficulty in measuring the area caused this quantity to be reliable to ± 20%.

6.12 Anodised films.

The film thickness was taken as 12.7 Å V^{-1}. The observed thickness for both electrolytes was in agreement with this figure.

Taking 5V across the cell as a reference value, the conductivities of the oxide films were determined. The lowest conductivity (6.7×10^{-15} mho cm^{-1}) was registered by the single crystal of aluminium anodised at 50V in the tartrate solution.

In all other cases, the variation within a given combination was always as great as that between combinations.

During the course of the measurements different solutions were made up from different batches and brands of A.R. grade reagents but no obvious trends in anodising or cell conductivity could be detected.

Because the behaviour of cells proved unpredictable at applied potentials near the forming voltage, most leakage current measurements were confined to appreciably less than this value.

Currents were measured for the gold electrode both positive and negative with respect to the aluminium electrode with no detectable difference.

In the light of the previous work, it was decided to look for linear relationships between current i (or current density, J) and applied voltage, V, sinh V, applied field E, and sinh E, or alternatively between ℓn i (or J) and V, $V^{\frac{1}{2}}$, E or $E^{\frac{1}{2}}$.

These curves were plotted for 1000 Å to 6500 Å films.

Similar to the situation found to exist for tantalum oxide (Mead 1962), the best approximation to a straight line was the log $J/V^{\frac{1}{2}}$ curve.

As reported in section 5.22, for the system $Ta/Ta_2O_5/Au$, the current density could be written

$$J = G_o E \exp(\beta V^{\frac{1}{2}} - W)/kT,$$

where $\beta = (e^3/\pi\epsilon d)^{\frac{1}{2}}$

It was observed that, since all the measurements were made at the same temperature, this relationship would be more useful when put in the form:

$$J = G_o E \exp(\gamma' V^{\frac{1}{2}}/d^{\frac{1}{2}} - W)kT$$

$$= G_o E \exp(\gamma E^{\frac{1}{2}} - K)$$

where $\log J = (\gamma E^{\frac{1}{2}}/2{\cdot}3) + K \log (G_o E)$,

where $\gamma = (e^3/\pi\epsilon)^{\frac{1}{2}}/kT$.

That is, for all film thicknesses, a plot of log J against the square root of the applied field would be a straight line of constant slope.

Figure 6.1 is a plot of the average measured current densities against the square root of the applied potential for films of 1000 Å (A) and 6500 Å (B) thick. The error bars are indicative of the range of values for individual films.

Figure 6.2 is the same information, with the abscissa being the applied field to the half power. Line C represents the expected slope of the curve if the Frenkel theory were applicable.

The corresponding values of γ are:

1000 A line . . . . . 3.15×10^{-4}

6500 A line (minimum slope) . . . 2.6×10^{-4}

6500 (maximum slope) . . . 5.6×10^{-4}

The expected calculated value (line c) is 4.5×10^{-4}

The errors in determining the thickness and the uncertainty in the permittivity are not sufficient to account for these variations.

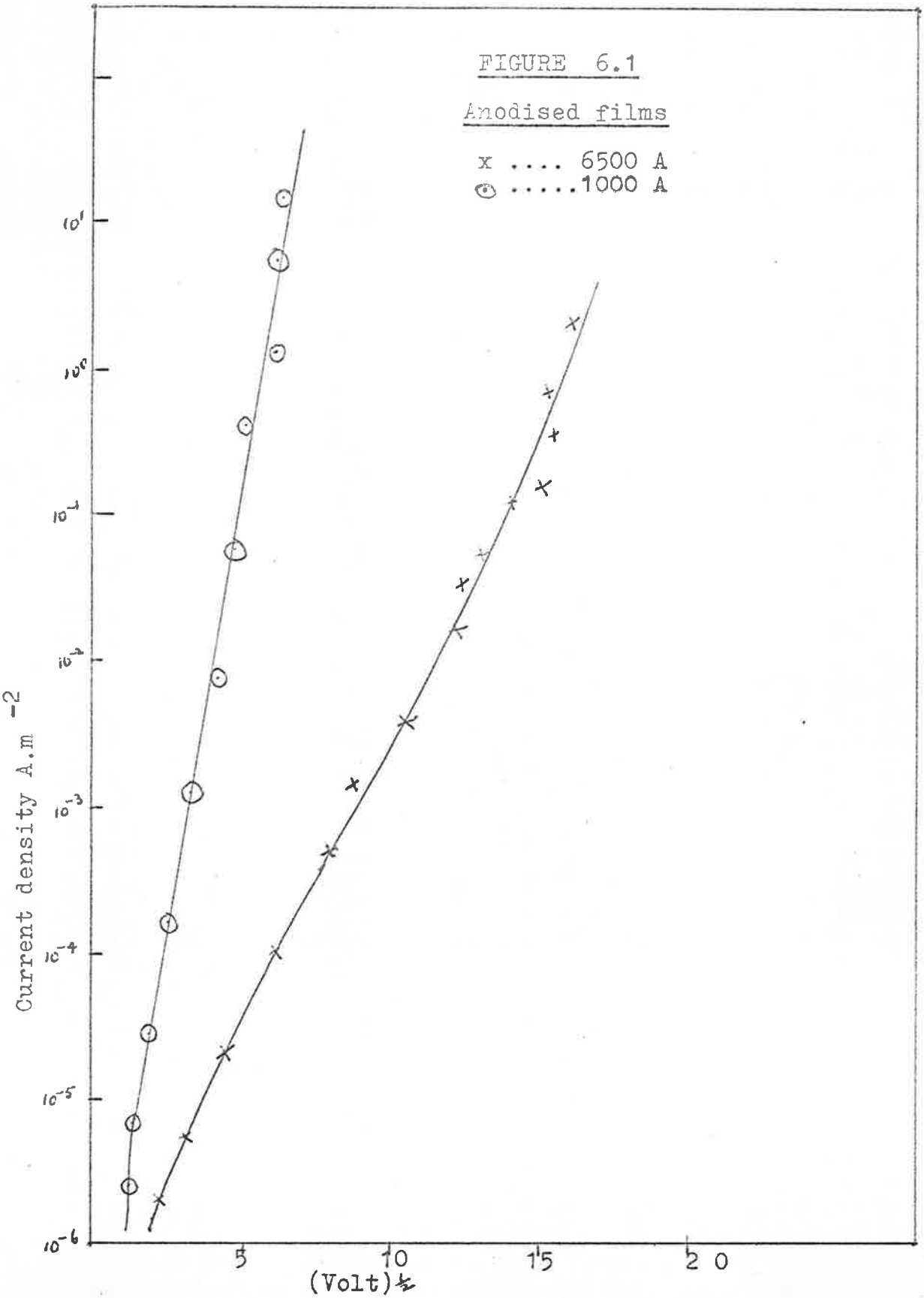
FIGURE 6.1
Anodised films
x .... 6500 A
⊙ .....1000 A
Current density A.m -2
10^1
10^0
10^-1
10^-2
10^-3
10^-4
10^-5
10^-6
5
10
15
20
(Volt)½

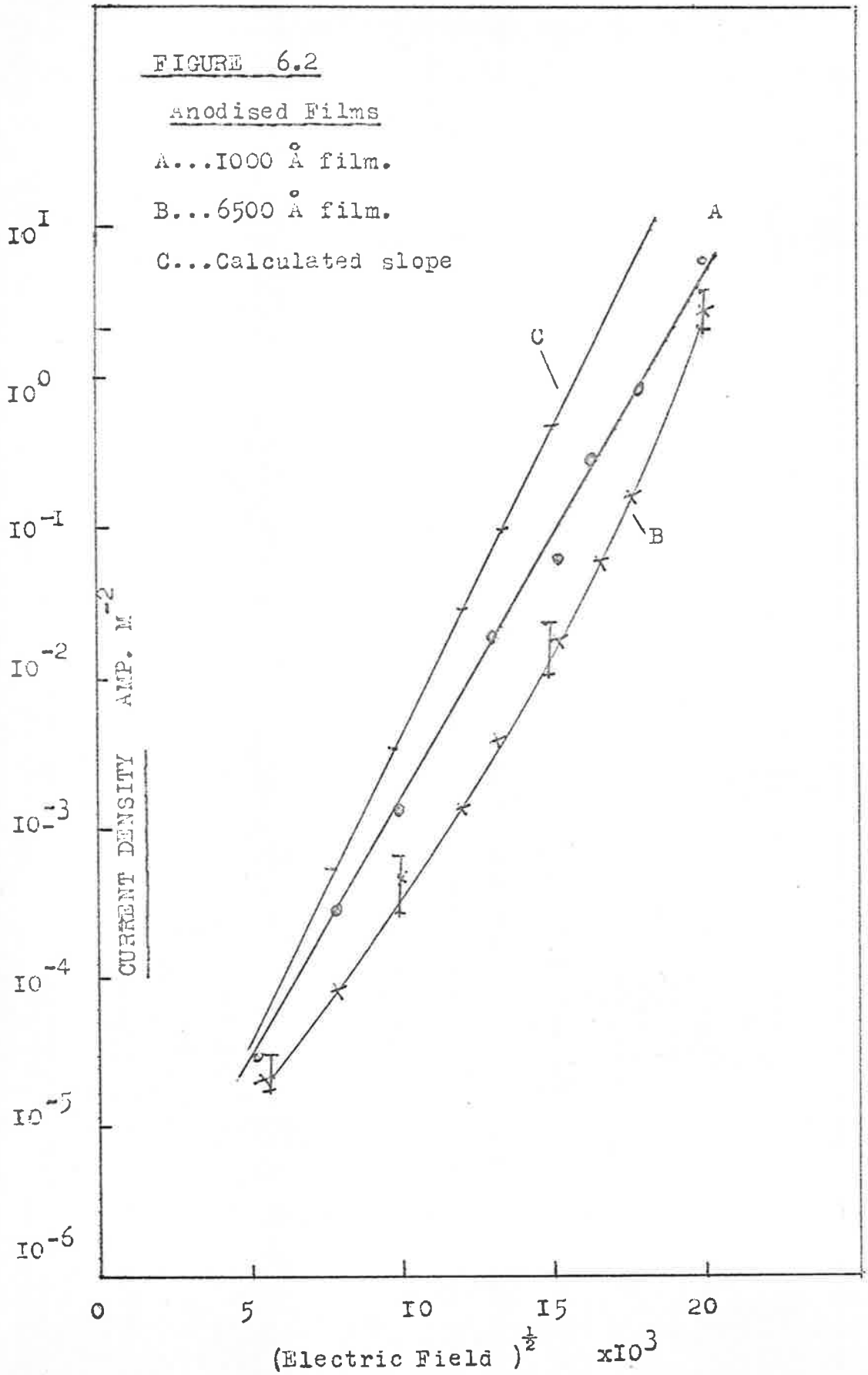
FIGURE 6.2
Anodised Films
A...1000 Å film.
B...6500 Å film.
C...Calculated slope
A
B
C
CURRENT DENSITY AMP. M^{-2}
10^{1}
10^{0}
10^{-1}
10^{-2}
10^{-3}
10^{-4}
10^{-5}
10^{-6}
0
5
10
15
20
(Electric Field)$^{\frac{1}{2}}$ x10^{3}

The concavity in the curve for the thicker film was evident in the individual curves for this thickness, as well as for the films of intermediate thickness. However, no simple direct relationship was observed.

A discontinuity in the tantalum oxide curve was ascribed to a change in permittivity. A continuous change in this same parameter would account for the changing slope. Alternatively some space charge limiting could be effective at low fields.

No consistent results were obtained for particularly low fields because the currents were nearing the lower limit of the electrometer. As a result, no effects characteristic of the difference in work function (0.86 V) between the aluminium and gold electrodes were detected.

The suggestion that $\log J \propto E^{\frac{1}{2}}$ for these films is generally borne out by the curves, although the magnitude of the slope is not in complete agreement with the predicted value.

However, the current-voltage relationship is consistent with a large number of trapping centres, and with the assumption that the measured conductivity is a property of the material of the films, rather than electrode processes.

Further, the conductivity of these films at low fields is sufficiently low that they do not impose a serious limit on the detection of low energy particles. The fact that so many traps exist in this form of the oxide reduces the possibility of the efficient collection of the released charges.

6.13 Evaporated films

Films were prepared by the evaporation of two different kinds of aluminium oxide powder on to glass substrates carrying aluminium electrodes, as described in section 4.25. The type of powder used did not have any measurable effect on the characteristics of the films.

The behaviour of the individual evaporated films was not predictable. A large number of specimens of active area ranging from 4 mm^2 to 8.6 mm^2 were examined; the thickness of the films lying generally from several hundred Angstrom units to 5000 Å. No reliable films of greater depth could be produced.

The limiting resolution of the interference microscope used for measuring the depth of the films was $\approx$ 1000 Å. For the thinner films, it was necessary to estimate the depth from the geometry (source-substrate distance) and the time of deposition. Some of the variations in results were no doubt due to this uncertainty.

However, by evaporating several cells on to the one substrate at the same time, a number of cells of the same thickness was obtained; thus permitting a comparison of supposedly similar elements.

Plots of the raw data similar to those of the anodised films were made, and several differences were observed.

Some 20% of the films showed an almost linear log J/V relationship, particularly in the low voltage region (figure 6.3), another 15% showed extremely low resistivity with a linear i/V relationship, another group of five exhibited marked current discontinuities and a further small group behaved similar to the anodised films. The remainder tended to be short circuited.

The darkening of the films reported in section 4.251 was most apparent in this last group.

The best film produced was 2130 ± 200 Å thick and its log $J/E^{\frac{1}{2}}$ curve is shown in figure 6.4. The low voltage conductivity was about 10^{-15} mho cm^{-1}, with five volts applied. This was less than the value for similar anodised films. Also shown in the same figure is a similar plot for the highest conductivity specimen (4000 Å) which had a log $J/E^{\frac{1}{2}}$ characteristic.

FIGURE 6.3.

Evaporated Al_2O_3 film.... 2000 Å

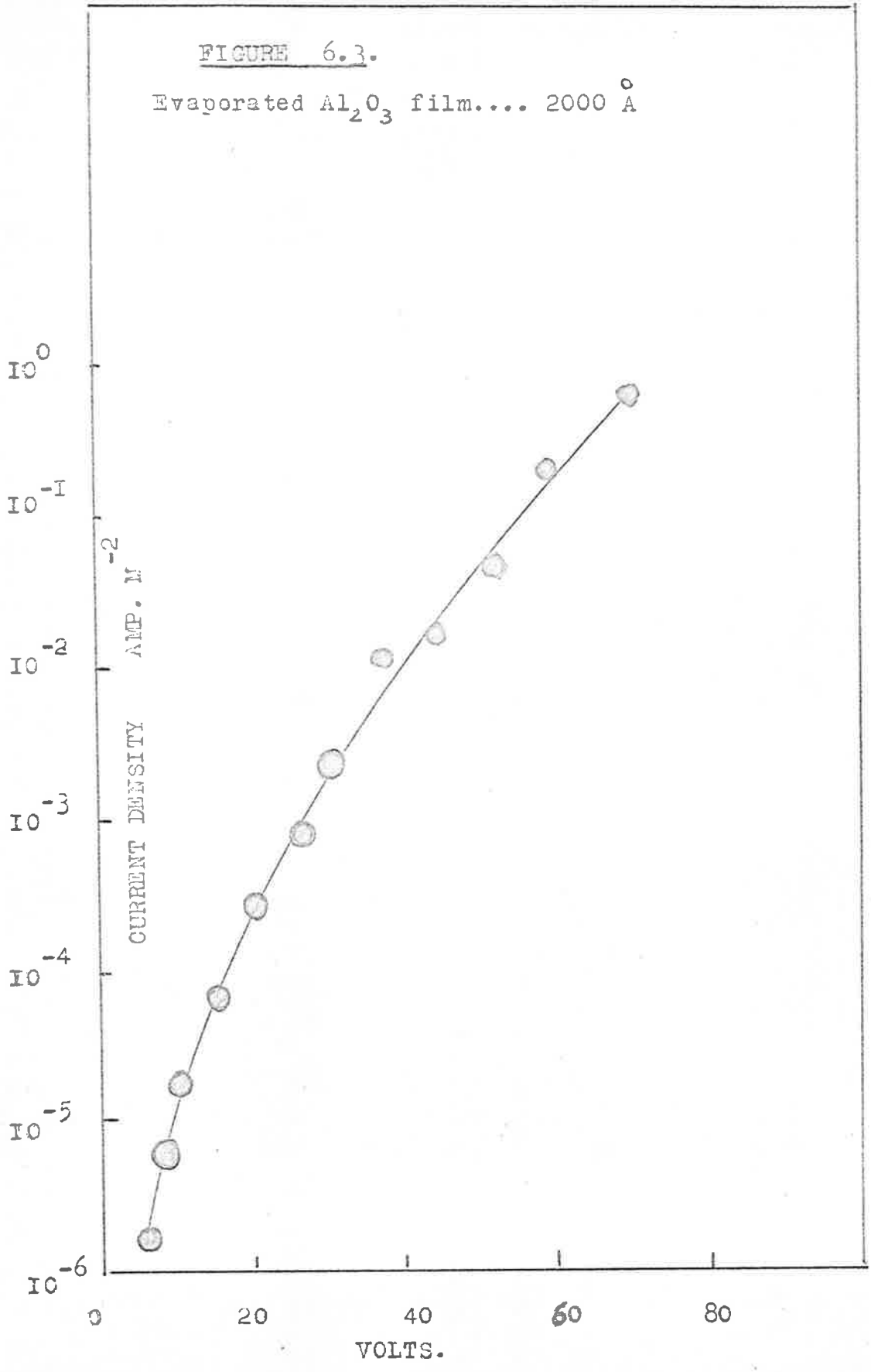

FIGURE 6.4

Evaporated Al_2O_3 Films

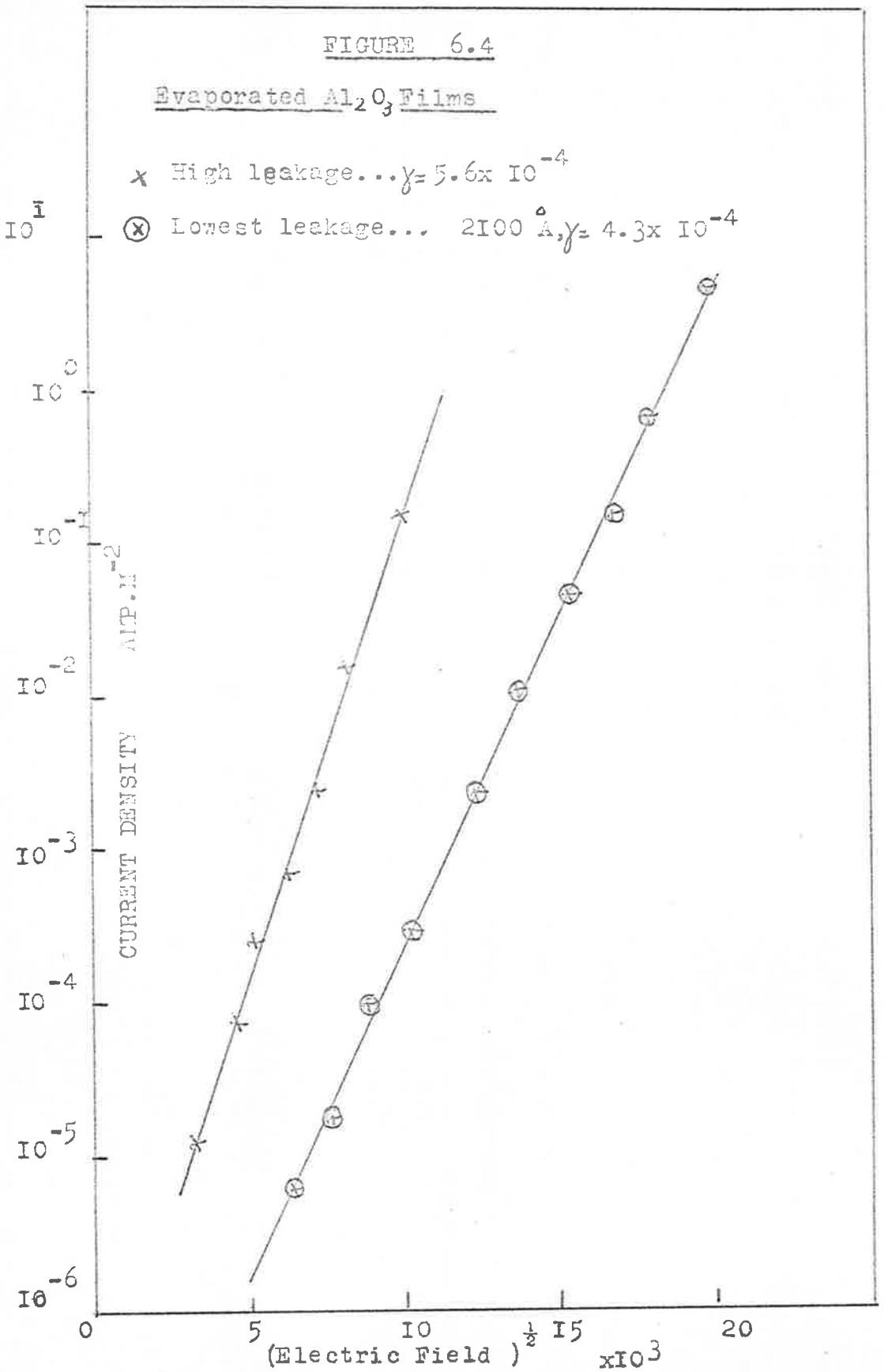

The corresponding values of γ are 4.3×10^{-4} and 5.6×10^{-4}. The former value has included in it, the inherent errors involved in measuring the thickness of the film. Some particular care was taken in determining this value. The photometric examination of an enlarged transparency as described in section 4.27 was used. The error of ± 200 Å in the 2100 Å, resulted in an error of about 5% in γ.

The agreement with the Frenkel theory is quite satisfactory for this film.

Five specimens showed marked current discontinuities. For low voltages, that is, say, less than one-tenth the voltage required to electrolytically form a film of similar thickness, the current-voltage relationships were similar to figure 6.5.

The initial section of log i/V line was almost straight (part A) and for higher values of V, the conductivity tended to Ohmic (part B) up to the point of breakdown (point C).

Up to the breakdown region, the currents flowing were only a little higher than the corresponding currents of the evaporated films which did not show this effect.

The increase in current corresponded to the film undergoing a permanent change because at no time did any film give rise to a curve similar to figure 6.5 once the point C had been exceeded.

If the breakdown potential were appraoched carefully using a high impedance power supply, the films did not short circuit immediately, although the current increased by several orders of magnitude. When the potential was reduced from the critical value the current was observed to increase still further.

Figure 6.6 represents the current-voltage characteristic after breakdown, firstly, as the applied potential was reduced to zero (as indicated by the arrows) and then increased up to the breakdown value. Curve I is typical of a thin film (≈ 500 Å) and curve II, for a thicker film (≈ 2000 Å).

FIGURE 6.5.

Evaporated Al_2O_3 (before breakdown)

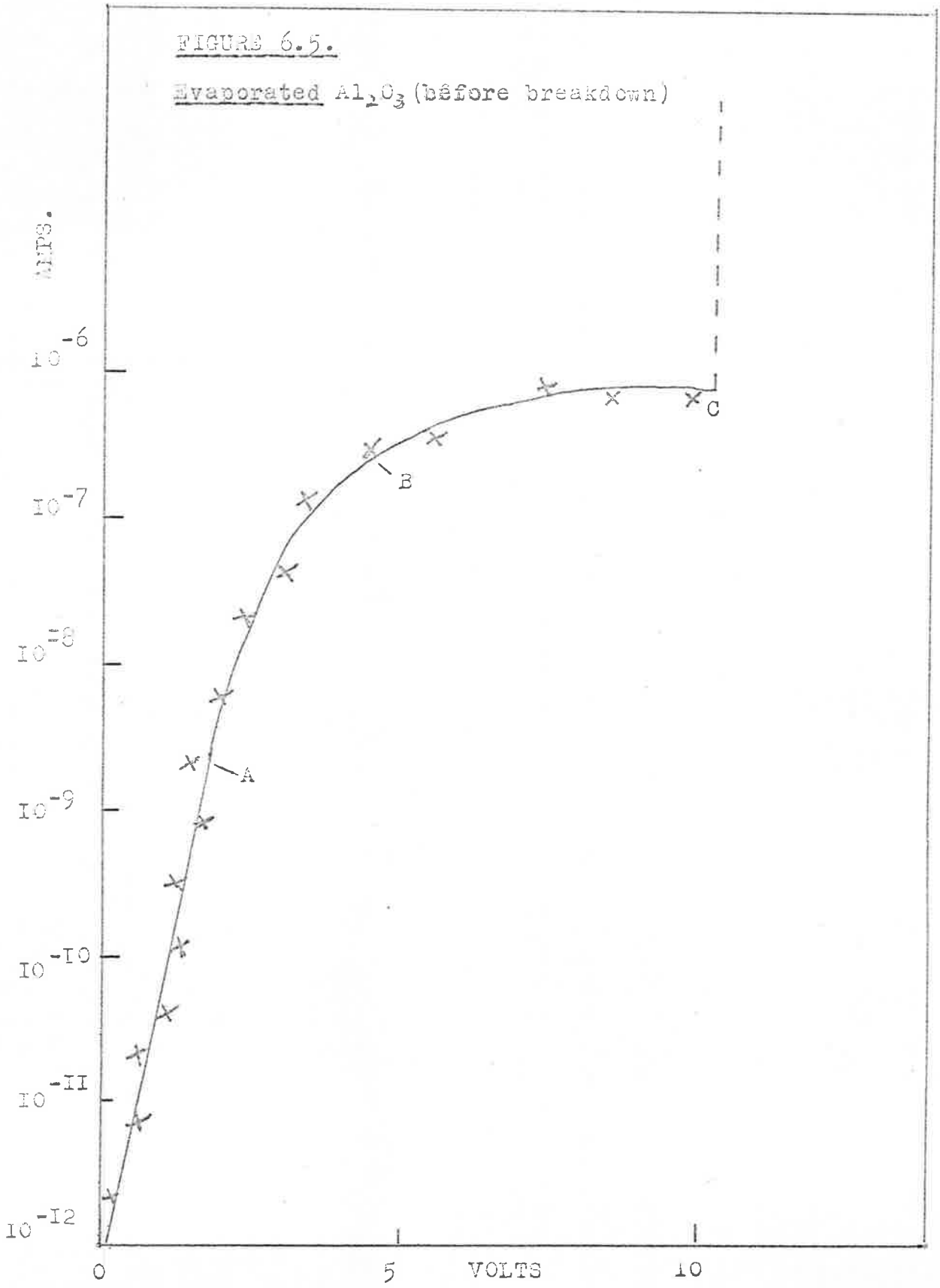

FIGURE 6.6

Evaporated Al_2O_3 (after breakdown)

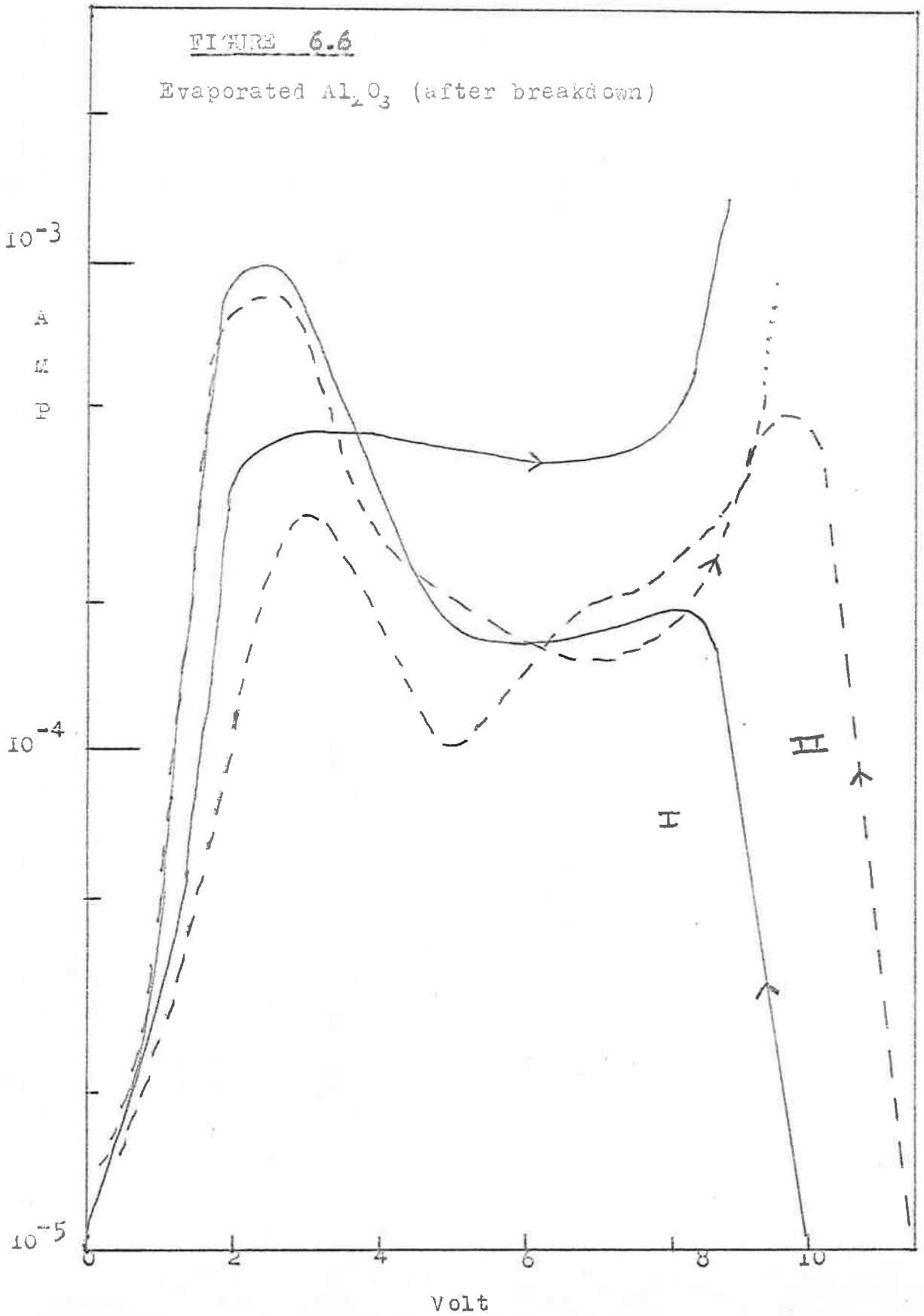

The marked negative resistance region just below the critical potential was well developed in the thinner films. The shape of the curve was not reproduced as the potential was cycled to zero and back to the vicinity of the breakdown voltage. On some cycles the current for a particular potential was less than that of the previous cycle, and vice versa.

On most occasions the current-voltage curves exhibited a second region in which the current increased as the voltage decreased. In this second regime the maximum peak to valley ratio was approximately 6.

Some films on some cycles passed sufficient current to eventually short circuit at quite low applied potential.

Reversing the direction of the applied potential did not introduce any additional, identifiable effects; the overall shape of the characteristics was generally independent of the polarity of the supply.

The material of the films in all probability consisted of a mixture of aluminium oxides, as well as hydrocarbon impurities. Because no low voltage critical voltage effects were observed with the other kinds of aluminium oxide films it is considered that the effects were produced by these impurities.

The measuring equipment was not fast acting, and no estimate could be made of the speed with which the change in properties first occurred, and no measurements were made using a rapidly alternating potential. The time taken for the changes to occur could well be the limiting factor in the use of these films as active circuit elements.

The structure of these films has not been determined, nor have any experiments been performed to identify the processes involved in the conduction mechanism.

It is intended to attempt to reproduce films of this type and perform a detailed investigation into the effect observed.

It is considered probably that the effect is highly localised at some part of the film, and that most of the increase in current above the critical potential occurs in this region. Many, slightly separated small electrodes distributed over the surface of the film would permit any particular area to be identified and isolated from the remainder.

Partially conducting dust particles on the substrate could also cause regions in which the film thickness was such that the breakdown potential was very low. This could account for the current increasing at a critical potential, but not for the two dynamic negative resistance regions.

A possible explanation would be that two closely spaced energy levels are present in the forbidden band due to the permanent change which occurs as a result of the breakdown, and that the mobility of the charge carriers is appreciably lower in the higher energy level than in the other level. If the conduction process involves carriers being field excited from one level to the next, the conductivity could decrease with applied field.

However, it is unlikely in films with this kind of highly disordered structure that, say, the effective mass of the charge carriers would vary so simply and sufficiently to cause effects of this magnitude.

The leakage current through most of the evaporated films was so high compared to the other types prepared, that they offered little likelihood of being satisfactory particle counters.

6.14 Cathodic Oxidation films.

Single crystal discs and polycrystalline rods were oxidised, after polishing and cleaning, by the method described in section 4.24.

Difficulties in accurately measuring film thickness were encountered, similar to the evaporated films. With this technique of film preparation however, it was relatively easy to produce films of depth in the

vicinity of 6000 Å, but difficult to control the process to produce thinner ones at will. The limitation in accuracy due to the interference microscope was not as significant for the thicker films, and it was used for all measurements.

The oxide produced by this process has been reported as growing epitaxially on the aluminium host (Hilbert and Lorenz 1963). The grain boundaries of the rod specimens were rendered visible by the electropolishing process and, although they were still visible after the oxidation process, the range of colours displayed did not indicate any really great difference in growth rate on the different surfaces.

The refractive index of the oxide was taken as 1.77.

As with the other films the plot of log $J/E^{\frac{1}{2}}$ resulted in a straight line. The slope for all films for which the thickness was accurately measured was remarkably constant at 4.4×10^{-3} as shown by line I of figure 6.7. There was little difference between all specimens, and the variation was within the accuracy of the thickness measurements.

The conductivity under given conditions was higher in the films produced on the polycrystalline rods than on the single crystal discs. The smaller the crystal size, the higher the conductivity. This was possibly because the depth of the film was not uniform (due to varying growth rates on different crystal planes), adding weight to the idea that the growth was epitaxial.

However, the increase in grain boundaries could have caused increased currents in these regions.

A planned experiment involves the oxidation of several single crystals of differing known orientations at the same time. After accurate depth measurements have been made the electron diffraction pattern of the stripped films will be observed. This will verify whether the growth is epitaxial or not.

FIGURE 6.7

Cathodic Oxidation Films

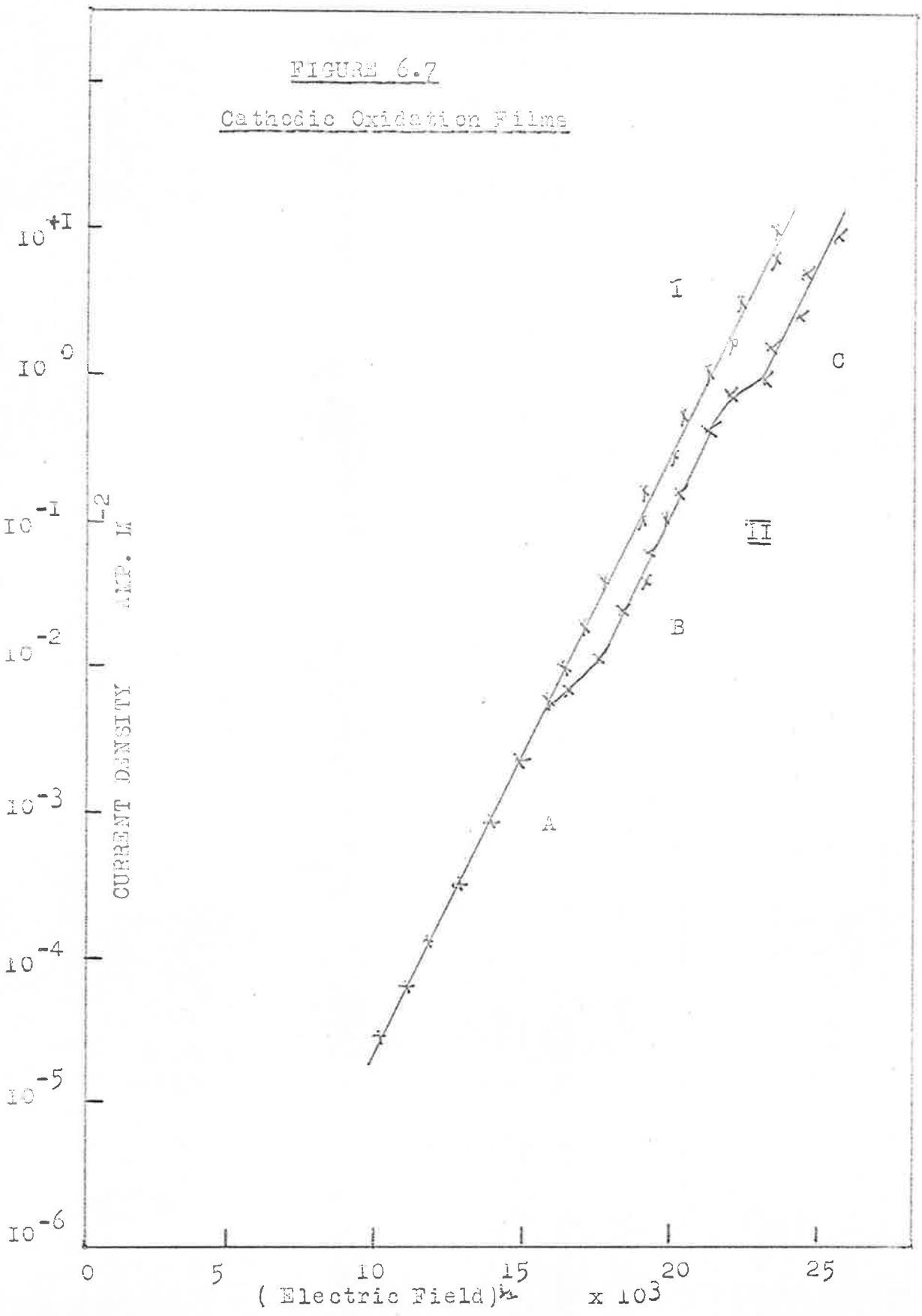

The effect of the argon ion cleaning process on the aluminium surface and the resultant oxide has not been investigated. Some imbedding of argon in the aluminium probably occurs. It is also not known how much sputtering of the aluminium occurs during the cleaning and oxidising procedures.

The conductivity at any point on the curves for this type of film was less than both the anodised and evaporated specimens. The values were almost an order of magnitude lower than the best (i.e. lowest conductivity) evaporated film, which, as reported earlier, was almost the same amount lower than the anodised films. Once again, the errors in thickness and area determination were insufficient to account for the differences.

An interesting property exhibited by several films is illustrated by line II of figure 6.7. This represents a log $J/E^{\frac{1}{2}}$ plot for a 5000 Å film.

Within the region, A, the line coincides well with the average line of the other films prepared by this method.

Over a relatively small range of values of $E^{\frac{1}{2}}$ the slope of the line changes until another straight segment B develops, parallel to, but displaced from the position of the extension of section A.

A somewhat similar, but slightly greater displacement separates segment C from segment B.

Some films showed no such variation, several had only two regions, and several had three regions similar to the ones depicted. Films of thickness 2000, 5000, and 7500 Å formed on single crystal hosts had relationships of this kind. Not all cells formed by the various gold electrodes on the same piece of oxide showed the effect, nor for those in whom it was well developed, did it occur at the same values of field strength. The lateral displacement of the lines, however, was about the same for each specimen.

It is significant, as will be discussed later, that most of the films that successfully counted alpha particles, either had relationships of this kind, or else were formed on the oxide film, some section of which displayed the effect.

Furthermore, the guard ring connection did not seem to be necessary for reproducible results with these films.

Discontinuities have been observed in tantalum oxide film characteristics (Mead 1962) but these have been discontinuities associated with voltage plots at constant current for varying depths of film. No discontinuities were reported for a given film with a variable field.

The tantalum oxide changes were satisfactorily accounted for by an assumed change in permittivity with thickness. It seems unlikely that the permittivity of these aluminium oxide films should be so field dependent. In any case a change in permittivity should produce a change in slope (i.e. in γ), rather than a displacement of the line.

If these cathodic oxidation films are single crystals, it is reasonable to assume that the trap density will be much less than the very disordered anodised or evaporated films. Similarly it would be expected that fewer trapping levels would lie between the valence and conduction bands.

Because the process of charge carriers being field excited into the conduction band accounts satisfactorily for the current-voltage relationship, for the time being an explanation in terms of this mechanism would be promising. One such possible explanation would be that there exists just below the conduction band (or alternatively, perhaps, just above the valence band) two defect produced energy levels, both of low concentration, and that at relatively low field these are effectively emptied, so that for higher fields they make no further contribution to the number of charge carriers, the process being somewhat akin to emptying of impurity induced energy levels in semiconductors as the temperature is raised.

It would be of interest to observe the current-voltage relationships for this type of film as a function of temperature to see how the points of changing slope depended on the applied field at these differing temperatures.

The optical absorption spectrum of the stripped films would also be worth investigation.

6.15 Aluminium oxide single crystal.

The 1 cm^3 single crystal of aluminium oxide current-voltage characteristic was measured for potentials of 500 to 2500 volt, applied between two gold electrodes evaporated on to opposite faces, separated by 1.0 cm.

Figure 6.8 line I, is a plot of log i against V, and line II, a plot of log i against $E^{\frac{1}{2}}$. This second line is essentially straight, with slope $4{\cdot}56 \times 10^{-3}$.

This is in close agreement with the corresponding slopes of the other kinds of aluminium oxide.

The applied fields in this case however, are much less than those of the films. A suitable higher voltage source was not available.

6.16 Summary.

For the electric field strengths considered, it appears as though the principal conduction mechanism in aluminium oxide films of various types, and in a single crystal, is field enhanced thermal excitation of trapped electrons into the conduction band, (or, possibly, field enhanced thermal excitation of electrons from the valence band into deep traps; this could account for the p type conductivity reported for the oxide single crystals).

FIGURE 6.8

Single crystal aluminium oxide

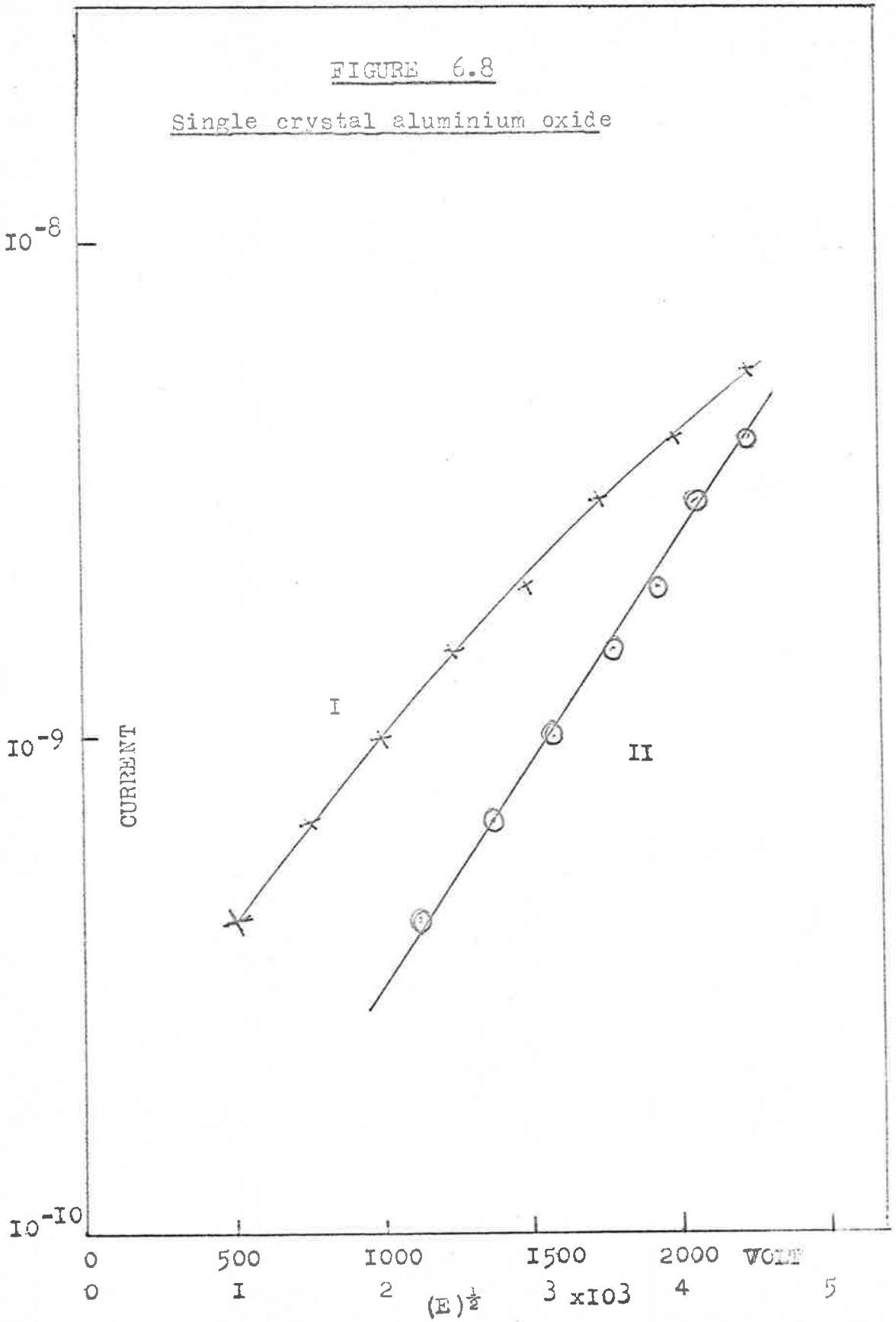

Anodised films, whilst easy to prepare for a given thickness, are highly disordered, and have significant conductivities. The variation from a linear log $J/E^{\frac{1}{2}}$ relationship for the thicker films indicates some additional or alternative processes.

Evaporated films, possibly because of the method of preparation, showed marked variations. The best film (that is, the lowest conductivity) was better than any of the anodised films, from this point of view. Once again the structure was highly disordered, and the low conductivity may have been due to an excessive trap density, rather than to high purity, low charge carrier concentration conditions. That is, high resistivity alone, and consequent low standing currents, is not a sufficient requirement for a particle counter.

The d.c. leakage characteristics of the cathodic films on the other hand, gave evidence of a reduced trap density, and even lower standing currents. On this basis alone they appeared the most promising as particle detectors.

Figure 6.9 shows the relative log $J/E^{\frac{1}{2}}$ for the various types of films considered.

6.2 Pulse characteristics.

6.21 Introduction.

The oxide film cells were placed in the vacuum chamber described in section 4.42 with an applied potential always appreciably less than the dielectric breakdown value. The gain of the system was adjusted so that no spurious noise pulses were registered by the scaler or displayed on the oscilloscope. The latter effect was achieved by adjustment of the sensitivity of the time base trigger.

Whenever the potential across the cell was altered, measurements were made without the gain being changed, and with the scaler and trigger sensitivity readjusted for zero noise counts.

FIGURE 6.9

Comparison of oxide types.

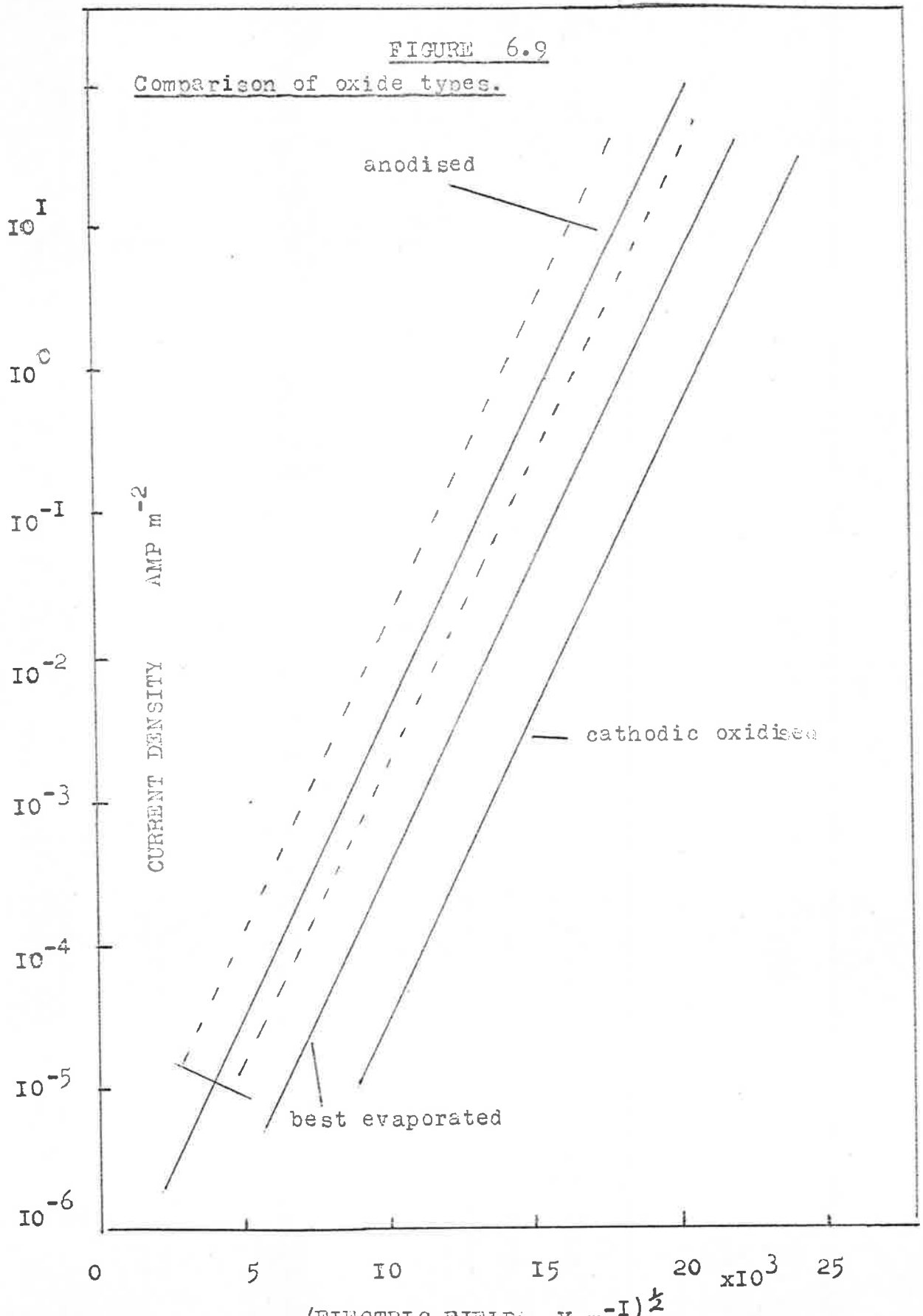

By this procedure close to optimum operating conditions for all cells were quickly determined. A fast discriminator controlling a linear gate with a delay amplifier would have been a better method of pulse selection. Such equipment was not available.

6.22 Anodised and evaporated films.

Many cells of differing thickness and area were formed by anodising single crystal and polycrystalline aluminium in two electrolytes, and by evaporation of two oxide powders from different sources.

In not one case was it possible to definitely associate any pulse response with the incidence of alpha particles. Some of the thinner anodised cells, at potentials approaching the formation value showed a slight (< 1%) increase in leakage currents on occasions. This was probably a spurious effect, since for the geometry shown in figure 4.7 the average particle flux incident on a 8·6 mm^2 specimen was 3 per second.

By dispensing with the alpha particle shield and the ability to rotate the source, the source to detector distance was reduced from 3·0 cm to 0·5 cm, with a consequent effective flux of 100 alpha particles per second. No further increased current was observed with this higher count rate.

This failure to count also applied to those evaporated films which exhibited current discontinuities (section 6.13 and figure 6.6). The greatly increased standing current of these films made pulse measurements more difficult.

The conclusion to be drawn from this is that the mean free path of the charge carriers produced by the alpha particles is substantially less than the thickness of oxide films of these kinds.

For both anodic and evaporated films the structure is highly disordered. In the former material however, the cells formed during oxidation are about the same size as the film thickness (section 3.21), and the films faithfully replicate the aluminium structure to at least 10 Å to 15 Å.

It was expected then that throughout the length of a given cell, the material was fairly well ordered. The earlier work on the structure of the cells (section 3.21) lend weight to this assumption.

Since the passage of the alpha particles, and the charge carriers they produced was along, rather than across the cells it was considered not unreasonable to expect some indication of the incidence of the particles.

The highly ordered structure of the single crystal aluminium which was anodised to produce the films also apparently has little effect on the ultimate small scale structure of the anodised films.

It would appear that the cell size or the number of cells per unit area is not a satisfactory measure of the small scale disordering in the films. Further it seems that the value of 5 Å for the mean free path of the charge carriers, determined by Collins and Davies (1964) is in agreement with these observations.

The mean free path of such carriers in evaporated films is probably of the same order.

The inability to detect alpha particles by using evaporated films is not surprising in view of the very obvious total disorder of the films and the observed optical darkening.

6.23 Cathodic oxide films.

Many of the films produced by the method described in section 4.24 on both single crystal and polycrystalline hosts, gave some indication of being able to respond to alpha particles. No really

reliable counting could be ascribed to films less that 3500 Å thick.

Furthermore, not all cells produced from the same rod behaved the same. In one instance a 5000 Å thick oxide film which detected alpha particles was produced on one of the polycrystalline rods. The gold electrode was then partially removed by gently rubbing with a lens tissue. The oxide was then removed in a sulphuric acid potassium bichromate bath, and the rod given a slight ($< 3\mu m$ removed) electropolish.

The rod was then oxidised under as near to identical conditions as previously. The resultant cell showed no tendency to count.

The consistency of behaviour was much higher for films formed on single crystals of aluminium.

However, once again, not all cells formed simultaneously on the one crystal behaved identically. Some would count well, others not at all, even though no visible difference was discernible, and their static leakage current characteristics were similar.

The most promising cells were those that were in some way related to those described in section 6.13 in which there were discontinuities in the log $J/E^{\frac{1}{2}}$ line as shown in line II of figure 6.7. That is, either cells which showed this effect, or else which were in close proximity to other cells showing this property. Most measurements were made with fields corresponding to section B of figure 6·7.

The several larger area cells manufactured were not satisfactory as counters. The increased leakage current, due to the increased area, and the decreased sensitivity resulting from the increased capacity possibly were the principal causes.

The small total energy deposited in the films, coupled with the relatively high value of the energy required to generate a charge

carrier pair (ϵ) in aluminium oxide, and the high capacity of the cells made direct observation of the electrical pulse impossible. Hence no rise time measurements were possible, and therefore no estimates could be made of the carrier mobility and trapping time. Carrier transit times of the order of 10^{-12} seconds were estimated in section 5.32, and high speed sampling techniques would be necessary.

The low noise charge sensitive amplifier of section 4.442 was used for all measurements with these films. Even so, the residual noise was sufficient to make pulse counting somewhat unreliable.

The shape of a representative pulse of the best detector made was copied from a Polaroid print and forms figure 6.10. This detector was one of front electrode area 8·6 mm^2 on a 6200 Å film formed on a single crystal of aluminium. Most of the neighbouring parts of the film also responded to alpha particles.

The rise time of the recorded pulse was that of the preamplifier.

The maximum pulse height delivered by the charge sensitive preamplifier was 0·18 mV, corresponding to a charge release in the detector of $8{\cdot}8 \times 10^{-16}$ coulomb, which is in turn equivalent to 5,500 electrons if trapping and recombination does not occur.

On the basis of 22·7 eV per electron-hole pair (calculated in section 6·24) this corresponds to an energy loss by the alpha particle of 120 keV. This is higher than would be expected from a film of this thickness.

It could be that some kind of multiplication process was taking place, because it is considered unlikely that the "direct" electron-hole generation energy would be significantly less than 22 eV, and in addition the total error involved in film thickness, electrode area and gain measurements would be less than 20%.

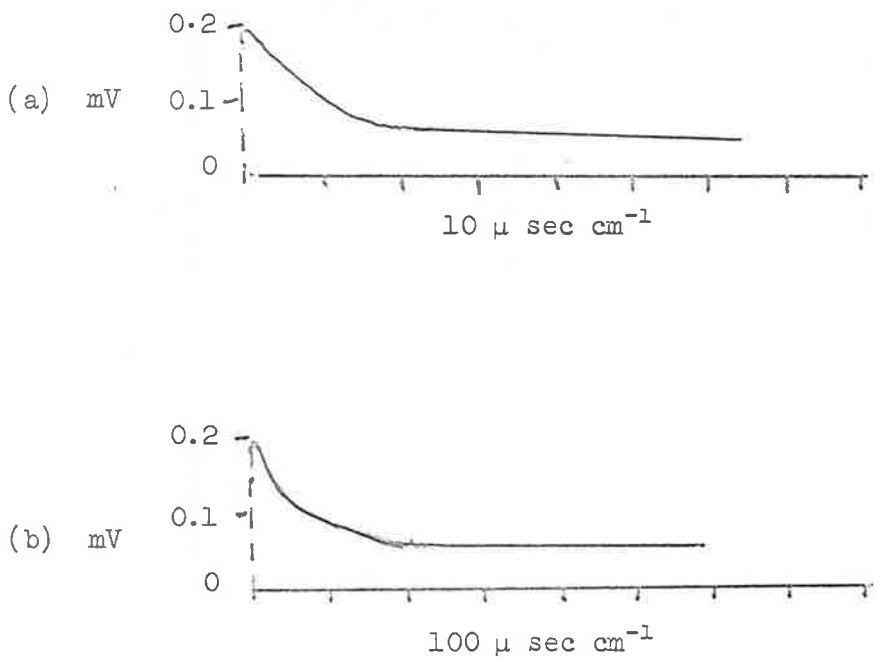

Pulse Shape - Cathodic Oxide Film

FIGURE 6·10

A further factor associated with most of the films was the relatively long decay of the tail of the pulses. This was difficult to measure accurately because of the noise associated with the system. However many pulses seemed to persist for times longer than the decay time of the input of the preamplifier. The indication is that some trapping of minority carriers may be occurring, giving rise to some effective pulse amplification (Northrop and Simpson, 1964).

The counting efficiency was difficult to determine precisely because the low source activity rendered the statistical variation large, and some noise pulses could have been counted, or, alternatively, some small signal pulses may have been excluded. An estimate would put the counting efficiency in the vicinity of 50%.

A height analysis of the generated pulses was attempted. A single channel analyser was used, but once again, the count rate was so low that this was a tedious time consuming task. There was appreciable variation from one detector to the next.

For the best one whose pulse response has just been described, the FWHM was of the order of 30 keV, with the peak corresponding to about 120 keV. Most other films showed a greater variation.

It is not known how much of this spread is due to the variation in the amount of energy given up by the alpha particles to the particular layer of oxide.

6.24 Oxide single crystal.

Two electrode configurations were used on the Semi-Elements crystal described in section 4.26.

In the first case gold electrodes were evaporated on opposite sides of the crystal, resulting in a detector of active area 0·75 cm^2 and depth 1·0 cm. A potential of up to 3000 V could be maintained across this cell.

The electrical capacity was approximately 2 pF in parallel with the input of the amplifier.

No evidence of counting of alpha particles was observed.

The maximum applied electric field strength was not very large (3×10^8 V cm^{-1}, being limited by the available supply) and this may have been a limiting factor, although in the light of the experience with the second electrode configuration, the limitation seems more likely to be due to the trap density.

In the second configuration the two equal area electrodes were vacuum deposited on the same face of the crystal with a measured gap of $4{\cdot}95 \times 10^{-2}$ mm running across a diameter of the crystal.

The arrangement was similar to that of Ahearn et al (Ahearn, Burton and Wooldridge 1947).

The potential across the gap could be varied from 0 to 200 V. Reliable counting occurred at about 100 V, corresponding to a field strength across the gap of $2{\cdot}0 \times 10^4$ V cm^{-1}.

Because the rise time of the pulses was required to enable a calculation of carrier trapping time to be made, the wide band amplifier (section 4.443) was used in conjunction with the Tektronix 585 oscilloscope, which was set at its most sensitive position (10 mV cm^{-1}).

Furthermore, the total charge generated by the alpha particles, and hence ϵ for aluminium oxide, as well as carrier mobility could be determined from the total charge collected, and the initial time rate of change of charge.

The former quantity was measured using the charge sensitive preamplifier, and the latter by extrapolating the rate of change of charge to zero time.

For these calculations it was necessary to know the capacity of the detector and the input circuit of the wide band amplifier.

The detector capacity, measured at 27 MHz on a Marconi Circuit Magnification Meter ("Q" meter) type TF3296., was approximately 2 pF.

The input capacity of the amplifier was about 10 pF.

To reduce the error introduced in the calculated quantities by the uncertainties of these capacities, an additional 20 pF capacitor was added to the input circuit. Whilst this reduced even further the magnitude of the signal produced by the passage of the alpha particle, it did make a worthwhile reduction in the relative uncertainity of the total capacity.

The input capacity under these conditions was 32 pF, with an estimated error of ± 6 pF.

The second quantity which introduced a considerable error in the finally calculated values, was the determination of the point of entry of the alpha particles.

The assumption was made that particles incident through the electrodes (rather than the gap between them) did not contribute to the collected charge.

In addition, to simplify the analysis photographs were required of pulses produced by particles incident near one electrode, thus allowing one type of carrier to be collected promptly.

Another limiting factor was the small angle subtended by the active area of the detector. The calculated number of particles incident on the total gap was 25 per minute., when the separation was 2·0 cm.

The level control of the time base of the oscilloscope was adjusted so that noise pulses did not produce regular triggering.

Photographic prints were made on type 47 Polaroid film with exposure times of one minute. Most prints had from 10 to 12 pulse outlines of varying heights, indicating a counting efficiency of the order of 50% (similar to the oxide films).

The smallest consistently occurring pulse was considered to be representative of the charge released by the alpha particle incident near the electrode remote from the collecting electrode. To facilitate the identification of this particular pulse type, long term multiple exposures (10 and 20 minutes) were made. Having identified the pulse type, the nearest pulse to this on the one minute exposures was copied.

This procedure was used for two different sweep times, viz 10 μsec cm^{-1} and 0·5 μsec cm^{-1}. The same minimum pulse could be identified on each occasion.

Figures 6.11 (a) and (b) are copied from these traces, whilst figure 6.12 is an enlargement of the pulse rise in terms of the collected charge.

The decay times of the pulses are consistent with an amplifier input capacity of 30 pF shunted by 0·5 MΩ.

Figure 6·13 is a plot of the logarithm of the rate of change of collected charge against collection time.

It will be observed that over an appreciable part of its length the trace is straight, the deviations occurring at the extremities of the line. The departure from linearity in the vicinity of 2 μsec is probably caused by the time constant in the amplifier input circuit. The initial part of the curve was not displayed because of the sensitivity setting of the time base.

Use can be made of the simplified analysis outlined in section 5.32 to determine the charge trapping time for ionising radiation incident near one electrode.

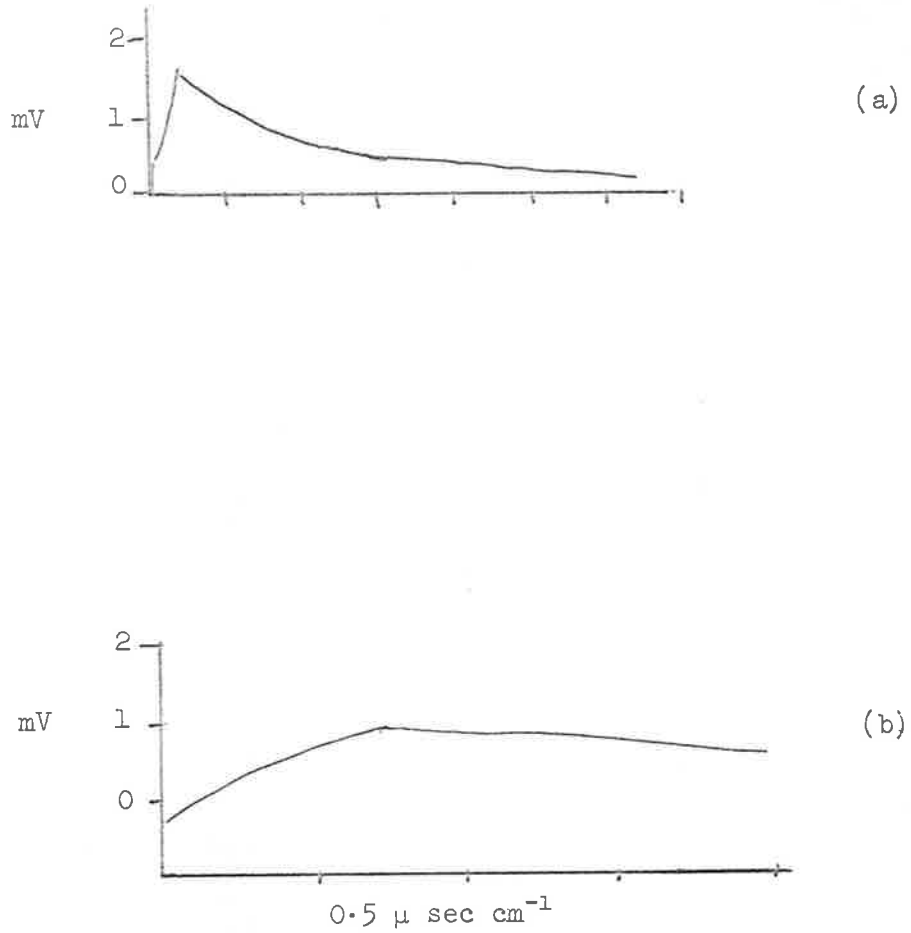

Pulse Shape - Single Crystal Al_2O_3

FIGURE 6·11

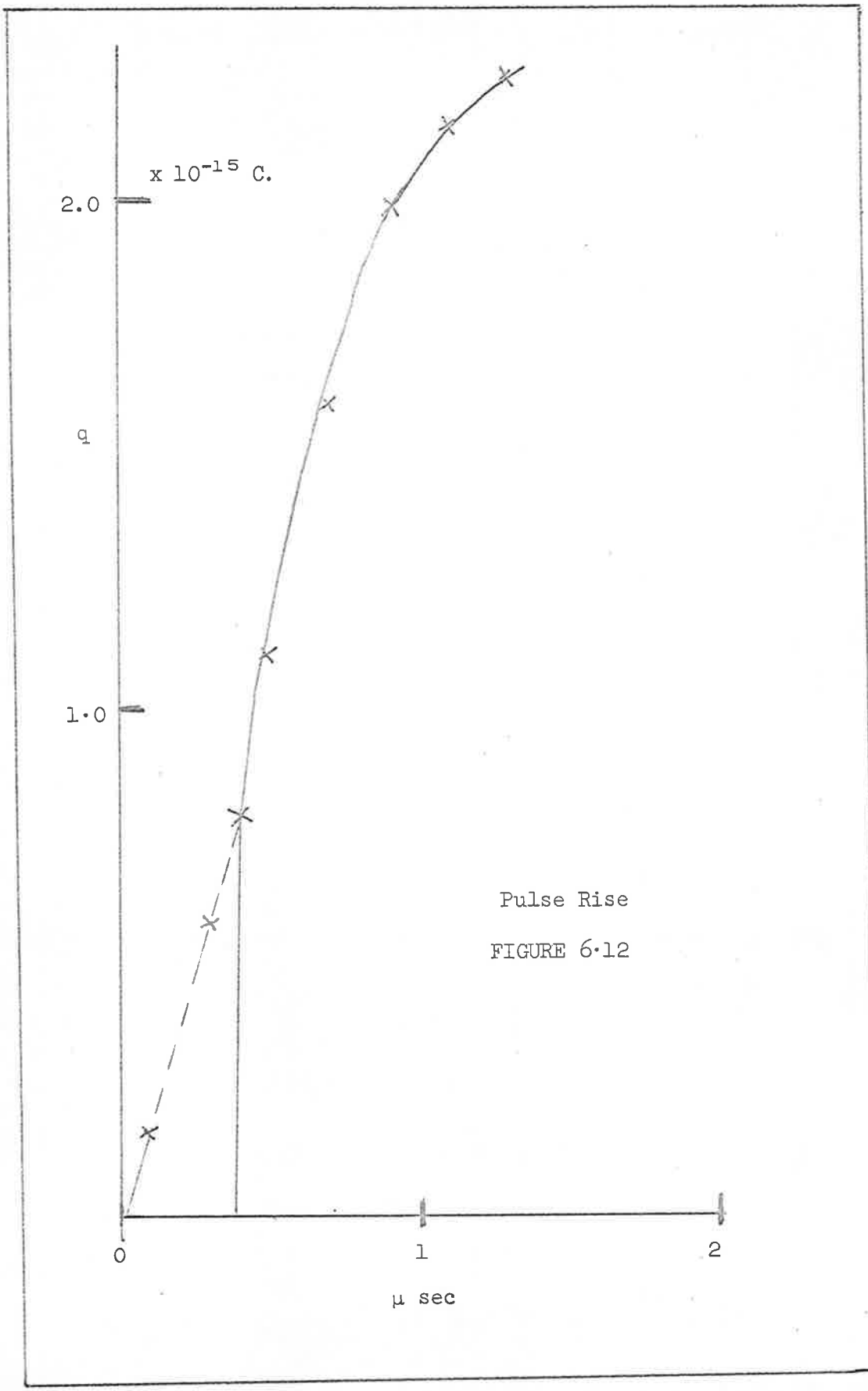

Pulse Rise

FIGURE 6·12

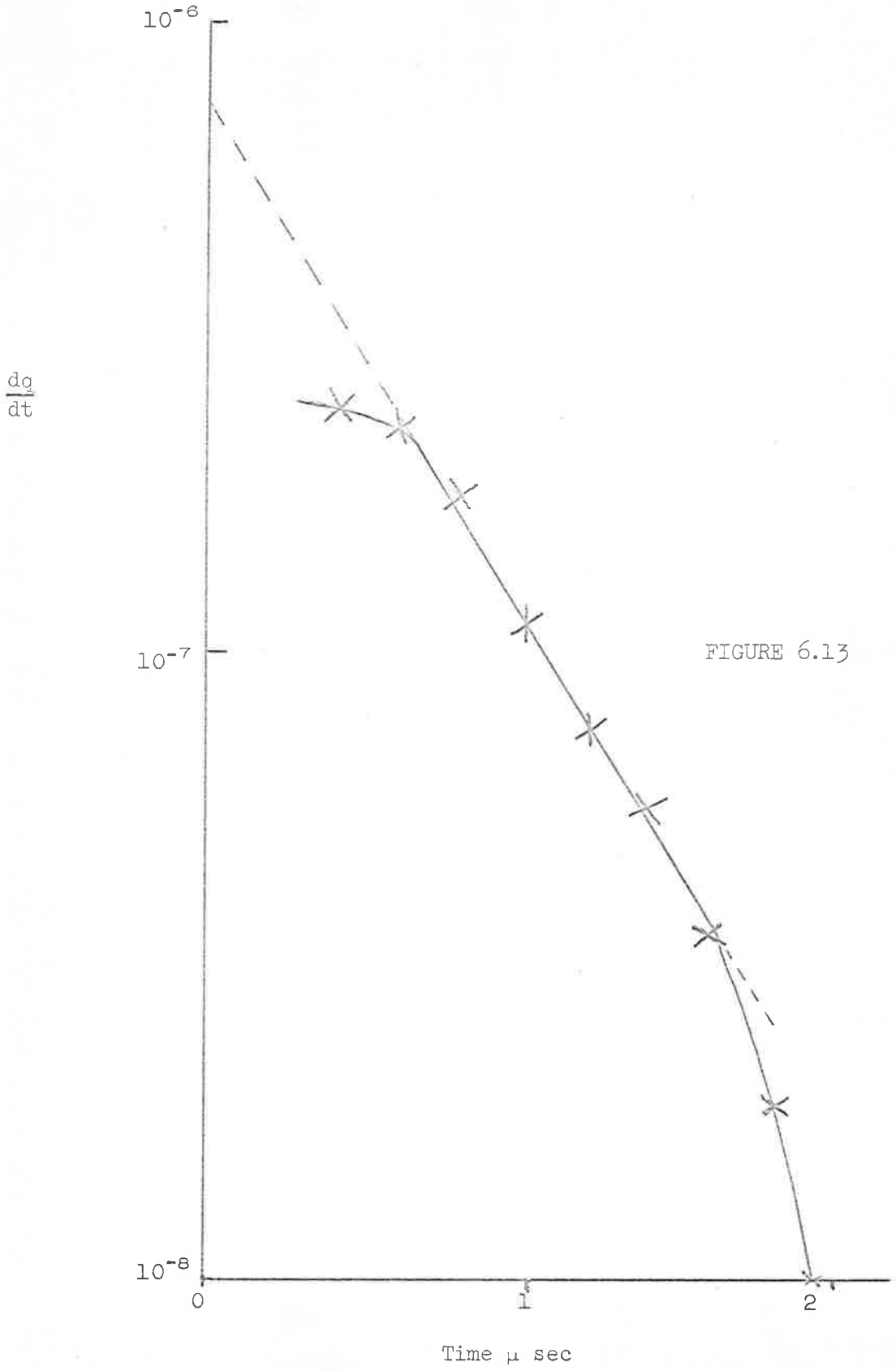

FIGURE 6.13

Under these conditions,

$$dq/dt = (n_g \, e \, \underset{\sim}{E} \, \mu/d) \exp(-t/T), \quad \text{then}$$

$$\log(dq/dt) = -t/2{\cdot}3\,T + \log(n_g \, e \, \underset{\sim}{E} \, \mu/d).$$

The value of T is taken from the linear part of figure 6.13 and results in

$$T = 4{\cdot}5 \pm 0{\cdot}2 \times 10^{-7} \text{ sec.}$$

If the line had been straight throughout its length the intercept on the ordinate would give the quantity

$$\log(n_g e \, \mu \underset{\sim}{E}/d).$$

The assumption is made that the straight portion of the line extended back to the (dq/dt) axis does give this quantity.

That is, $(n_g \, e \, \mu \, \underset{\sim}{E}/d) = 7{\cdot}6 \times 10^{-7}$

Since $d = 4{\cdot}95 \times 10^{-3}$ cm and V = 100 V,

then $n_g \, \mu = 116.$ (MKSA units.)

Similar analyses were made for pulses produced when the collecting potential was 130 V and 170 V. The variations in the slope of the straight portion of the curve was about 5% and the value of the product $n_g \, \mu$ determined by the same procedure varied by 30% The latter difference was probably due to the method of selecting and measuring the pulse, and the extrapolation of the line.

The curvature was about the same for these slightly higher fields.

The total charge collected was measured in a similar manner to the output pulse, except that in this instance the first stage of amplification was the charge sensitive preamplifier, the voltage output of which was proportional to the input charge.

The output voltage had a peak value of 6·8mV, corresponding to a collected charge of $3{\cdot}41 \times 10^{-14}$ coulomb.

This total collected charge is given by:

$$q = (n_g e \mu \underset{\sim}{E} T/d) [1 - \exp(- d/\mu \underset{\sim}{E} T)].$$

Substituting the measured value of q, and the other calculated quantities in this equation gives:

$$\mu = 5{\cdot}3 \pm 2 \times 10^{-4} \text{ m}^2 \text{ V}^{-1} \text{ sec}^{-1} \text{ (Or } 5{\cdot}3 \text{ cm}^2 \text{ V}^{-1} \text{ sec}^{-1})$$

and $n_g = 2{\cdot}3 \pm 0{\cdot}8 \times 10^5$ electrons.

Since $\epsilon = (E/n_g) = 5{\cdot}1 \times 10^6/2{\cdot}25 \times 10^5$ eV

$= 22{\cdot}7$ eV,

$\epsilon = 23 \pm 8$ eV.

An assessment of the uncertainties involved in the methods and measurements used would place an upper limit of error of about 40% in these last three calculated quantities.

The carrier mobility measured is that of the surface region of the crystal; this need not be representative of the bulk of the crystal. Some appreciable changes could well have occurred as a result of the polishing and etching processes, as well as by the evaporation of the gold electrodes.

The agreement of this mobility value with that calculated by the Frohlich-Mott model is perhaps somewhat fortuitous.

It is intended to repeat the experiments with other single crystals of aluminium oxide in which some attention has been given to the manner of preparation of the surfaces. The relative chemical inertness of the material makes non-mechanical cutting and polishing difficult.

In addition single crystals of depth (≈ 1 mm) between the two values used for this specimen will be prepared and their behaviour

examined.

The physical arrangement of source and detector, and the type of electrode assembly made pulse height resolution studies unrealistic.

Further the experiments did not permit the type of charge carrier to be determined.

6.3 Conclusions.

As a result of the experimental investigations conducted the following conclusions can be drawn.

(a) Oxide films can be produced on polycrystalline and single crystal aluminium by anodisation and cathodic oxidation. These films have reproducable electrical properties.

(b) For films of these types at room temperature the rate limiting step in the conduction process is field enhanced thermionic emission of trapped electrons into the conduction band, (or the equivalent process of excitation of electrons from the valence band into traps, with hole conduction resulting). Some of the cathodic films behaved in a manner suggesting a relatively low occupancy of these traps.

(c) Evaporated oxide films tend to be erratic in behaviour; some showing negative resistance characteristics after having under gone some permanent change.

The evidence is generally in favour of the concept that these films are highly disordered.

(d) None of the anodised or evaporated oxide films investigated were suitable as conduction alpha particle detectors, even though the leakage currents were not limiting factors. The high trapping density associated with the disordered structure of the films was probably the limiting factor.

(e) Cathodic oxide films which are capable of detecting alpha particles can be readily prepared. The small amount of recombination shown by the detectors indicates that efficient charge collection can take place over greater lengths, making possible low capacity, higher sensitivity detectors. Some evidence exists that charge multiplication effects occur in these films.

(f) The one commercially supplied single crystal of aluminium oxide displayed current-field characteristics similar to those of the prepared films, indicating similar conduction mechanisms.

(g) A surface alpha particle counter constructed on this single crystal permitted the determination of the following parameters for aluminium oxide:

(i) charge carrier mobility, $\mu = 5 \pm 2$ cm^2V^{-1} sec^{-1};

(ii) mean energy to generate a charge carrier pair, $\epsilon = 23 \pm 8$ eV;

(iii) mean charge carrier trapping time, $T = 4.5 \pm 0.2 \times 10^{-7}$ sec., where the errors have probably been overestimated.

6.4 Future work.

In addition to the areas already suggested in the body of this thesis, viz specimen preparation, structure and properties, and improved measuring technique, it is considered that several other experiments would be justified.

Some preliminary experiments have been performed on the effect of alpha particle irradiation on the emission of hot electrons from aluminium oxide films. These will be continued.

The accuracy of the magnitude of the values of carrier mobility and the like, can be improved by better methods of recording the shape of the pulses. A signal averaging techniques centred around a 256 channel pulse height analyser is being developed and should be capable of reducing the error to less than one percent.

Finally attempts will be made to use the developed detectors for the counting of low energy protons.

Acknowledgements.

The advice and assistance of Dr. S.G. Tomlin was much appreciated. Professor D.N.F. Dunbar made helpful suggestions, and made available the Soild State Radiations Detector used. Thanks are also expressed to Professor D.E. Swan for fruitful discussion and encouragement. This work was supported by the Department of the Army.

APPENDIX

Several electronic circuits were developed during the course of the experiments. Brief descriptions and circuit diagrams follow.

Charge Sensitive preamplifier:

A charge sensitive preamplifier based upon the ORNL Q-20693-3 design in which the cascode stage tubes were replaced by E810F valves, and the following stages by E180F was built. The feedback capacitor was adjusted to 5 pF; the output voltage (V) is related to the output charge (Q) by:

$$V = {}^{Q}/_{C} = 2Q \times 10^{11} \text{ volt.}$$

The circuit diagram is figure A.1. The main operating characteristics are described in the main text.

Wide band amplifier.

An amplifier with bandwidth 150 MHz, and an equivalent input noise resistance of 130 ohm, and gain per stage of 5 times was modelled on the design of Moody (Electronic Engng. 24 214, 1952). In the final design (circuit diagram figure A.2) the high input capacity (23 pF) of the E810F was counteracted by interposing a similar valve as a cathode follower between succeeding stages. A filter coupling network of characteristic impedance of 100 ohm was used between amplifying stages and the adjacent cathode follower. The bandwidth of the amplifier was improved by using ferrite cored inductors in the anode leads and ferrite beads on the heater and supply leads.

Amplifiers of gain 5 times and 25 times were made so they could be coupled in cascade.

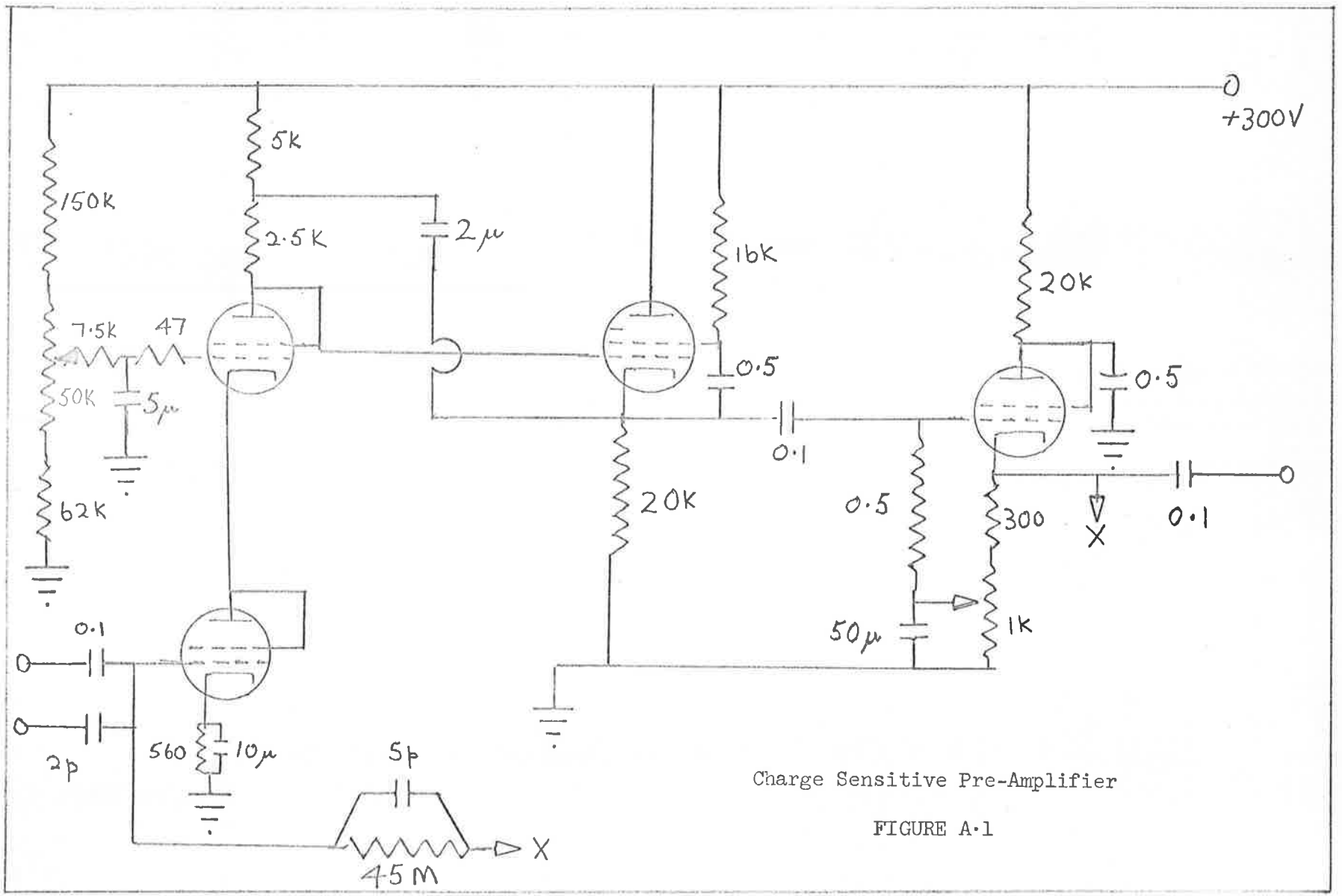

Charge Sensitive Pre-Amplifier

FIGURE A·1

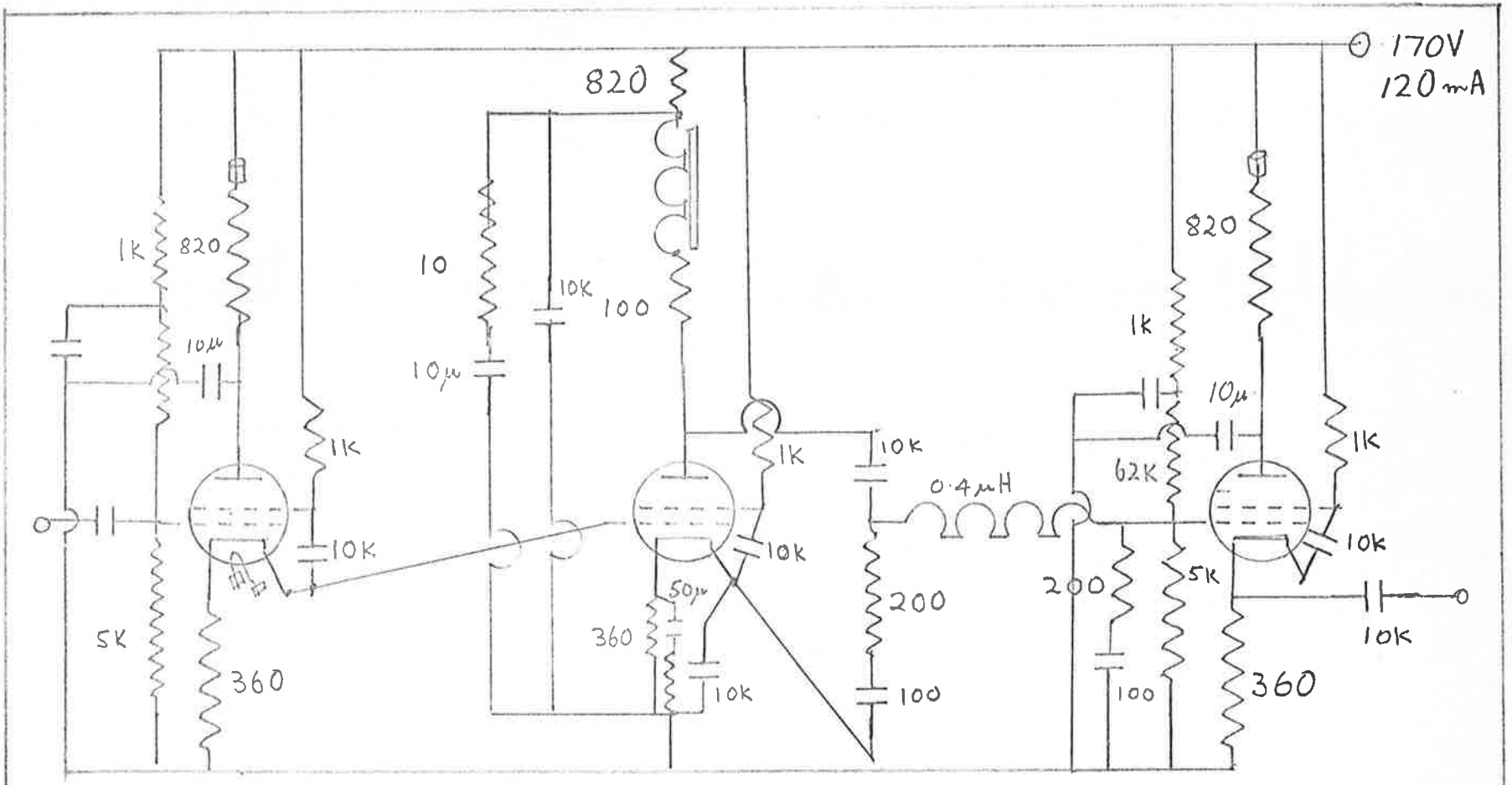

Wide Band Amplifier

FIGURE A.2

Post amplifier.

A two stage amplifier of adjustable gain and with variable integration and differentiation time constants was built. The maximum gain is 100 times. Figure A.3 is the circuit diagram. The amplifier was used in conjunction with the charge sensitive amplifier.

Motor drive control.

A control circuit for the spark-cutter blade drive motor was devised to permit cutting, without welding, larger diameter rods. The negative going pulse produced by the spark discharge cuts off the 6AQ5, which in conjunction with the diodes effectively disconnects the drive. The maximum sparking rate is 20 per second - at this frequency the motor drive ceases completely. The control circuit forms figure A.4.

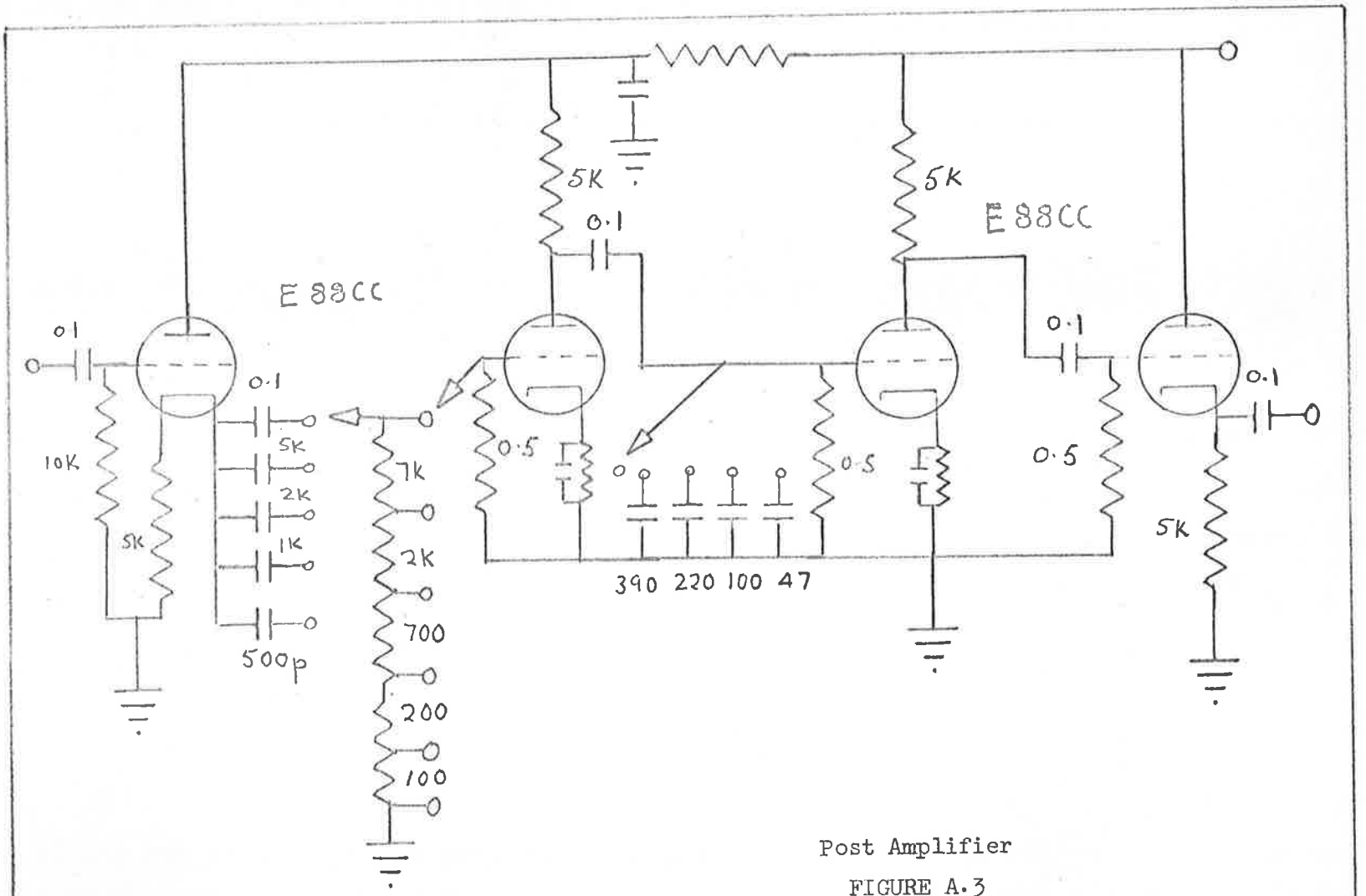

Post Amplifier

FIGURE A.3

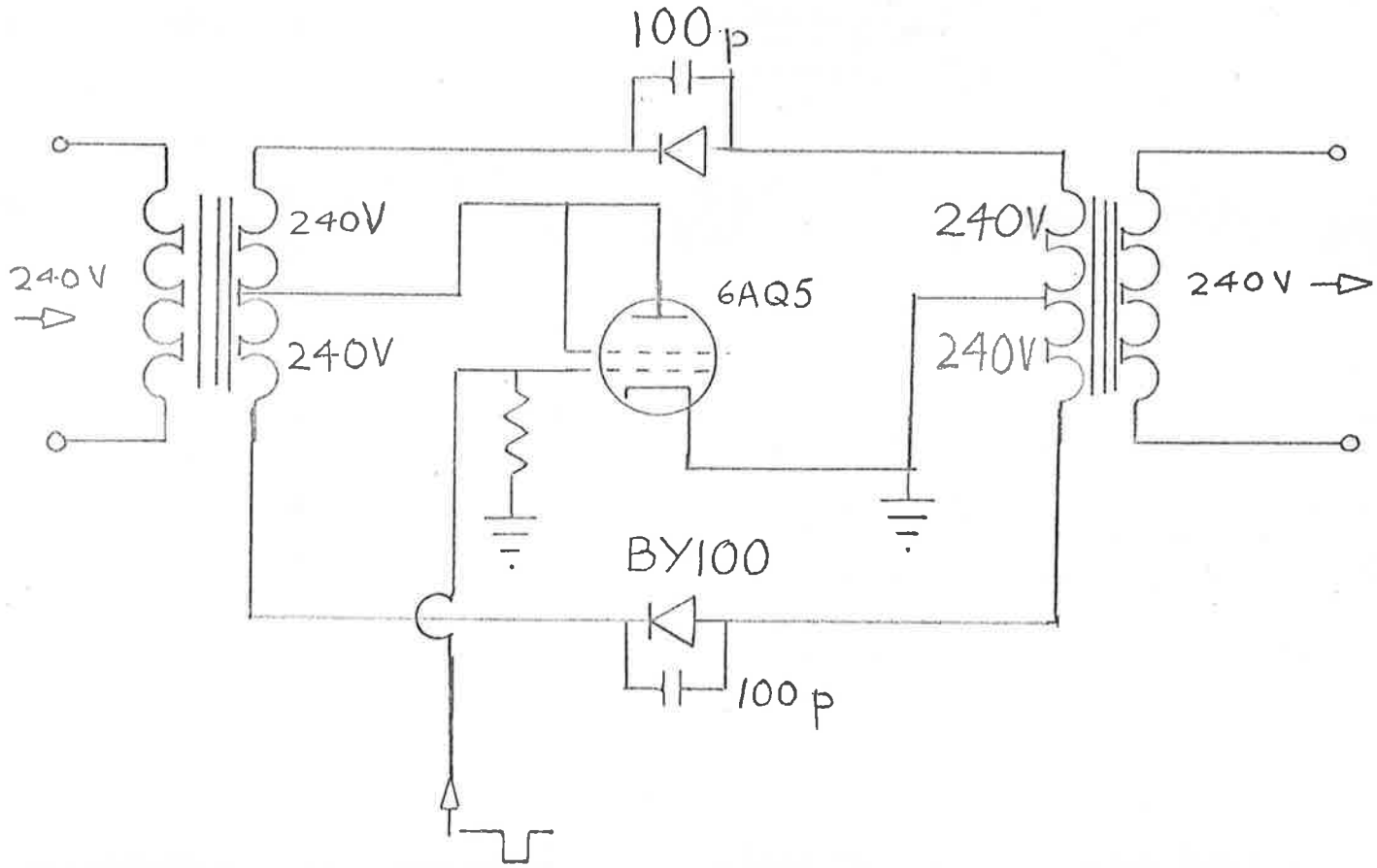

Motor Drive Control

FIGURE A·4

REFERENCES

Ahearn, A.J., J.A. Burton and D.E. Wooldrige. Phys. Rev., 71, 913 (1947)

Ahearn, A.J., Phys. Rev., 73, 524 (1948)

Barrett, M.A., and A.B. Winterbottom, First International Congress on metallic Corrosion. Imperial College, London, 1961.

Baumann, W., Z. Phys., 111, 708 (1939)

Bersohn, R., J. Chem. Phys., 29, 326 (1958)

Biondi, M.A., Rev. Sci. Instrum, 30, 831 (1959)

Blewe, E., Z. Phys., 100, 192 (1936)

Bosman, J., private communication.

Bureman, O., T.E. Cranshaw, and J.A. Harvey; Can. J. Research, A-27, 191, (1949).

Burthers. W.G., A. Claasmen and J. Zernike, Z. Phys., 74, 593 (1932)

Chang and Rosenblum, Phys. Rev., 67, 222 (1945).

Charlesby, A., Prac. Phys. Soc., B. Vol. LXVI, 317 (1953).

Chase, R.L., NAS-NRC Publication 871, 221, Edited by T.W.T. Dobbs and P.J. Walter (1961).

Chynoweth, A.G., "Progress in Semiconductors" Vol. 4, (John Wiley and sons Inc. New York 1960).

Cohen, J., Bu.. Amer. Ceram. Soc., 38, 441 (1959).

Cole, M., I.A. Bucklow and C.W.B. Grigson, Brit. J. appl. Phys. 12, 296 (1961).

Collins, R.E., and L.W. Davies, Solid State Electron, 7, 445 (1964)

Cottini, C., E. Gatti, G. Giannelli and G. Rossi, Il Nuovo Cimento 3, 473 (1956).

Curtis, M.L., J.W. Heyd, R.G. Olt, and J.F. Eichelberger: Nucleonic, 13, 38 (1955).

Czarnecki, R. and F. Hilbert, Kernenergi, 5, 586 (1962) (1)

Czarnecki, R. and F. Hilbert, Neutte Hiitte, 7, 765 (1962) (2).

Das Gupta, N.N., and S.K. Ghosh, Revs. Mod. Phys., 18, 227 (1946).

David, I., and A.J.E. Welch, Trans. Faraday Soc., 52, 1642 (1956).

Dearnaley G., and D.C. Northrop, Semiconductor Counters for Nuclear Radiations. 1st Ed. (E and F.N. Span Ltd. London 1964).

Defence Standards Laboratory, Department of Supply (Australia) Annual Report, 1961-1962.

Davies, D.K., private communication.

Edwards, J.D. and F. Keller, J. electrochem. Soc., 79, 135 (1941)

Edwards J.D. and F. Keller, Trans. Amer. Inst. min. met. Engr. Inst. Met. Rev., 156, 288 (1944)

Emery, F.E., and T.A. Robson, Phys. Rev., 140, A2089 (1965).

Engel Kemeir, D., Rev. Sci. Instr., 27, 589 (1956)

Ess, H., and J. Rossel, Helv. Phys. Acta., 24, 247, 1951.

Evans, V.R. The Corrosion and Oxidation of Metals. (Edward Arnold Ltd. London 1960)

Fairstein, E., I.R.E. Trans. Nucl. Sci., NS-8, No. 1, 129 (1961)

Franklin, R.W., Nature, 180, 1470 (1957).

Frenkel, I., J. Exptl. Theoret. Phys. (USSR), 8, 1893 (1938)

Frisch, O.R., British Atomic Energy Rept. BR-49, (1944).

Frohlich, H., Prac. Roy. Soc., A188, 521, (1947).

Gamble, F.T., R.H. Bantram, C.G. Young, O.R. Gilliam and P.W.Levy, Phys. Rev. 134, A589 (1964).

Gibbons, D.J., private communication.

Gibson, W.M., and G.L. Miller, Brookhaven National Laboratory Report. No. BNL5391.

Gregg, E.C., "Handbook of Chemistry and Physics", 43rd ed., p. 2564. The Chemical Rubber Publishing Co., 1961.

Greinacher, Helv. Phys. Acta. 9, 950 (1936)

Grosskeutz, J.C. and G.G. Shaw, J. Appl. Phys., 35, 2195 (1964).

Harrington, R.A., and H.R. Nelson, Trans. Amer. Inst. min. met. Engr. Inst. Met. Div., 137, 62 (1940).

Harrop, P.J., and R.H. Creamer, Brit. J. appl. Phys., 14, 335 (1963).

Hartman, T.E., and J.S. Chivian, Phys. Rev., 134, A1094 (1964).

Hass, G., Z. anorg. Chem., 254, 96 (1947).

Hass, G., J. opt. Soc. Amer., 39, 532 (1949).

Hass, G., and H. Kehler, Koll. Z., 95, 26 (1941).

Heidenreich, R.D., and V.G. Peck, J. appl. Phys., 14, 23 (1943).

Henenguel, J. and P. Lang, C.R. Acad. Sci. Paris 232, 2218 (1951).

Hilbert, F., Neute Hiitte, 7, 368 and 416 (1962).

Hilbert, F., and H. Lorenz, Jena Review, 5, 218 (1963).

Hoar, T.P., and N.F. Mott, J. Phys. Chem. Solids, 9, 97 (1959).

Hofstadter, R., Nucleonics, 4, 2, 29 (1944).

Holland, L. "Vacuum Deposition of Thin Films" (Chapman and Hall, London, 1956).

Huber, K., Helv. Chem. Acta., 28, 1416 (1945).

Huber, K., and A. Gangler, Experientia, 3, 277 (1947).

Huber, K., and A. Gangler, J. Coll. Sci., 3, 197 (1948)

Iredale, P., Nuclear Inst. Methods, 11, 336 (1961).

Johnson, P.D., J. Amer. Cerma. Soc., 33, 168 (1950).

Keller, F., and A.H. Geisler, J. appl. Phys., 15, 696 (1944).

Keller, F., M.S. Hunter and D.L. Robinson, J. electrochem. Soc., 100, 411 (1953).

Keller, F., M.S. Hunter and D.L. Robinson, J. electrochem. Soc., 101, 335 (1954).

Laurance, N., E.C. McIrvine and J. Lambe, Phys. Chem. Solids, 23, 515 (1962).

Lewis, J.E., and R.C Plumb, J. electrochem. Soc., 105, 496 (1958).

Liechti, F., and W.D. Treadwell, Helv. Chem. Acta., 30, 1204 (1947).

Livingston, S. and H. Bethe, Revs. Modern Phys. 9, 203 (1937).

McCuthceon, D.M., J. appl. Phys., 20, 414, (1949).

McCutcheon, D.M., and W. Pohl, Metal Progress, 56, 674 (1949).

McKay, K.G., Phys. Rev., 74, 1606 (1948).

McKay, K.G., Phys. Rev., 76, 1537 (1949).

McKenzie, J.M., and J.B.S. Waugh, I.R.E. Trans. Nucl. Sci. NS7, 195 (1960).

Mead, C.A., Phys. Rev., 128, 2088 (1962).

Miles, J.L., and P.H. Smith, J. electrochem. Soc., 110, 1240 (1963).

Mott, N.F. and W.O. Twose, "Advances in Physics", Vol. 10, edited by N.F. Mott (Taylor and Francis Ltd., London, 1961).

Newnham, R.E., and Y.M. de Haan, Z. Krist., 117, 235 (1962).

Northrop, D.C. and O. Simpson, Prac. Phys. Soc., 80, 262 (1962).

Olsen, L.O., C.S. Smith, and E.C. Crittenden, J. appl. Phys. 16, 425 (1945).

Orman, C., N.Y. Fan, G.J. Goldsmith and K. Lark-Horovitz, Phys. Rev. 78, 646 (1950).

Piper, W.W., and F.E. Williams, Phys. Rev., 98, 1809 (1955).

Plumb, R.C., J. electrochem. Soc., 105, 498 (1958).

Powell, C.F., I.E. Campbell and B.W. Ganser, "Vapour Plating" Ch. 7, (John Wiley and Sons Inc., New York 1955).

Preston, J.S., Proc. roy. Soc., A.202, 449 (1950).

Price, W.J., "Nuclear Radiation Detection", 2nd ed., (McGraw-Hill Book Co., London 1964).

Rummel, Th., Z. Phys., 99, 518 (1936).

Rhyshkewich, E., "Oxide Ceramics" (Academic Press, New York, 1960).

Sharpe, J., and Taylor, Prac. I.E.E., 98, 210 (1951).

Sharpe, J., Nucleonics, 11, 40 (1953).

Sharpe, J., "Nuclear Radiation Detectors", 2nd ed., (Methuen and Co. Ltd., London, 1964).

Shockley, W., Solid State Electron, 2, 35 (1961).

Simpson, J.A., Rev. Sci. Instrum, 18, 844 (1947).

Smith, A.C., Can. J. Phys., 35, 1151 (1957).

Smith, A.C., Can. J. Phys., 37, 591 (1959).

Snouse, T.W., Rev. Sci. Instrum. 36, 866 (1965).

Snowden, M., Article in "Progress in Nuclear Physics", vol. 3., O.R. Frisch (ed.) (Academic Press, Inc., New York, 1953).

Stern, M., and H.H. Uhlig, J. electrochem. Soc., 99, 389 (1952).

Suchet, J.P., "Chemical Physics of Semiconductors", (Van Nastrand series in Physical Chemistry, T.M. Sugden, ed.), D. Van Nostrand Co. Ltd., London, (1965).

Taylor, C.S., C.M. Tucker, and J.D. Edwards, J. Electrochem. Soc., 88, 325 (1943).

Taylor, C.J., W.K. Jentshke, M.E. Remley, F.S. Eby and P.G. Kruger, Phys. Rev., 89, 1034 (1951).

Taylor, R.L. and H.E. Haring, J. electrochem. Soc., 103, 611 (1956).

Tegart, W.J., McG., "The Electrolyte and Chemical Polishing of Metals in Reserach and Industry." (Pergamon Press Ltd., London, 1956).

Tibol, G.J., and R.W. Hull, J. electrochem. Soc., 111, Dec. (1964).

Tibol, G.J., and W.M. Kaufman, Proc. I.E.E.E. Dec. 1964. p. 1465.

Treadwell, W.D., and A. Obrist, Helv. chem. Acta., 24, 998 (1941).

Tyler, W.W., R. Newman and H.H. Woodburg, Phys. Rev., 97, 699 (1955).

van Geel, W., Ch. , Physica, 17, 761 (1951).

van Geel, W., Ch. , Halbeiterprobleme, 1, 291 (1955).

van Geel, W., Ch. , and B.J.J. Schelen, Philips Res. Rep. 12, 240 (1957).

van Heerden, P.J., "The Crystal Counter" (N.V. Noordhollansche Uitgevers Maatschappij, Amsterdam) (1945).

van Scriver, W., and R. Hofstadter, Phys. Rev., 97, 1181, (1955).

Verkerk, B., P. Winkel and D.G. de Groot, Philips Res. Repts. 13, 506 (1958).

Vermilyea, D.A., Acta. Metallurgica, 2, 482 (1954).

Vermilyea, D.A., J. appl. Phys. 27, 963 (1950).

Verwey, E.J.W., Z. Kryst., 91, 65 (1935).

Veszi, G.A., J. Brit. Instr. Radio Eng., 13, 183 (1953).

Warterberg, H.U., and H. Moehl, Z. phys. Chem., 128, 439 (1949).

Weinrich, A.R., Brit. Pat. 650, 173 (Nov. 1947) (Quoted in Holland L. 1956, p. 464).

Whaling, W., "Handbuch der Physik", 34, 193, Julius Springer, Berline (1958).

Wilkinson, D.H., "Ionisation Chambers and Counters" (Cambridge University Press, London, 1950).

Wilson, J.G. "The Principles of Cloud-Chamber Technique", (Cambridge University Press, London, 1951).

Wilms, O.R. and J.B. Wade, Metallurgica, 54, 263 (1956).

Winkel, P. and D.G. de Groot, Philips Res. Repts., 13, 489 (1958).

Winkel, P. and B. Verkerk, Philips Res. Repts., 13, 501 (1958).

Yamakawa, J., Phys. Rev., 75, 1774, (1949).

Yamakawa, J., Phys. Rev., 82, 522 (1951).

Young, L., Trans. Faraday Soc., 51, 1250 (1951).

Young, L., Trans. Faraday Soc., 55, 842 (1959).

Young, L., "Anodic Oxide Films" (Academic Press Inc., New York, 1961).

Zhuze, V.P., Zh. Tekh. Fiz. 25, 2079 (1955).